Modeling of Microbially Induced Calcite Precipitation for the Immobilization of Strontium-90 Using a Variable Velocity Streamtube Ensemble

Final Technical Report
DOE-FG02-07ER64403
Submitted 26 August 2013

Timothy R. Ginn trginn@ucdavis.edu
Tess Weathers tess.weathers@gmail.com

Table of Contents

Abstract

Biogeochemical modeling using PHREEQC2 and a streamtube ensemble approach is utilized to understand a well-to-well subsurface treatment system at the Vadose Zone Research Park (VZRP) near Idaho Falls, Idaho. Treatment involves *in situ* microbially-mediated ureolysis to induce calcite precipitation for the immobilization of strontium-90. PHREEQC2 is utilized to model the kinetically-controlled ureolysis and consequent calcite precipitation. Reaction kinetics, equilibrium phases, and cation exchange are used within PHREEQC2 to track pH and levels of calcium, ammonium, urea, and calcite precipitation over time, within a series of one-dimensional advective-dispersive transport paths creating a streamtube ensemble representation of the well-to-well transport. An understanding of the impact of physical heterogeneities within this radial flowfield is critical for remediation design; we address this via the streamtube approach: instead of depicting spatial extents of solutes in the subsurface we focus on their arrival distribution at the control well(s). Traditionally, each streamtube maintains uniform velocity; however in radial flow in homogeneous media, the velocity within any given streamtube is spatially-variable in a common way, being highest at the input and output wells and approaching a minimum at the midpoint between the wells. This idealized velocity variability is of significance in the case of ureolytically driven calcite precipitation. Streamtube velocity patterns for any particular configuration of injection and withdrawal wells are available as explicit calculations from potential theory, and also from particle tracking programs. To approximate the actual spatial distribution of velocity along streamtubes, we assume idealized radial non-uniform velocity associated with homogeneous media. This is implemented in PHREEQC2 via a non-uniform spatial discretization within each streamtube that honors both the streamtube's travel time and the idealized "fast-slow-fast" pattern of non-uniform velocity along the streamline. Breakthrough curves produced by each simulation are weighted by the path-respective flux fractions (obtained by deconvolution of tracer tests conducted at the VZRP) to obtain the flux-average of flow contributions to the observation well.

1. Introduction

A well-to-well treatment system that incorporates *in situ* microbially-mediated ureolysis to induce calcite precipitation for the immobilization of strontium-90 has been explored at the Vadose Zone Research Park (VZRP) near Idaho Falls, Idaho. PHREEQC2 (Parkhurst and Appelo, 1999) is utilized to model the kinetically-controlled ureolysis and consequent calcite precipitation. Subsurface contamination is often approached with treatment schemes involving an injection/extraction well system. An understanding of the impact of heterogeneities on the idealized radial flowfield is critical for modeling, prediction, and remediation of the subsurface. This is addressed with a Lagrangian approach: instead of depicting spatial extents of solutes in the subsurface the focus is on the arrival distribution at the control well(s). PHREEQC2 provides a one-dimensional advective-dispersive transport option that can be and has been used in streamtube ensemble models. Traditionally, each streamtube maintains uniform velocity; however in radial flow in homogeneous media, the velocity within any given streamtube is variable in space, being in general highest at the input and output wells and approaching a minimum at the midpoint between the wells. This idealized velocity variability may be of significance if kinetic reactions are present with multiple components, if kinetic reaction rates vary in space, if the reactions involve multiple phases (e.g. heterogeneous reactions), and/or if they impact physical characteristics (porosity/permeability), as does ureolytically-driven calcite precipitation. Streamtube velocity patterns for any particular configuration of injection and withdrawal wells are available as explicit calculations from potential theory, and also from particle tracking programs.

To approximate the actual spatial distribution of velocity along streamtubes, we assume idealized non-uniform velocity associated with homogeneous media. This is implemented in PHREEQC2 via a non-uniform spatial discretization within each streamtube that honors both the streamtube's travel time and the idealized "fast-slow-fast" nonuniform velocity along the streamline. Breakthrough curves produced by each simulation are weighted by the path-respective flux fractions (obtained by deconvolution of tracer tests conducted at the VZRP) to obtain the flux-average of flow contributions to the observation well. Breakthrough data from urea injection experiments performed at the VZRP are compared to the model results from the PHREEQC2 variable velocity ensemble.

Analytical methods as described in Charbeneau (2000) can be implemented to solve three, four, and five spot injection/extraction patterns. However, these solutions require ideal, homogeneous, confined aquifers: constant and known regional gradient and water table height, uniform porosity, etc. The VZRP does not reflect these ideal characteristics and thus the travel times are found empirically. The streamtube ensemble was parameterized from bromide tracer tests that were conducted simultaneously with the urea injection. Thus, parameterization should reflect regional gradients and hydraulic characteristics of the site.

2. Background

2.1 Site Description and Motivation

Strontium is a radioactive metal that is part of the Department of Energy legacy. Strontium-90, the longest living of the artificially created strontium isotopes with a half-life of 28 years, was produced in large quantities as a result of the fission process. A bioremediation option currently being explored is the co-precipitation of strontium with calcite in a perched groundwater system as a part of the Idaho National Engineering and Environmental Laboratory (INEEL) (Fujita, et al. 2004). This *in situ* bioremediation strategy employs bacterial ureolysis to trigger calcite precipitation and strontium co-precipitation, thus immobilizing the contaminant.

Humans are typically exposed to strontium through contaminated drinking water. Strontium is relatively mobile which poses a particular risk to groundwater; as the Eastern Snake River Plain Aquifer, an unconfined and continuous aquifer, is the drinking water source for southeastern and south-central Idaho, immobilization of this radioactive contaminant is critical (Fujita, 2008; Wood, 1986).

Due to the chemical similarities between strontium and calcium, strontium can ultimately become concentrated in bones where it emits radiation and can cause cancer (US DOE, 2003; Fujita, 2008). Strontium-90's radioactivity makes the metal difficult to dispose if it is physically removed from an aquifer, thus *in situ* remediation techniques are often the most viable options. Additionally, cost effective *in situ* methods are sought for a variety of Department of Energy remediation strategies due to the large quantities of contaminated material and the difficulty of accessing the deep subsurface (Fujita, 2008). Typical treatment methods such as "pump and treat" systems are often inappropriate for aquifer media as many contaminants may be associated with the aquifer material, rendering pumping ineffective (Fujita, 2008). There are many advantages to bacterial ureolysis; as noted by Mitchell (2005) and Fujita (2004), the addition of foreign bacteria is most likely not required. Urea is an organic compound often found in natural environments; many subsurface organisms inherently maintain the ability to catalyze ureolysis.

In order to test calcite precipitation via microbially induced ureolysis strategies in a safe environment, the Vadose Zone Research Park (VZRP) is utilized. Sites within the INEEL are contaminated with strontium-90; the VZRP however, is not. Performing experiments in this location provides similar hydrology, geology, chemistry, and bacterial life that may be present in actual contaminated sites, while mitigating the risk of exposing equipment and researchers to radiation during the testing phase of this project. The VZRP is used for a variety of research projects; thus large quantities of data are available for this site. The VZRP is located at the new percolation ponds at the Idaho Nuclear Technology and Engineering Center (INTEC) facility as a part of the Idaho National

Engineering and Environmental Laboratory, and can be seen in the south-western corner of the map in Figure 1. These percolation ponds are implemented by INTEC as a remediation scheme to prevent contaminants from migrating into the aquifer system. The releases into the pond from INTEC often include cooling water, but may also contain waste from ion exchange or reverse osmosis processes (Baker, 2004). To mitigate algae growth, the discharge can be switched between the North and South ponds as needed. Discharge events may last anywhere from one to four days. The wells used for various injection and extraction schemes are located immediately south of the new percolation ponds; because of their close proximity, groundwater flow and water chemistry between the wells is highly dependent on the percolation pond usage, and thus is highly variable. The Idaho Nuclear Technology and Engineering Center reports that 99% of the Strontium on site is sorbed onto the aquifer material. This strontium is primarily sorbed onto ferrihydrite mineral surfaces in a manner consistent with surface complexation in a system that is supersaturated with calcite (Fujita, 2004). Tests in the Snake River Plain Aquifer (SRPA) establish an initial pH of 7.3 (Smith, 2006).

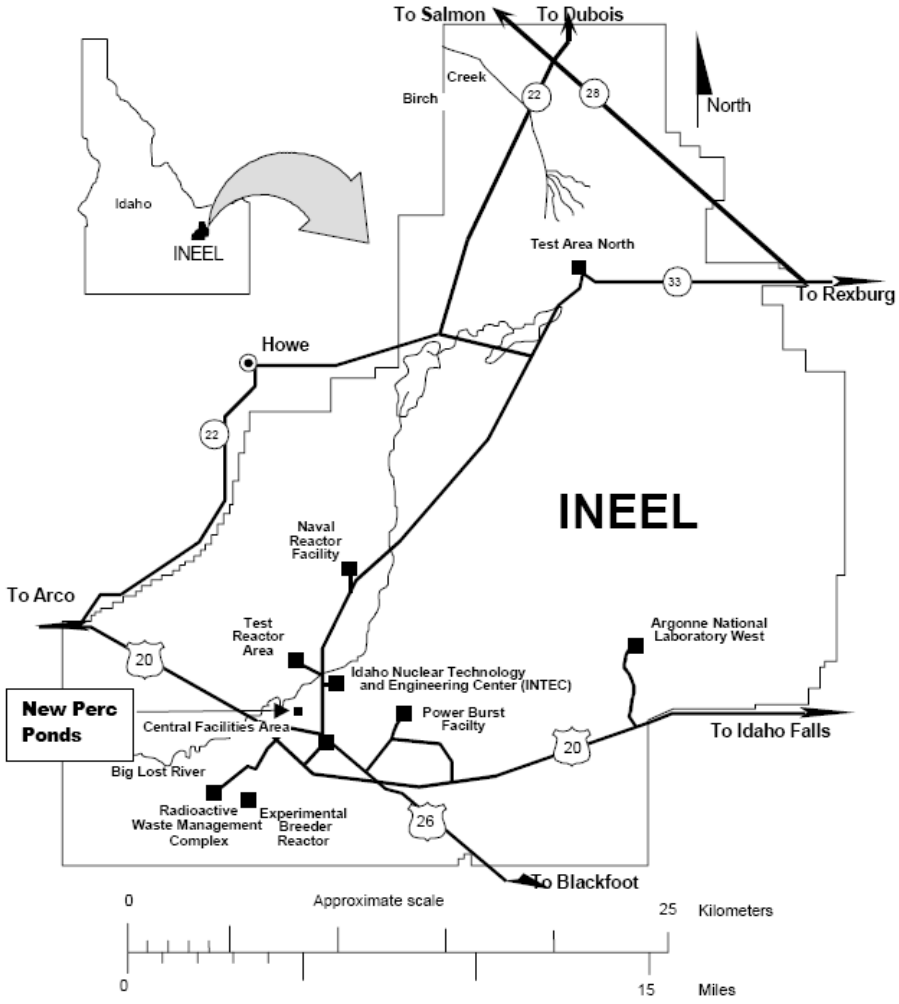

Figure 1: Map Depicting Location of Percolation Ponds (Baker, 2004)

Five wells are available for VZRP experiments; their configuration can be seen in figure 2. The studies presented here utilized injection in 2025 and extraction in 2024 and 2026.

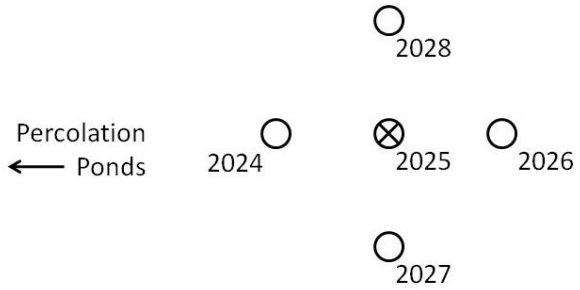

Figure 2: Test well layout

The experiments modeled herein are meant to simulate an injection/extraction system. Well 2025 is the injection well; 2024 and 2026 are extraction wells, each pulling at approximately half of the injection rate. If this study and other preliminary tests regarding microbially induced calcite precipitation at the VZRP are deemed successful, this remediation strategy can be safely applied to areas containing strontium-90.

2.2 Ureolysis and Calcite Precipitation

The application of urea to promote urea hydrolysis is an innovative idea that capitalizes on systems and reactions that naturally occur. Urea hydrolysis by microbial life results in production of ammonium and increases in pH. The pH increase triggers calcite precipitation; if strontium is present it will coprecipitate, forming a solid solution. This idea has been implemented not only in the field of remediation, but also for geotechnical applications and minor structural repairs in concrete, granite, or other media (Booster et al, 2008; Harkes et al, 2008; Fujita 2004). Calcite precipitation has been used for calcium removal in wastewater (Fujita, 2004) and for mineral plugging (Mitchell, 2006b). Porosity and permeability changes resulting from mineral precipitation have also been used for manipulation of fluid flow in porous material (Fujita, 2004).

Booster et al (2008) approach calcite precipitation for geotechnical modification purposes. They summarize and compare an experiment and a model developed within Excel. The bacteria chosen for urea hydrolysis in their study is *Sporosarcina pasteurii*. The authors make a notable point of including changes in porosity (as caused by calcite precipitation) with a simple algorithm; they state the result will have a "restricted reduction of the permeability." The authors note that there are many factors that can influence the urea hydrolysis rate, and suggest that future experiments should focus on urease activity as a function of relative parameters. They provide the same kinetic rate law from Fidaleo et al (2003) that is used in the VZRP study. Similar to the study by Booster et al. (2008), Harkes et al (2008) evaluate bacterial suspension throughout the sand column and develop an empirical relationship between strength and carbonate content for a specific sand type. The final objective is to up-scale the column experiments to suit commercial applications. Up-scaling is an issue that is at the forefront of calcite precipitation applications (Martinez, 2009).

Many studies have been conducted to verify the effectiveness of urea hydrolysis to induce calcite precipitation and the ability of calcite to coprecipitate with divalent metals. Ferris et al (2004) demonstrate a temperature dependence on the urea hydrolysis rate; Mitchell et al (2006b) demonstrate that the mineralogy and morphology of calcite is not influenced by the presence of bacterial cells, but rather from changes in bulk solution chemistry. Curti (1999) addresses the lack of knowledge regarding radionuclide coprecipitation as a remediation strategy and provides a set of partitioning parameters for radionuclides in calcite. With a similar objective to that of Curti (1999), Tesoriero (1996) assesses solid solution partitioning of Ba, Cd, and Sr. Warren (2001) investigates the potential for contaminant capture within carbonates. Evaluation of UO_2, Sr, and Cu yields that Sr has the greatest potential for incorporation in calcite. This study also evaluates the occurrence of calcite, aragonite, and vaterite as microbially induced precipitates; calcite was most commonly observed. Davis (1987) relates the adsorption of Cd^{2+} into calcite in systems saturated with respect to calcite, but undersaturated with respect to $CdCO_3$. This is similar to the VZRP system: saturated with respect to calcite and undersaturated with respect to $SrCO_3$. Pingitore et al (1992) focuses on strontium coprecipitation; this study was to determine the mechanisms of strontium incorporation into calcite to infer the stability of sequestered strontium. These experiments do not exhibit precipitation of strontianite, instead they witness occupation of Sr^{2+} in the Ca^{2+} sites in the calcite structure, creating a solid solution. Strontium will not be leached or mobile relative to calcium as it is a part of the solid solution, however mineral dissolution may occur. All of these findings support the hypothesis that Strontium may be sufficiently immobilized within calcite.

Fujita et al (2004) also evaluates the incorporation of strontium into calcite as a result of bacterial ureolysis. Three experiments are performed: one with *Bacillus pasteurii* and urea, the second with a non-ureolyzing bacteria and carbonates, and the third with *Bacillus pasteurii* and carbonates, no urea. The first and third cases are utilized to demonstrate differences in calcite precipitation rate in the presence of ureolysis versus induced precipitation by addition of carbonates. The second case is utilized to show whether or not the presence of bacterial cells is critical for the precipitation process. The results demonstrate that strontium is incorporated at depth in the calcite particles after ureolysis, and that faster calcite precipitation rates are associated with greater strontium uptake in the solid. In another study by Fujita et al (2008), molasses is injected in a single well over two weeks to promote microbial activity, followed by an injection of urea in order to estimate ureolysis rates in the subsurface. They determine that nutrient addition (molasses) increases ureolysis rates in the subsurface. As a result of this study, molasses has been added to most of the experiments at the VZRP to stimulate bacteria and potentially increase strontium uptake.

Most of these studies take place in laboratory-scale environments and include models that are built to represent bench scale processes. Currently there is no published research regarding three-dimensional field scale calcite precipitation modeling; the streamtube ensemble and reaction network supplied here will ideally address this void of knowledge and provide insight for future experiments and remediation efforts.

2.3 Streamtube Ensemble Methods

A practical method to simulate well-to-well transport in terms of arrival time distributions (breakthrough curves) is to construct a streamtube ensemble. A set of streamlines can be utilized to approximate flow throughout the entire field. Streamtubes are used in geochemical simulations in order to provide a continuum mechanical basis to calculate reaction kinetics and biological functions streamtube-representative streamlines. This amalgamation of transport and chemistry is used to approximate what may be happening underground. The arrival time distribution associated with particular streamline networks applied in homogenous media in a well-to-well pattern aligned with the hydraulic gradient is presented in Charbeneau (2000), building from the work of Grove and Beetem (1967).

Streamlines and streamtube ensembles have been widely used since the work of Simmons et al. (1995). In hydrology and petroleum engineering they are utilized to understand and predict capture zones, estimate oil recovery from reservoirs, and to visualize flow fields (Crane and Blunt, 1999). In Luo and Cirpka (2008, based off Grove and Beetem 1967) an ensemble is used to describe the kinetic mass transfer between mobile and immobile phases. As is performed in this VZRP study, Luo and Cirpka (2008) identify mixing parameters and estimate travel time distributions from breakthrough curves. Crane and Blunt (1999) implement the streamline method in a variety of contaminant transport problems: transport in a fully saturated confined aquifer; conservative, sorbing, and decaying species flow; radioactive decay; and saltwater intrusion in a temporally varying flow field. Travel-time based approaches for transport have been adapted for reactive transport. Ginn et al. (1995) describe a travel-time approach using streamlines to simulate biodegradation with microbial growth in theory. Ginn (2001) and Ginn et al. (2001) extend the Ginn et al. (1995) approach to a streamtube method and apply to data from an experiment involving aerobic biodegradation of benzoate in a two-dimensional heterogeneous flow field with microbial growth and attachment-detachment to surfaces. Cirpka and Kitanidis (2001) use this method for vertical recirculation to stimulate cometabolic dechlorination of trichloroethene by alternating oxygen and toluene injections. Luo et al (2006) approach a nested cell approach for bioremediation of uranium VI with potential theory. They propose a nested cell system to mitigate erratic regional flow conditions that may negatively affect the performance of traditional well-to-well systems. In Cirpka and Kitanidis (2001) a travel-time based approach is used to simulate bioreactive transport in a vertical circulation well system. Their approach is a modification of that by Crane and Blunt (1999). Their, and essentially all streamtube approaches, utilize the following advection-reaction equation:

$$\frac{\partial c(t,\tau_i)}{\partial t} + \frac{\partial c(t,\tau_i)}{\partial \tau} = r(t,\tau_i) \qquad \text{(EQ 1)}$$

where c [mol/L] is the aqueous species concentration, t [s] is time, τ [s] is travel time (τ_i relates to the inflow boundary,) and r [mol/L/s] is the reactive source/sink term (Ginn et al., 1995; Ginn, 2001; Cirpka and Kitanidis, 2001; Crane and Blunt, 1999). This equation is applied with the following boundary condition:

$$c(t, \tau_i = 0) = c_{in}^{i}(t) \quad \text{(EQ 2)}$$

Development of this equation assumes that the reaction term depends only on the travel time, not its spatial location. Essentially, two locations are assigned with the same concentration if they have the same travel time. The travel times in Cirpka and Kitanidis (2001) were determined using particle tracking developed by Pollock (1988); those in Ginn et al. (2001) were determined by transient deconvolution of the breakthrough curve of a passive tracer.

The study at the VZRP assumes steady-state flow and spatially uniform reactive parameters. These assumptions are also made in Cirpka and Kitanidis (2001) as reactive parameters are not dependent on location. In the future, the streamlines may be adapted to represent the changes in flowfield due to changing physical characteristics (i.e. porosity and permeability changes as a result of mineral precipitation). For example, Crane and Blunt (1999) calculate reactive transport repeatedly over streamlines that are updated over time.

Streamline approaches commonly are based on concentrations associated with fluid particles that move with the velocity field; these are essentially particle tracking, or Lagrangian methods. An advantage to Lagrangian methods is the ability to avoid directly solving the advection-dispersion equation by representing the solute mass with a set of particles; this makes characterization of the hydraulic conductivity field , that is generally not possible, uneccessary. The associated limitation is that streamline methods cannot delineate plumes and they require the traveltime distribution as input data. Another advantage to streamline methods is that transport becomes essentially one-dimensional versus the traditional multi-dimensional domain (Simmons et al, 1995; Crane and Blunt, 1999; Cirpka and Kitanidis, 2001; Luo and Cirpka, 2008). Unlike Eulerian approaches, streamline methods do not require limitations on step size or heavy reliance on grid orientation. The Eularian approach generally solves transport with a fixed spatial grid; linking concentrations to fixed points or spatial elements. This technique handles dispersion controlled transport problems with ease, but suffers from numerical dispersion, and therefore increased computation time for further discretization in time and space (e.g., Crane and Blunt, 1999). A critical advantage of streamline methods is the ability to simulate transport in non-uniform or highly heterogeneous or unknown subsurface conditions. In this case, tracer tests can be easily implemented to evaluate travel time distributions which eliminate the need for classification of many aquifer properties (Simmons, et al, 1995; Ginn et al., 2001; Luo and Cirpka, 2008). This is advantage is a primary reason a streamtube ensemble was selected for studies at the VZRP. Additionally, streamline methods can be useful in cases where variable velocity fields exist, resulting in unpredictable transport and unexpected breakthrough curves. For instance, Ginn et al. (2001) found a trimodal traveltime distribution governing transport in a bimodal heterogeneous porous medium. Long-term remediation strategies are also well-modeled with streamline methods; these models can be easily updated as conditions

change or as more information is discovered about the system, versus traditional methods (Luo and Cirpka, 2008).

Streamline methods based on potential theory , where the streamlines are contours of cumulative flux, denotes that in steady, two-dimensional flow, the flux between two streamlines is constant if the domain is defined between the two streamlines. A set of streamlines is termed an ensemble; this ensemble is a distribution of solute flux over time (e.g., Simmons et al., 1995). Each streamline obeys conservation equations while the integrated breakthrough curve is the weighted average concentration of all streamlines crossing an observation plane (Simmons et al., 1995) which in the case of the VZRP system is an extraction well. In most streamtube ensemble approaches, the difference between each streamline is the travel time and all other transport parameters are constant (e.g., Luo and Kitanidis, 2008). Seeboonruang and Ginn generalize the approach to the case where reaction parameters vary among the streamtube ensemble.

2.4 Objective and Scope

This study consists of five main objectives:

1. Develop and implement a reaction network
2. Deconvolve tracer test data to estimate travel times
3. Develop a variable velocity streamtube ensemble
4. Compare model results to experimental results
5. Utilize the model to predict calcite precipitation

Objective 1, development of the reaction network, consists of establishing the basis and secondary species; relevant speciation, precipitation and dissolution reactions; establishment and verification of kinetic ureolysis; and their subsequent implementation into PHREEQC. To obtain Objective 2, a cumulative density function is fit to each set of tracer test data resulting in overall distribution of solute fluxes over travel times. Objective 3 utilizes bins of fluxes per discrete travel times to create a streamtube ensemble. MathCAD is implemented to create a variable velocity ensemble; this requires a mathematical description of the velocity between an injection and extraction well pair that can be divided into varying cell lengths. To complete Objective 4, the model breakthrough curves are graphically compared to the experimental breakthrough curves and a comparison of a first-order ureolysis constant is performed. Objective 5 utilizes the model to predict quantity and general location of calcite precipitation. This objective innately demonstrates how this model may be used to evaluate possible *in situ* effects as a result of this remediation strategy.

This project focuses on a particular tracer test at the VZRP, although it could be applied to any well-to-well injection/extraction site with a tracer test and known groundwater chemistry. Ideally, this model will be developed for future use in predicting strontium immobilization by providing a modeling platform that could predict future experimental and applied uses for strontium immobilization.

3. Approach

To develop a model that can be used for prediction of strontium remediation, a series of steps must be taken. Throughout the process it is critical to maintain strong communication between the modeling group, the laboratory experimentalists, and the experimentalists at the field site. After the understanding of the general bioremediation technique, reaction network, and field tests is achieved, the model can be developed, shared, and implemented.

3.1 Conceptual Model

The development of this model has two distinct parts: the reaction network as implemented in PHREEQC2, and creation of the variable velocity streamtube ensemble with travel times derived from the tracer test. As described in section 2.1.1, there is an injection well (2025) and two extraction wells (2024 and 2026). For computation, this system is split into two separate well-to-well systems with equal injection and extraction rates. Each well-to-well system, 2025 to 2026 and 2025 to 2026, has its own ensemble of 14 streamtubes. Because of symmetry, the model runs can be reduced to 7 streamtubes. Each streamtube contains chemistry and transport and is run independently in PHREEQC2. In total, there are 14 runs to determine the breakthrough curves and calcite precipitation for wells 2024 and 2026.

3.1.1 Reaction Network

Urea hydrolysis is a process mediated by urease catalyzing bacteria. The addition of urea to the system results in ammonium and bicarbonate production, and an increase in pH which favors kinetic calcite precipitation (Fujita, 2004, 2008; Mitchell, 2005, 2006a, 2006b; Warren, 2005). The ammonium is present in such quantities that can exchange with strontium, calcium, or other metals currently sorbed to the surface material, releasing them into the aqueous phase where it can be readily subjected to reactions and redeposition. Because strontium and calcium are both divalent ions, they precipitate together in a reaction that can be considered irreversible while the saturation index of the solid solution remains high. This allows for long term containment (mineral precipitation) over the previous sorbed state (Fujita, 2004, 2008). The overall reaction is shown below (Smith, 2006).

$$\text{Solid} - (^{90}Sr^{2+}) + H_2N(CO)NH_2 + 2H_2O \rightarrow {}^{90}SrCO_3 + \text{Solid} - (NH_4^+)_2 \qquad \text{(EQ 3)}$$

On the right side of the equation, strontium is sorbed to the aquifer. The other reactants are urea ($H_2N(CO)NH_2$) and water. The final products are a strontianite mineral solid with ammonium sorbed to the aquifer. Note here that this is just a simplification of the reaction process, and does not include the contribution from the calcite precipitation reaction. This overall reaction can be broken down into secondary reactions to better describe the process.

$$H_2N(CO)NH_2 + 3H_2O \rightarrow 2NH_4^+ + HCO_3^- + OH^- \quad \text{(EQ 4)}$$

The above reaction (Fujita 2004; Mitchell 2005, 2006a, 2006b; Warren, 2005) demonstrates the breakdown of urea in water into ammonium (NH_4^+), bicarbonate (HCO_3^-), and hydroxide (OH^-) after being catalyzed by the enzyme urease. The creation of OH^- provides an increase in pH; Smith (2006) notes that the pH in this network will rise to and remain constant at 9.1. Evaluation of the carbonate system at equilibrium at this pH demonstrates that bicarbonate is the dominant species at this pH range (Morel, 1993).

In aquatic systems, the following precipitation reaction is likely to occur (Warren, 2005):

$$Ca^{2+} + 2HCO_3^- \rightarrow CaCO_3(s) + CO_2 + H_2O \quad \text{(EQ 5)}$$

As addressed in section 2.1.2, many studies have documented that the strontianite will coprecipitate with calcite as a solid solution. Coprecipitation is the process through which a constituent (in this case strontium) is trapped in a solid product formed during the interaction of the aqueous solution with the groundwater material (Curti, 1999). This mineral form will effectively immobilize the radioactive strontium-90.

Incorporation of this reaction network into PHREEQC will require the definition of all species implemented in the reactions, selection of a database to provide the appropriate thermodynamic values, surface exchange, a kinetic system to simulate urea hydrolysis, and a precipitation mechanism to represent calcium and strontium coprecipitation. To simulate reactive transport in this particular three-well system, the final program contains relevant species, cation exchange, kinetic ureolysis, and equilibrium precipitation. To ensure complete modeling of the system, the necessary master species must be included in the database or defined. The chosen database for this application is a modified minteq.v4. This is an oxidation/reduction decoupled database. This is chosen for the VZRP because redox systems are not critical, and inclusions of redox reactions (specifically within nitrogen cycling) may incorrectly skew the urea hydrolysis and ammonium production. In addition to the species described in the database, urea and a fictive enzyme species "Z" are added (see section 4.1.1). The initial concentrations of chosen constituents are based on the measured concentrations of observed solutes in each well and are initially assigned to every cell between the injection and extraction wells.

Initially, surface complexation with ferrihydrite was desired for modeling of the exchange surface. However, due to a lack of knowledge of the surface characteristics, a general cation exchange model was selected. This only requires an initial quantity of exchange sites that can be estimated as a fitting parameter. Utilization of cation exchange may represent the initial sorption of strontium, exchange with ammonium or other cationic species, and sites for precipitation just as well as PHREEQC2's surface complexation given the quantity of available data. This exchange is modeled as an equilibrium process. Calcite precipitation is also modeled as an equilibrium process. There are many types of calcite precipitation and crystal growth mechanisms that occur kinetically. A single mineral may be described by a variety of rate laws (Bethke, 2008).

Mitchell and Ferris (2006a, 2006b) demonstrate that crystal growth is highly dependent on precipitate surface area; equilibrium precipitation in PHREEQC2 only evaluates the saturation index.

The kinetic formulation is a modified Michaelis-Menten equation and is discussed in section 4.1.1. Cation exchange, precipitation, and kinetics are set to occur in every cell for every transport step. Advective transport in PHREEQC2 is a shift wherein the contents of one cell are 'shifted' to the next after reaction calculations. Parameterization of the bromide tracer tests mitigates the need for specification of additional subsurface parameters such as diffusion or porosity. Dispersivity, however, is specified; its implications are discussed in section 5.2.

3.1.2 Streamtube Incorporation

The urea injection experiment was conducted by injecting into well 2025 for 230 minutes at 2 gpm. Wells 2024 and 2026 extracted at 1.25 gpm. Instead of analyzing this three-well system at once, the simulation is broken into two distinct parts: injection in 2025 and pulling from 2024, and injection in 2025 pulling in 2026. For the separate analysis, the pumping rates are both assumed to be 1 gpm. This assumption stems from the idea that 50% of the injectate into 2025 will flow towards 2024 and the other 50% towards 2026. In PHREEQC2, the theoretical injection and extraction rates must be theoretically equal, as the shift operator does not truly account for pumping rates, only a shift of matter. The chosen boundary conditions for both the inlet and outlet cells in this simulation are a flux, or Cauchy boundary condition. This is most suitable for column-type simulations and is defined as follows (Parkhurst and Appelo, 1999):

$$C(x_{end}, t) = C_0 + \frac{D_L}{v}\frac{\partial C(x_{end},t)}{\partial x} \qquad \text{(EQ 6)}$$

Each well-to-well segment will be broken up into an ensemble of fourteen tubes; due to symmetry they can be run as seven separate simulations. From deconvolution of the tracer tests, seven travel times are determined that correspond to seven equal flux percents. This simplifies analysis; each streamtube is multiplied by the same factor. The streamlines are defined from potential theory and are assigned based on the angle of exit from the axis between the wells to the streamline. This angle (termed α in this document) is assigned in increments of $\pi/7$. These angles are defined in table 1 below. Note the first streamtube with $\alpha = 0$ is the direct path streamtube connecting the two wells.

Table 1: Designation of streamtubes. Angle is measured from the axis between the two wells to the tangent from the potential line.

Streamtube Number	Angle (α)	
	Radians	**Degrees**
1	0	0
2	$\pi/7$	25.71429
3	$2\pi/7$	51.42857
4	$3\pi/7$	77.14286
5	$4\pi/7$	102.8571
6	$5\pi/7$	128.5714
7	$6\pi/7$	154.2857

A schematic of the chosen streamlines are shown below in figure 3. Only the streamtubes for one half are actually computed within PHREEQC2, but are accounted for due to symmetry. The first streamtube corresponds to the straight line between the wells, with the seventh streamtube being the one with the longest path.

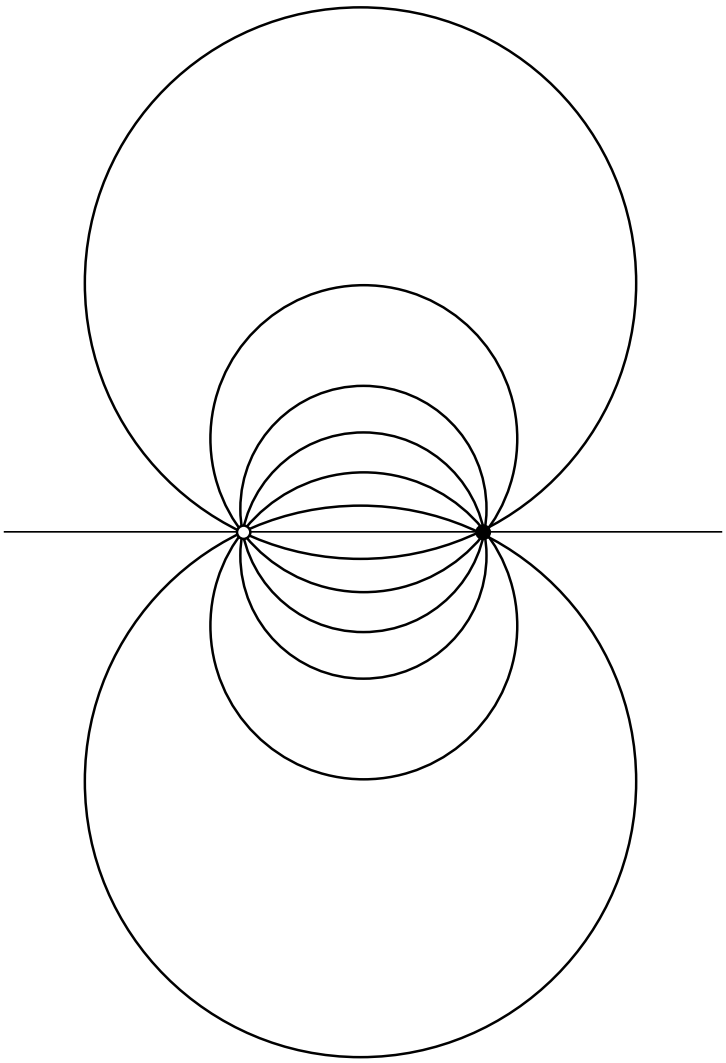

Figure 3: Streamline schematic between two wells with streamtubes radiating from each well at $\pi/7$.

The streamlines were chosen to be evenly spaced to further promote simplicity of analysis. The actual location of a streamline or a particle's path that will not likely follow this pattern is not critical for this type of analysis. Results from the VZRP are solely concerned with arrival times, not the extent or path of the solutes. A constant timestep for all of the streamtubes (amount of time spent in each cell, required for calculation of transport within PHREEQC) is chosen based on the first streamtube. By adjusting the lengths of each cell, velocity along a streamtube can be variable. MathCAD is used to assign lengths that match typical velocity profiles for a well-to-well flowfield. Selection of the travel times for each streamtube, timesteps, and cell lengths are discussed in section 4.2.4.

3.2 PHREEQC Program Background

PHREEQC2 is a computer program written in C that is used to simulate chemical reactions and one-dimensional transport. Some capabilities of PHREEQC are:

- Mixing
- Addition of net irreversible reactions to solution
- Dissolution and precipitation to achieve aqueous equilibrium
- Effects of temperature change
- Ion exchange
- Surface complexation
- Fixed-pressure and fixed-volume gas-phase equilibria
- 1D transport
- Kinetic reactions
- Solid solutions

It can be used for equilibrium calculations as well as kinetic reactions that implement user-specified rate equations that can be fully linked with the equilibrium reactants. PHREEQC2's transport operator includes advection, dispersion, and diffusion (including dual-porosity diffusion). PHREEQC2 comes with a database that includes common species and reactions, as well as the capability to utilize a custom database. PHREEQC2 uses a variety of methods to simulate the many capabilities it provides. The following sections describe PHREEQC2's standard processes and background theory for many of the capabilities that were utilized throughout this project.

3.2.1 Speciation and Forward Modeling: Aqueous Speciation

PHREEQC allows speciation or equilibration with respect to a single aqueous phase. Dissolved species in the aqueous phase are assumed to exist at thermodynamic equilibrium, with the exception of the initial solution composition that can be defined with disequilibrium among valence states of redox elements. Unknowns for each of the aqueous species (i) are activity (a_i), activity coefficient (γ_i), molality (m_i), and moles in solution (n_i). PHREEQC calculates chemical equations in terms of "master species." In other programs, such as MINEQL+ (Schecher and McAvoy, 1991) the term "component" is used to describe the master species. Master species must be linearly independent (no master species can be expressed as a function of other master species), and every species must be able to be defined from the selected master species (245a lecture4-2-8). The master unknowns, for which PHREEQC solves using iterative methods, are the natural logs of the master species' activities, the activity of water, the ionic strength, and the mass of the solvent water in the aqueous solution (W_{aq}). A species' activity is a basic measures of the "livelihood" of that species; activity describes its interaction with other species. In ideal solutions, the activity coefficient is equal to 1. In non-ideal solutions, the activity will be less than 1. The following relationships are universally applicable to aqueous species and demonstrate the relationship between activity coefficients and species concentrations:

$$a_i = \gamma_i m_i \qquad \text{(EQ 7)}$$

$$\boldsymbol{n_i = W_{aq}\, m_i} \qquad \text{(EQ 8)}$$

The activity coefficient of a species, γ_i, is determined with either the Davies Equation or with a form of the Debye-Hückel (D-H) equation. The Davies equation is an empirical fit of the D-H equation that provides a nearly constant activity coefficient for ionic strengths between 0.3 and 0.7 (Young, 2008). The Davies equation is:

$$\boldsymbol{log\gamma_i = -Az_i^2\left(\frac{\sqrt{\mu}}{1+\sqrt{\mu}} - 0.3\mu\right)} \qquad \text{(EQ 9)}$$

where z_i is the ionic charge of the aqueous species *i,* μ is the ionic strength, and A is a temperature dependent constant. Unless otherwise specified, PHREEQC utilizes the Davies equation for charged species and the D-H equation for uncharged species. The WATEQ D-H equation found in Truesdell and Jones (1974) is:

$$\boldsymbol{log\gamma_i = -\frac{Az_i^2\sqrt{\mu}}{1+Ba_i^0\sqrt{\mu}} + b_i\,\mu} \qquad \text{(EQ 10)}$$

with B as another temperature dependent constant. The extended D-H equation is as above, but with b_i equal to zero. In this case, a_i^0 is a size dependent parameter (often the radius of an ion, within the range of 3-10 Å). If b_i is not equal to zero, it is the "salting out" coefficient, and a_i^0 is another ion specific parameter. For uncharged species the WATEQ D-H equation is utilized with the first term becoming zero, resulting in the Setchenow equation (Langmuir, 1997):

$$log\gamma_i = b_i\mu \qquad \text{(EQ 10)}$$

where b_i is 0.1 unless otherwise defined within the database or input file.

To achieve equilibrium in ion-association models, all mass-action equations for an aqueous species must be satisfied. These governing equations can fully describe the equilibrium state of a geochemical environment (Bethke, 2008). The general mass action equation below

$$K_i = a_i \prod_m^{M_{aq}} a_m^{-c_{m,i}} \qquad \text{(EQ 12)}$$

can be implemented for each species, i. K_i is a temperature dependent equilibrium constant, and M_{aq} is the total number of aqueous master species. The stoichiometric coefficient, $c_{m,i}$, of the master species m in species i, can be either positive or negative: positive for the terms on the left side of an association reaction, negative for the terms on the right. For example, the association reaction for calcite is: $Ca^{+2} + CO_3^{-2} = CaCO_3$ with a logK of 3.2 at 25°C (minteqv4-ns6b.dat). The corresponding mass-action equation is:

$$10^{3.2} = \frac{a_{CaCO_3}}{a_{Ca^{2+}}\, a_{CO_3^{2-}}} \qquad \text{(EQ 13)}$$

Combining equations 7, 8, and 12 will provide a formula for determining the number of moles in species *i*:

$$n_i = K_i \, W_{aq} \, \frac{\prod_m^{Maq} a_m^{c_{m,i}}}{\gamma_i} \qquad \text{(EQ 14)}$$

3.2.2 Speciation and Forward Modeling: Exchange Species

To facilitate ion exchange equilibrium calculations, PHREEQC utilizes mass-action equations and mole balances for exchange sites. Within the EXCHANGE_MASTER_SPECIES block, a theoretical unoccupied exchange site can be defined. The theoretical nature of the exchange master species implies that it has no physical concentration (thus will not affect mole balance calculations) and possesses an activity only to ensure that the exchange sites will be filled with other species.

PHREEQC employs the Gaines-Thomas convention (Gaines and Thomas, 1953) to describe and incorporate exchange species and mass-action calculations. For example, an associative reaction for an exchange species is written as:

$$Ca^{2+} + 2X^{-} = CaX_2 \qquad \text{(EQ 15)}$$

where X^{-} represents the exchange master species. Exchange species reactions are not included in the minteq-v4.ns6b database; thus the necessary reactions are incorporated into the input file. The default activity coefficient for an exchange species is 1.0, but can be calculated with the Davies or D-H equations if desired. Mass-action and mole balance calculations are evaluated in the same manner for these reactions as for those discussed in the Aqueous Species section, however K_i represents the half-reaction selectivity coefficient.

3.2.3 Speciation and Forward Modeling: Surface Species

PHREEQC provides the framework to incorporate surface exchange reactions, wherein the surface will exist in equilibrium with the aqueous phase. The differences between an exchange species assemblage and a surface exchange assemblage are:

1. Exchange reactions are implemented as half-reactions, absolving the need for mole balance calculations on the exchange species. Surface reactions are not implemented as half reactions, and thus are "real" species that must be accounted for in mole balances.
2. Exchange reactions are neutral, whereas surface reactions can be defined as anionic, cationic, or neutral

In some studies hydrous ferric oxide (HFO) is the solid surface in which calcite and the incorporated strontianite matrix will precipitate. To implement the HFO surface, PHREEQC requires the number of active sites, the specific area, and the mass of the surface.

3.2.4 Equations for the Newton-Raphson Method

Equilibrium conditions are solved using the Newton-Raphson method. When equilibrium is satisfied, a set of functions based off mass-action and charge-balance equations are equal to zero. These zeroes are found with the Newton-Raphson method. The functions are developed for equilibrium with pure phases and solid solutions, for the activity of water, and for ionic strength, and are shown in the following sections.

3.2.4.a Activity of Water and Ionic Strength

The following function regarding the activity of water is solved by the Newton-Raphson method.

$$f_{H_2O} = W_{aq}\left(a_{H_2O} - 1\right) + 0.017 \sum_i^{N_{aq}} n_i \qquad \text{(EQ 16)}$$

The second term on the right side of the equation is derived from Raoult's Law, which provides an approximation for the activity of water. When evaluated for the partial derivative with respect to the activity of water, $\ln(a_{H_2O})$ becomes the master unknown. When the ionic strength is the master unknown, the following function is utilized:

$$f_\mu = W_{aq}\mu - \frac{1}{2}\sum_i^{N_{aq}} z_i^2 n_i \qquad \text{(EQ 17)}$$

Each function is then differentiated with respect to the appropriate master unknown and is incorporated into the Jacobian matrix as a linear equation. The solutions to these linear equations are found iteratively; providing approximate solutions to the nonlinear equations.

3.2.4.b Equilibrium with Pure Phases

The mass-action equation for a pure phase, e.g. calcite, is based off a dissolution reaction in PHREEQC. PHREEQC adopts the convention that the activity of a pure solid is 1.0 (Parkhurst and Appelo, 1999). The following function is utilized for pure phases by the Newton-Raphson method to obtain a zero:

$$f_p = (\ln K_p + [\ln(10)]\, SI_{p,target}) - \sum_m^{M_{aq}} c_{m,p}\ \ln(a_m) \qquad \text{(EQ 18)}$$

where $SI_{p,target}$ is the desired saturation index as specified by the user, and can represent supersaturated, undersaturated, or equilibrium conditions. The subscript *m* represents characteristics of the master species associated with the pure solid; the *p* represents characteristics of the pure solid itself.

3.2.4.c Equilibrium with Solid Solutions

An incorporated form of calcite and strontianite can be represented in PHREEQC by defining a solid solution. Solid solutions interact with the aqueous phase in equilibrium by following the same laws of mass-action, also subject to the constraints of Gibbs'

Phase Rule which limits the number of phases that can coexist at equilibrium (Morel and Hering, 1993). The activity of an ideal solid solution is equal to 1.0; for a non-ideal or binary solid solution, as a calcite-strontianite solution would be, PHREEQC defines activity coefficients with Guggenheim parameters. The particular Guggenheim parameters are currently unknown and are thus approximated from similar complexes (aragonite-strontianite, see example in manual).

3.2.4.d Mole Balance for Exchange Sites

A mole balance on the exchange sites requires that the number of moles of exchange species be equal to the number of available exchanger, *e*. The following function equates to zero when this condition is fulfilled:

$$f_e = T_e - \sum_{i_e}^{N_e} b_{e,i_e}\ n_{i_e} \qquad \text{(EQ 19)}$$

where T_e is the total moles of exchange sites as defined by the user and b_{e,i_e} is the number of exchange sites occupied by the exchange species.

3.2.4.e Mole Balance for Elements

A mole balance is performed for each element in the system. The function utilized by the Newton-Raphson technique must equal zero at equilibrium. This function is simply the difference between the total moles known to be in the system and the moles found in the pure and aqueous phases, solid solutions, gas phases, and exchange assemblages.

3.2.4.f Aqueous Charge Balance

To evaluate charge balance, exchange sites and aqueous cations and anions are summed. Charges must maintain balance in real systems, however analytical errors within PHREEQC may perpetuate charge imbalances in the initial solution calculations. In this case, the same imbalance is maintained throughout the simulation. Initial solutions can be balanced by either adjusting pH or by modifying the initial concentration of a specified cation or anion. The function to balance all charges is shown below:

$$f_z = T_z - \sum_{i}^{N_{aq}} z_i\ n_i - \sum_{e}^{E} \sum_{i_e}^{N_e} z_{i_e}\ n_{i_e} \qquad \text{(EQ 20)}$$

where f_z will equal zero when the charges are balanced. T_z is any charge imbalance, the first summation represents the aqueous species charges, and the second summation set represents charges on the exchanger.

3.2.5 Numerical Methods

Newton-Raphson iteration is performed on the functions (*f*) that were previously described. For equilibrium solutions, when the residuals of these functions equal zero or

fall within a specified tolerance, a solution has been found. To begin iterations, initial estimates for the master unknowns must be established.

For many geochemical applications, kinetic reactions are needed to accurately portray natural systems. Ordinary differential equations are often utilized to solve kinetic systems as reaction rates generally vary with reaction progress. PHREEQC utilizes a Runge-Kutta algorithm which generates an error estimate for each evaluation. If the error from the first three evaluations remains within a specified tolerance, a final rate is directly calculated.

PHREEQC is capable of modeling a variety of 1D transport processes: diffusion only, advection only, advection and dispersion, and advection and dispersion with dual porosity diffusion. The governing equation for transport is the advection-dispersion equation, included in PHREEQC with reactions:

$$\frac{\partial C}{\partial t} = -v\frac{\partial C}{\partial x} + D_L\frac{\partial^2 C}{\partial x^2} - \frac{\partial q}{\partial t} \quad \text{(EQ 21)}$$

where C is concentration of the solute (mol/kgw) and t is time (s). The first term, $-v\frac{\partial C}{\partial x}$ represents advective transport where v is pore water flow velocity (m/s), and x is distance (m). The last term, $-\frac{\partial q}{\partial t}$, is the reaction term that represents the change in the solid phase; q is defined as the concentration in the solid phase (mol/kgw). The middle term, $D_L\frac{\partial^2 C}{\partial x^2}$, represents dispersive transport where D_L is the hydrodynamic dispersion coefficient defined as the following:

$$D_L = D_e + \alpha_L v \quad \text{(EQ 22)}$$

where D_e is the effective diffusion coefficient and α_L is the dispersivity (m).
The graphic below visually represents the conservation of mass used to derive the advection-dispersion equation above.

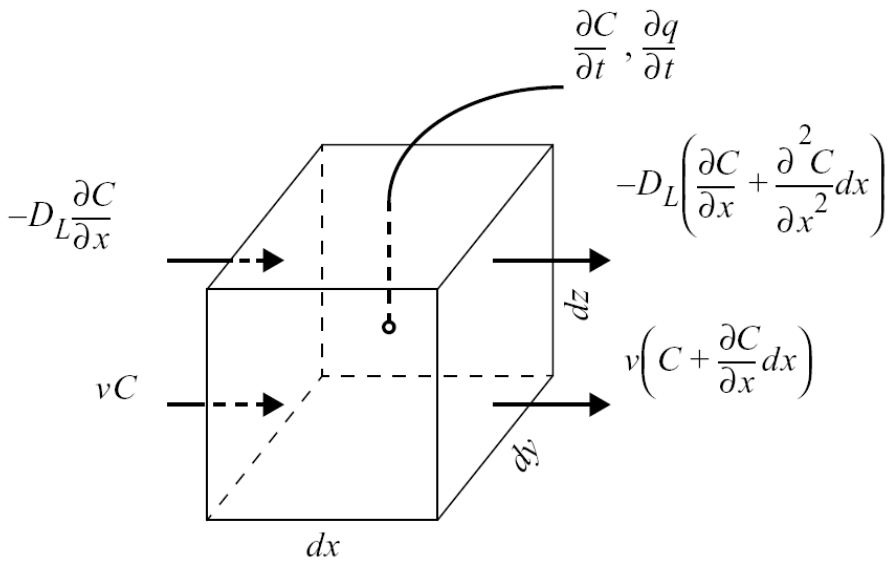

Figure 4: Depiction of conservation of mass used for the transport equation (Parkhurst, 1999)

The advective and dispersive transport pieces of equation 21 are solved using an explicit finite difference method that is forward in time, central in space for dispersion and upwind for advection. The numerical approach utilized in PHREEQC is a split-operator scheme: for each timestep advection is calculated first, followed by equilibrium and kinetic reactions. Next, the dispersive transport is calculated, again followed by equilibrium and kinetic calculations. Double calculation of equilibrium and kinetic reactions after both transport calculations differs from most other hydrogeochemical codes; it reduces numerical dispersion and iterations between transport and chemistry. This split-operator scheme minimizes numerical dispersion by always maintaining that the following equation is upheld:

$$(\Delta t)_A = \frac{\Delta x}{v} \qquad \text{(EQ 23)}$$

This states that the timestep for advective transport, $(\Delta t)_A$, must always be equal to the cell length, or change in distance, Δx, over the pore velocity. Not only does the split-operator scheme promote numerical accuracy and stability, but it provides the opportunity to effectively specify differing velocities to chosen cells (see section 4.2.1.b for an application of this concept), as long as the timestep fulfills the Courant condition for advective transport. Numerical instabilities are eliminated by maintaining the following relationship:

$$(\Delta t)_D \leq \frac{(\Delta x)^2}{3D_L} \qquad \text{(EQ 24)}$$

where $(\Delta t)_D$ is the timestep for dispersive/diffusive transport, subject to the Von Neumann Criterion for dispersive transport. If a fine grid is used to reduce numerical dispersion, multiple dispersion steps will be used that equal one advective step, with equilibrium and kinetic calculations being performed after every dispersion step.

The capabilities of PHREEQC2 easily lend themselves to streamtube applications. Its ability to compute one-dimensional reactive transport makes it an ideal program for the geochemical modeling of well-to-well systems. To determine the specifics of transport, such as timestep and cell lengths that are needed as input values in PHREEQC2, MathCAD 13 is utilized.

3.3 MathCAD 13 Program Background

MathCAD 13 (Mathsoft, 2005) is a mathematical calculation program with a visual interface. It provides a clear way to quickly solve complicated problems. A few key features in MathCAD 13 that are utilized in this project are:

- Calculation documentation using unit-aware notation
- The ability to import and export data to and from other programs, such as Excel or ASCII
- High-end numerics: summations, products, derivatives, integrals, trigonometry, exponentials
- The ability to use and update variables throughout a worksheet
- Functions for system solving and root-finding
- Programming for repeated calculations
- Graphics generation: x-y, 2D, 3D.

MathCAD 13 uses a numerical solver for its root-finding function. Adequacy of the achieved solution is dependent on the initial user-provided guess. If a guess is provided, MathCAD 13 uses the Secant or Mueller method. The Secant method connects two points along the function and traces it to the intersection with the x-axis. The corresponding x-value on the function is one of the next points for the following iteration. The process is repeated until a solution within the convergence criteria is reached. Mathematically, the Secant method is defined as:

$$x_{n+1} = x_n - \frac{(x_n - x_{n-1})f(x_n)}{f(x_n) - f(x_{n-1})} = \frac{f(x_n)x_{n-1} - f(x_{n-1})x_n}{f(x_n) - f(x_{n-1})} \qquad \text{(EQ 25)}$$

where x_{n+1} is the x-coordinate of the next point we are finding (ideally the point closer to the root,) x_n is the x-coordinate of the current location while $f(x_n)$ is the function value at that point. x_{n-1} is the x-coordinate of the previous point and $f(x_{n-1})$ is the function value at the previous point (Jensen, 2000). The Muller method is similar to the Secant method, but instead uses three points to create a parabola (Muller, 1956).

When PHREEQC2 and MathCAD 13 are used in conjunction with one another, they are useful tools that can be applied to model development.

4. Model Development

This section discusses the formulation of the model. The reaction network, including kinetics developed by Fidaleo and Lavecchia (2003) is described as well as a detailed description of the specific input code of PHREEQC2 used to run the batch systems and streamtubes. Preliminary speciation calculations are also discussed to verify that the initial conditions as measured at the VZRP can be accurately modeled and will behave according to theory. General theory and development of the streamtube ensemble is also discussed, as well as a detailed description of the MathCAD computations.

4.1 PHREEQC

PHREEQC2, a chemical modeling program, is used to replicate a remediation strategy of this system. Kinetic reactions and equilibrium phases were both used to track pH and levels of calcium, ammonium, urea, and calcite over time or space. Model results are compared with experimental outcomes. Utilization of PHREEQC to model this remediation strategy shows positive implications for the effectiveness of this method.

4.1.1 Fidaleo and Lavecchia Evaluation

A critical process to address in the reaction network is the hydrolysis of urea, which catalyzes the entire reaction network by increasing the pH of the system. For this project, biomass degradation is not considered, but rather urea hydrolysis is governed by the chemical reaction, equation 4, with the modified Michaelis-Menten kinetic model for ammonium and hydroxyl production as described by Fidaleo and Lavecchia (2003). In PHREEQC2, the formula for urea hydrolysis can be programmed and the parameters can be defined for the rate equation per Michaelis-Menten as follows (Fidaleo and Lavecchia, 2003).

4.1.1.a Summary

Urea hydrolysis, or ureolysis, is the process by which urea is converted via subsurface microbiota into ammonium and carbonate. It is the capstone process of this remediation strategy. The kinetic reaction implemented in PHREEQC2 is derived from Fidaleo and Lavecchia (2003).

Fidaleo and Lavecchia (2003) developed a urea hydrolysis rate expression that is dependent solution properties and pH. They hypothesized that in an aqueous solution, the reaction products (ammonia and carbon dioxide) will be present in varied ionic states, thus affecting the reaction rate. They performed different sets of experiments to explore the effects of urease concentration and the influence of pH on the reaction. Additional experiments were conducted to estimate the activation energy of the reaction and product inhibition effects. Finally, validation runs were performed to verify the kinetic expression.

These experiments focused on the ureolysis of urea by jack bean urease. Urease is an enzyme that is also found in bacteria; this study was prompted by the wide range of biotechnological uses of urease as a degrader of urea. Ureolysis is defined by the following reaction:

$$(NH_2)_2CO + 2H_2O \rightarrow 2NH_4^+ + CO_3^{2-} \quad \text{(EQ 26)}$$

where the first term is the substrate, urea. The overall reaction produces both ammonium and carbonate, however, only the concentrations of the product NH_4^+ were reported from these experiments.

Fidaleo and Lavecchia began with the assumption of a non-competitive mechanism for ammonium inhibition. This leads to the following rate expression:

$$r = \frac{v_{max}\,[S]}{(K_m + [S])\left(1 + \frac{[P]}{K_P}\right)} \quad \text{(EQ 27)}$$

where r is the rate expression, v_{max} is the maximum reaction rate, $[S]$ and $[P]$are the substrate (urea) and product (ammonium) ion concentrations, respectively. K_m is the Michaelis constant, and K_P is the inhibition term. Next, the effects of initial urease concentration were evaluated. Conclusively, they found that the reaction rate was proportional to the urease concentration; thus the specific enzyme activity remained constant and protein denaturation did not occur within this concentration range.

To evaluate the effects of pH variation, Fidaleo and Lavecchia begin with the assumptions that the product inhibition term, K_P, is negligible with respect to the overall kinetics, and that K_m and v_{max} are both parameters that are pH dependent. They adopt the Tripton and Dixon (1979) mechanism for molecular dissociation. However, over the pH range considered (pH from 4 to 9), K_m was shown to be essentially pH independent. To evaluate temperature effects, k was assumed to be only parameter acting as a function of temperature and was defined through experimental data to be as follows:

$$k(T) = exp\left[\frac{-E_a}{R}\left(\frac{1}{T} - \frac{1}{T^*}\right)\right] \quad \text{(EQ 28)}$$

where the temperature, T, is in degrees Kelvin, R is the universal gas constant at 8.314 J/(K mol), E_a is the activation energy and T^* is the temperature at which k is 1 mol/g/min. These last two values were experimentally defined to be 35.3 kJ/mol 414.6 K, respectively.

At this point, Fidaleo and Lavecchia revisit the product inhibition term. They utilize the kinetic expression developed thus far coupled with the assumption of a non-competitive inhibition mechanism to empirically determine that K_P. This varies from the case of Cirpka and Kitanidis (2001) where they implement competitive inhibition for TCE degradation.

The following expression is the final version of the rate law implemented by Fidaleo and Lavecchia. The values for each parameter are shown in table 2.

$$r = \frac{exp\left[\frac{-E_a}{R}\left(\frac{1}{T} - \frac{1}{T^*}\right)\right]\ [E]_0[S]}{(1 + \frac{[H^+]}{K_{ES,1}} + \frac{K_{ES,2}}{[H^+]})(K_m + [S])(1 + \frac{[P]}{K_P})} \quad \text{(EQ 29)}$$

Parameter	Value	Units
K	$(1.83 \pm 0.05)\ 10^{-2}$	mol g^{-1} min^{-1}
K_M	$(2.31 \pm 0.36)\ 10^{-3}$	mol/l
$K_{ES,1}$	$(7.57 \pm 0.41)\ 10^{-7}$	mol/l
$K_{ES,2}$	$(1.27 \pm 0.08)\ 10^{-8}$	mol/l
K_P	$(1.22 \pm 0.11)\ 10^{-2}$	mol/l
E_a	35.3	kJ/mol
T^*	414.6	K

Table 2: Parameters utilized by Fidaleo and Lavecchia (2003) in the overall rate expression.

The quantity of $[E]_0$ is the total enzyme concentration in g/l. This is an input concentration, and was implemented as 0.1 g/l for most of the experiments. The final rate model was subject to statistical analyses that determined the approximation to be statistically correct. This study verified that a Modified Michaelis-Menten equation with a pH dependent rate constant and a non-competitive product inhibition term has the ability well describe ureolysis kinetics within pH 4-9.

4.1.1.b Implementation

The comprehensive rate expression developed by Fidaleo and Lavecchia (2003) for urea hydrolysis is implemented within PHREEQC to replicate field experiments and provide future predictions or even recommendations. Due to the nature of PHREEQC, equation 29 developed by Fidaleo and Lavecchia is adjusted to promote computing efficiency, clarity within the code, and to properly represent kinetic ureolysis within the VZRP.

All of the experiments at the VZRP occur at approximately 25°K. This simplifies equation 28 to a constant: $k(25°C) = 1.83\text{x}10^{-2}$. Concentrations in PHREEQC need to be entered in the same units, thus the quantity of $[E]_0$ must be entered in mol/kgw. To convert the given units of g/l to mol/kgw, the molecular weight of urease is approximated at 480,000 g/mol (Tanis et al. 1968). Additionally, for dilute solutions as this, 1 liter of water is approximately 1 kg of water.

Fidaleo and Lavecchia committed a significant portion of their urease exploration to the effects of pH. Their rate expression contains the Tripton and Dixon (1979) mechanism, however, this term is not required when the rate is programmed into PHREEQC. To eliminate the need for this term, protonation and deprotonation reactions for the enzyme urease are defined within the input code. The following reactions and logK values were added to the PHREEQC input file (Spycher, 2009):

$Z^- + 2H^+ \leftrightarrow ZH_2^+$ logK = 14.017
$Z^- + H^+ \leftrightarrow ZH$ logK = 7.896
$Z^- + H^+ + NH_4^+ \leftrightarrow ZHNH_4^+$ logK = 9.81

(EQ 30, 31, 32)

For these reactions, 'ZH' is the user defined species name for urease. As PHREEQC calculates the reactive chemistry (details on PHREEQC's solution method is provided in section 3.2.4) the effects of pH on urease are automatically included per the protonation/deprotonation reactions provided above and in the thermodynamic database. This eliminates the need for the pH term in equation 29.

For computing efficiency and for clarity when reading the code, equation 29 is broken up into three different functions before being implemented within PHREEQC. The following reaction is the final version of Fidaleo and Lavecchia's kinetic rate expression as developed for use in PHREEQC:

$$r = [ZH]\, C\, f_1\, f_2 \quad \text{(EQ 33)}$$

where $[ZH]$ is implemented as the current number of moles of urease (this varies as the kinetic reaction progresses) and

$$C = 146.4\ \text{mol}_{\text{urea}}/\text{mol}_{\text{urease}}/\text{s} \quad \text{(EQ 34)}$$

$$f_1 = \frac{[Urea]}{(K_m + [Urea])} \quad \text{(EQ 35)}$$

$$f_2 = \frac{K_P}{(K_P + [NH_4^+])} \quad \text{(EQ 36)}$$

$$C = k\ \frac{480{,}000 mol_{urease}/g_{urease}}{60 sec/min} \quad \text{(EQ 37)}$$

As you can see above, C is equivalent to the product of all of the constants: $k(25°C)$ and the various unit conversions. For clarity of notation, $[S]$, the molarity of the substrate urease has been renamed $[Urea]$; similarly $[P]$, the molarity of the product ammonium has been renamed $[NH_4^+]$.

4.1.1.c Batch Verification

Within their study, Fidaleo and Lavecchia performed a batch experiment to verify their mathematical model's ability to simulate urea hydrolysis. Two different solutions were prepared at 25°C: one at pH 5 and one at pH 8. The product, ammonium, was measured over 65 minutes for each solution. The initial conditions for this experiment are shown below in table 3. To maintain appropriate pH levels, acetate and borate buffers were used for pH 5 and 8 respectively. Fidaleo and Lavecchia then used their mathematical network to predict the ammonium production over time and compared the results graphically.

Component	**pH 5**	**pH 8**
Buffer	Acetate	Borate
T	25°C	25°C
Urease	0.1 g/l	0.1 g/l
Urea	20 mmol/l	20 mmol/l

Table 3: Initial batch conditions

To verify adequate performance for this kinetic reaction as programmed in PHREEQC, the experiment was replicated with the same initial conditions. The concentration of initial buffer in solution was iteratively estimated to provide a near constant pH throughout the simulation. The graphical results are shown in figure 5 below.

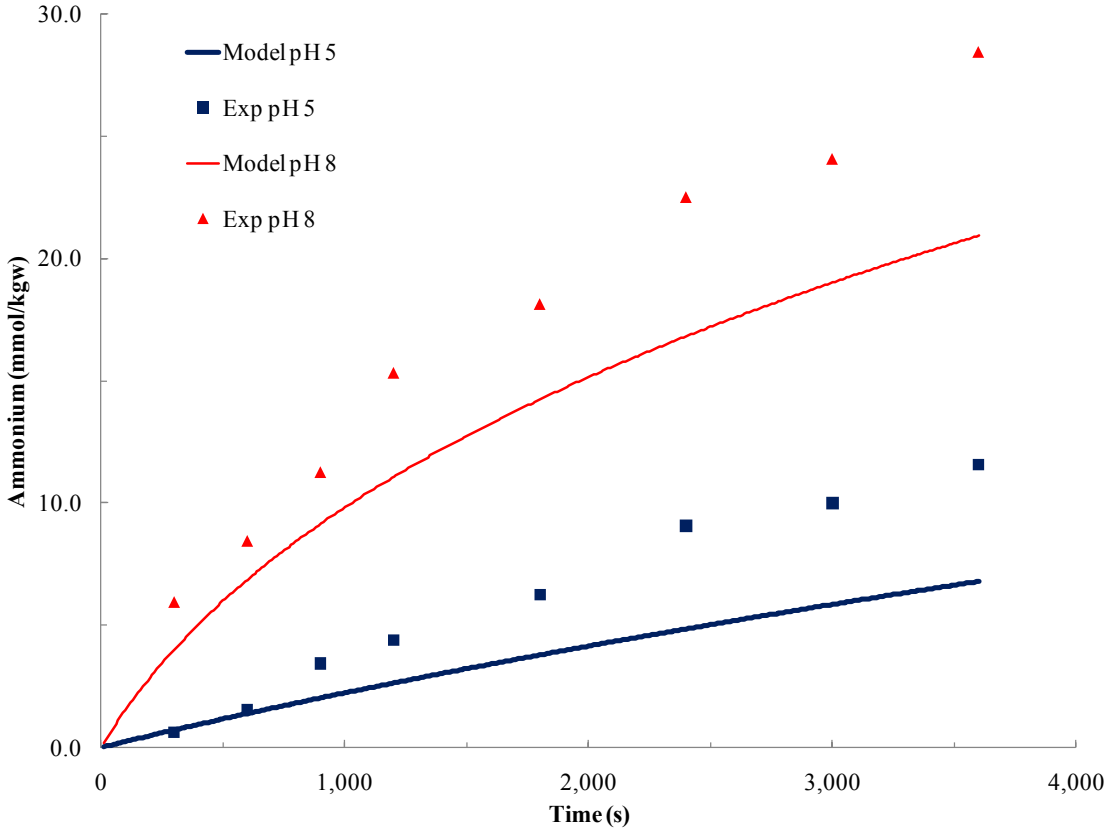

Figure 5: Model results compared to Fidaleo and Lavecchia 2003 data

As is apparent, the modeled results under predict the ammonium output, essentially under predicting the rate of ureolysis. Although beginning steps have been taken to invert the urease enzyme fictive parameter "Z," a convergent value and statistical analysis has not been reached or performed. A similar inversion problem has been explored through the use of Geochemist's Workbench to simulate work of Grant and Ferris (2006a). This problem will be addressed in Future Work (section 5.6). These parameters, although they do not provide a perfect match to the results in Fidaleo and Lavecchia, is sufficient for the VZRP application.

There are many limitations of the adaption of Fidaleo and Lavecchia's rate model as implemented in a streamtube ensemble. First, the VZRP study approximates Fidaleo and Lavecchia's urease as a measure of microbial activity. There is no urease in the experiments performed at the VZRP, simply naturally-occurring bacteria. The most appropriate value for "urease" in the VZRP system would be one evaluated from data collected directly from the site such that the value represents the bacterial activity that would actually be occurring. Additionally, "urease" cannot reflect any bacterial transport or attachment/detachment. Currently, researchers are unsure whether there is bacterial transport significant enough to effect results (Fujita, 2004). Research suggests that bacterial transport may be likely in one-dimensional column experiments. Another limitation of this application is that the parameters determined by Fidaleo and Lavecchia are specific to their batch experiments and are empirically estimated or selected by minimization of the objective function. Batched determined parameters rarely scale to

field-site applications (Martinez, 2009), in the VZRP case where chemical reactions are occurring in a highly heterogeneous perched aquifer system. Also, the treatment of urease's "enzymatic protonation" is a significant uncertainty. Approximations in the VZRP study only include three protonation speciation reactions, when in reality, many more could occur given the quantity of exchangeable protons urease includes. This assumption also infers that enzymatic protonation is only occurring at equilibrium, versus the gradual breakdown of the enzyme (Bob Smith, personal correspondence).

4.1.2 Complete System

Accurate representation the reaction network within PHREEQC2 is critical to the replication and prediction of experiments at the VZRP. Details of each section within the PHREEQC program are provided here. The entirety of a sample streamtube run can be found in the appendix.

The first step in creating a PHREEQC run is to define the master and secondary species. Many applicable master species are already defined in the chosen, but in this case urea and "urease" need to be added. The first line of the SOLUTION_MASTER_SPECIES block defines urea; "Urea" is stated twice to define the element name and the formula for the master species. The formula for the master species remains "Urea" as the relevant speciation reactions involving urea are included later. the first number after the specification of the master species (in this case 0.0) is the alkalinity contribution of the corresponding master species. the next number, 1.0, is the formula (in this case meaning 1 Urea = 1 Urea). The last number, 1., is the element weight. This is just a default value; the actual element weight of "Urea" is not actually needed. "Z," the fictive urease species, is defined similarly, but with the valence included in the definition of the master species (Z-) to link urease with protonation reactions.

The next section is the SOLUTION_SPECIES block, which defines the log K values and the relevant reactions pertaining to the previously defined master species. First, the association reaction is defined (Urea = Urea); this is an identity reaction for this particular primary master species. Next is the log K at 25degC for this association reaction, which will be 0.0. Because this code includes kinetic ureolysis, this is the only reaction for urea that needs to be defined. The urease "Z" association reaction and corresponding log K is defined similarly. The fictive protonation reactions of the urease enzyme based on the Tripton and Dixon mechanism (1979) is defined here as three separate reactions: the first is the dual protonation of the urease enzyme to create H_2Z^+ with a log K of 14.017, the second is a protonation reaction creating HZ with a log K of 7.896, the last defines the urease – ammonium relationship with a log K of 9.81.

To replicate surface complexation and exchange reactions, the EXCHANGE_MASTER_SPECIES block is needed. Here, "X" is defined as the exchange site in the same way that urea and urease "Z" were defined in the SOLUTION_MASTER_SPECIES and SOLUTION_SPECIES blocks. In the

EXCHANGE_SPECIES block, the exchange site "X" is defined a negative valence state so it can be readily utilized for cation exchange with sodium, potassium, hydrogen, ammonium, calcium, magnesium, and strontium. The relevant half-reactions and their log K and Debye-Hückel parameters (if applicable) are specified. See section 3.2.1 for a description of the gamma values and Debye-Hückel parameters. The Davies equation may also be used to calculate activity coefficients, if desired.

The next block, SOLUTION, describes the initial makeup of the aquifer. The numerical range after the SOLUTION statement defines which cells will have this composition. Each streamtube run will have every cell between the injection and extraction wells begin with these concentrations. The constituents and their concentrations (excluding urease,) the pH, and temperature are all measured values from the VZRP tracer test. Values for well 2024 are assumed to be constant between the injection well and 2024, while the measured values in 2026 are assumed to be constant between the wells. This is intuitively not what is actually occurring in the subsurface, but is a logical assumption considering the availability of data. Another option is to interpolate concentrations between the wells, however this would introduce its own set of instructions. A third option would be to use UCODE or another inversion code to invert concentrations; this method was explored for the value of urease along the length of a soil column by Barkouki (Master's Thesis, 2009). The chosen value for urease, Z, is used as an estimate for bacterial activity and has been estimated from data by Fidaleo and Lavecchia (2003). The default pe value within PHREEQC is 4.0; it is included here as a reiteration. No ion is selected for charge balance here; it is not needed as the charge balance is acceptable at the defined concentrations. The next block, EXCHANGE, defines the quantity of the exchanger in the specified solution cells. Again, this is applied to the initial conditions between the injection and extraction wells. The specified quantity of the exchanger "X" was set to 0.0005 moles to ensure an adequate amount of exchange sites. It is critical to remember that this exchange definition is the only an approximation to account for surface exchange in a system where exchange sites are in equilibrium, as specified by the previous line of code: "-equil with solution (...)".

The next block defines calcite as one of the possible equilibrium phases that can be formed and the amount with which it can react with the aqueous phase. The phase name, calcite, is followed by the target saturation index. Again this is specified for the initial conditions between the injection and extraction wells. The target saturation index initially is 0.0 (before initial composition speciation) with an initial amount of 0 moles. This amount is the maximum quantity of the mineral that *can* dissolve if the solution becomes supersaturated with calcite. Defining calcite as an equilibrium phase is a large assumption; no consideration is granted to the mechanism or rate of calcite precipitation. According to Curti (1999) and Tesoriero (1996) the rate of calcite precipitation may have a significant effect on coprecipitation. Future work (see section 5.6) will address this concern by replacing EQUILIBRIUM_PHASES with the SOLID_SOLUTIONS block, or equivalent, to represent coprecipitation with strontium. The next three commands, USE, SAVE, and END, are used to specify that solution 1 is used in the following batch reaction calculations, that the solution is saved for later calls if needed, and that the end of data input has been reached, respectively.

The injection solution defined in SOLUTION 0 is required for transport. This is the solution that represents the urea-bromide injectate. As implemented in the initial solution definition, most of these values were directly measured from the injectate utilized at the VZRP. Again, no specification for charge balance was needed and the urease concentration is the same as implemented previously.

The description of the kinetic rates begins with the next block: RATES. This block assigns a rate titled "ureolysis". This section of the code is written in Basic. "-start" begins this basic loop, followed by statements 30, 60, and 90. These lines define Km, Kp, and k as parameters that will be used in the rate equation. Statements 94 and 96 describe the mathematical fragments used in the rate equation that are combined in the final rate equation in statement 100. The amount of moles is linked with the rate and time in statement 110, the final value is saved in statement 200. The basic loop ends with "-end." The next block, KINETICS, specifies the chemical formula of the reaction taking place as well as the parameter values. The ureolysis reaction shown below is described within the KINETICS block by specification of the stoichiometric coefficients.

$$(NH_2)_2CO + 2H_2O \rightarrow 2NH_4^+ + CO_3^{2-} \quad \text{(EQ 38)}$$

The next line beginning with "-parms" specifies the values of parameters parm(1), parm(2), and parm(3) as initiated in the RATES block.

The USER_GRAPH block describes what sort of data should be written to the grid and chart graphic output within PHREEQC. Two different varieties of the USER_GRAPH are utilized in this experiment. The first is used to track the breakthroughs (concentration at the final cell over time) of the specified constituents. The second reports the quantity of calcite precipitated at each timestep along the length of the column. A description of each of the lines in the USER_GRAPH block for the first print scenario, concentration verses time, is shown below:

- -headings: The name of each series that will be recorded;
- -chart_title: The customized chart title;
- -axis_titles: The names of the axes, if there is a secondary axis it is also titled on this line;
- -axis_scale: This line is specified for each axis defined in the axis_titles line. The applicable axis is labeled (x_axis, y_axis, or secondary_y_axis in this case) followed by the minimum value for that axis, the maximum value, the major unit, and the minor unit;
- -initial_solutions false: this line specifies whether or not the initial solution calculation results will be plotted. False denotes that the initial solution will not be graphed;

- -plot_concentration_vs time: this line specifies that concentration is the dependent variable and time is the independent variable;
- -start: this signifies the beginning of the Basic program which actually executes the plotting;
- 10 GRAPH_X: This statement defines that TOTAL_TIME will be the x-values on the graph;
- 20 GRAPH_Y: This statement defines the results that will be plotted along the y-axis, in this case it is either the molality of the specified surface species (multiplied by a factor to ensure tracking of units) or the amount of moles of an equilibrium phase;
- 30 GRAPH_SY: This statement defines the y-values to be plotted on the secondary axis, here pH;
- -end: This signifies the end of the Basic program.

To plot calcite precipitation at specific timesteps along the length of the column, the following critical differences are needed instead of or in addition to the ones described above:

- -plot_concentration vs x: This critical statement ensure that the concentrations are plotted over distance, x;
- 10 GRAPH_X: This statement, as part of the Basic program, defines DIST (distance) as the independent variable.

The other key differences will occur as changes in the TRANSPORT block. The TRANSPORT block defines the one-dimensional transport processes that will occur during the simulation. The default unit setting for the TRANSPORT block is meters; the first specified aspect is the number of cells followed by the lengths. The number of the cells vary according to the desired velocities (see section 4.2.4b). The "-length" lines represent the length of each cell. If there are less length values entered than cells, PHREEQC will automatically apply the last specified length to all of the remaining cells. For this simulation, each length has been specifically calculated to achieve a desired velocity; every value will be different. Next, the number of shifts, or advective transport steps, is assigned. This is the number of times a solution will be switched into the next cell. The number of shifts for each streamtube is dependent on the number of shifts required to complete approximately one pore volume. Shifts are defined by the following relation:

$$Shifts = \frac{TT}{dt} \qquad \text{(EQ 39)}$$

where TT is the total time of injection, 230 minutes, and dt is the timestep, or the amount of time of each advection step calculated to be 1.06 minutes. This provides a total shift quantity of 217. The timestep is also specified here. The dispersivity is assumed here to be 0.002 m for every cell. This is a general case assumption chosen because of its

common occurrence as an assumption within Parkhurst (1999). The dispersivity correction is implemented is this case, as recommended for simulations wherein the final cells are defined with flux boundary conditions and when effluent composition is being monitored. The correction multiplies the final cells' dispersivity by $1 + 1/cells$ where $cells$ is the number of cells in the simulation. Note here that a diffusion coefficient is not specified. This approximation is not needed when utilizing a streamtube ensemble.

The TRANSPORT block also includes information for printing. For monitoring concentrations at the final cell, the following lines need to be defined:

- -punch: This defines which cell will be recorded, for breakthroughs this is the final cell;
- -punch_frequency: This defines the frequency of shifts that will be recorded. A value of 1 will print every shift;
- -print_cells: This defines which cells are printed to the selected output file, very similar to the "-punch" option.

For printing calcite precipitation over the length of the column, the following print and punch options within the TRANSPORT block are required:

- -print_cells: In this case, this is defined as the entire range of cells (e.g. 1-108) in order to print the moles of precipitate in every cell;
- -print_frequency: The print frequency defines which shifts are printed. Selecting the entire range will provide a set of data at every sell for each shift, as is desired for printing calcite over length.

Finally, the TRANSPORT block is completed by statement of the "END" line.
The next block of code in PHREEQC is also what happens next in the physical system. After the transport of the Urea-Bromide injectate, the injection system is terminated and the ambient water is allowed to return while extraction continues. SOLUTION 0 here represents the ambient water and matches the initial compositions measured in wells 2024 or 2026. In actuality there is no more injection, only extraction. To model this in PHREEQC, however, some sort of injection solution is required. For that purpose, the initial solution is re-implemented. This is a major assumption as it is known that the composition in the wells varies widely over time and space; this approximation assumes that the composition after 230 minutes of pumping is suddenly the same as the composition before the injection began. To simulate the transport of this extraction-only period, another TRANSPORT block is needed. For the second TRANSPORT block, only the differences between it and the first block need to be specified. In this case, only the number of shifts has changed. The number of shifts, 300, was chosen as as it represents an adequate amount of time for the extraction-only solution to equilibrate for the longest streamtube. The final PRINT block and "-reset true" line establish that eh, equilibrium phases, exchange quantities, headings, kinetics, saturation indices, species, totals, and graphs be printed to the output file. The entire program is terminated by the final END.

4.1.3 Initial Speciation

To verify that the initial solution composition programmed within PHREEQC will provide relevant and realistic results, this section of the code is tested independently. If the initial and Urea-Bromide injection solutions are speciated within PHREEQC accurately and as predicted, the entire program is ready to be implemented. Initial solution speciation is tested at each well and for the injectate solution.

4.1.3.a Initial Speciation of Well 2024

Running a batch speciation is much more simple than creating an entire run with kinetics and transport. This program begins with specification of SOLUTION 1, which is the only solution described within these runs. This solution block represents the initial composition of well 2024 as measured before the tracer test began. Unit conversions were performed using molecular weights that are established within the chosen database. The measured and model input parameters are shown below in table 4.

Table 4: Initial parameters for well 2024

	Measured	Model Input
pH	7.33	7.33
pe	4	4
temp (deg C)	18.15	18.15
units	mg/L (Sr in ug/L)	mmol/kgw
Ca	40.71	0.001015769
C	40.37	0.003361058
Sr	259.5	2.96165E-06
Cl	41.96	0.001183539
Nitri (NO2)	0	0
Amm (NH4)	0	0
Mg	11.07	0.000455462
Na	40.05	0.001742077
K	2.4	6.13837E-05
Urea	0	0
Z (Urease)	--	2.083E-07
Br	0.62	7.75931E-06
Sulfate	21.98	0.000228801
F	0.25	1.3159E-05

These values are plugged directly into SOLUTION 1, with a few exceptions. The value for Eh is assumed (see section 4.1.2) and temperature is implemented as 25 degrees C. This temperature assumption is critical; the implications of which are discussed in section 5.6. The value for urease (titled “Z” within PHREEQC) is not actually measured from

the tracer test but is an assumed number as well (see section 4.1.1). Additionally, NO_3^- is measured in the tests, but is not included at all in the PHREEQC simulations. This is because oxidation-reduction systems are decoupled in the chosen database; inclusion of NO_3^- therefore is insignificant to the modeled chemical processes.

The speciation calculation runs in PHREEQC also include the same SOLUTION_MASTER_SPECIES and SOLUTION_SPECIES as described in section 4.1.2, as well as a PHASES block to replace the EQUILIBRIUM_PHASES block discussed previously.

The initial speciation was tested to check for an appropriate charge balance and to check the saturation of calcite. The charge balance for the initial solution in well 2024 is 1.282d-5 with a percent error of 0.14%. This is highly acceptable and can be assumed that future calculations with this ensemble will converge. To further explore the charge balance, "charge" was assigned to the most dominant anion, in this case Cl, to assess whether or not forcing a charge balance with that ion would make a significant difference. As expected, this brings the percent error to 0%, but as the previous case was well within acceptable percent error, charge balance will not be specified for this initial solution. Assessing these initial speciation results to view the saturation index of calcite could provide additional outlook into the future behavior of the system. After performing the batch reaction calculations, the saturation index of calcite is -0.24. This means that the system is undersaturated with respect to calcite, and thus has potential for calcite dissolution. A discussion of these implications and further evidence of this potential can be seen in sections 5.6 and 6.0.

4.1.3.b Initial Speciation of Well 2026

The initial composition as measured in well 2026 is shown below. These values were used to calculate the model input values, also shown in table 5 below.

Table 5: Initial parameters for well 2026

	Measured	Model Input
pH	7.77	7.77
pe	4	4
temp (deg C)	18.28	18.28
units	mg/L (Sr in ug/L)	mmol/kgw
Ca	44.13	0.001101103
C	40.94	0.003408514
Sr	238.7	2.72426E-06
Cl	45.26	0.00127662
Nitri (NO2)	0	0
Amm (NH4)	0	0
Mg	12.92	0.000531578
Na	42.45	0.001846471
K	2.55	6.52202E-05
Urea	0	0
Z (Urease)	--	2.083E-07
Br	1.114	1.39417E-05
Sulfate	21.32	0.000221931
F	0.24	1.26326E-05

The electrical balance for this simulation is 1.153e-4 with a percent error of 1.16%. This is again acceptable; there is no need to specify an ion for charge balance. The saturation index for calcite is 0.25. This means the system is supersaturated with respect to calcite and calcite will precipitate.

4.1.3.c Initial Speciation of the Urea-Bromide Injectate

The injection solution containing urea and the non-reactive tracer bromide that was injected into well 2025 is described by the following composition in table 6. The measured values are included as well as the values that were input into the model.

Table 6: Initial parameters of the urea-bromide injectate

	Measured	Model Input
pH	7.75	7.75
pe	4	4
temp (deg C)	21.69	25
units	mg/L (Sr in ug/L)	mmol/kgw
Ca	38.9	0.000970607
C	44.82	0.003731548
Sr	231.3	2.63981E-06
Cl	17.72	0.000499817
Nitri (NO2)	0.02	0.000434719
Amm (NH4)	0.25	0.014679632
Mg	11.14	0.000458342
Na	30.62	0.001331895
K	76.68	0.001961211
Urea	988.29	0.016455045
Z (Urease)	--	2.083E-07
Br	144.65	0.001810297
Sulfate	18.74	0.000195074
F	0.14	7.36904E-06

The electrical balance for this simulation is -1.640e-4 with a percent error of -1.34%. This is an acceptable percent error; inclusion of a forced charge balance on an ion is not required. The saturation index for calcite is 0.21. The system is supersaturated with calcite, and will precipitate if conditions become favorable.

4.2 Streamtubes

To simulate transport, PHREEQC2 operates by performing initial solution calculations, followed by batch reaction calculations, and finally reactive transport calculations (Parkhurst and Appelo, 1999). Multiple runs with PHREEQC's 1D advective-dispersive transport system can be assembled to form a streamtube ensemble along streamlines. Streamlines are the common paths of a fluid particles (e.g., Charbeneau, 2000), and when paired with reactive chemistry they are considered streamtubes (e.g., Ginn, 2001). Deconvolution using solute flux averaging of tracer test data from experiments performed at the VZRP resulted in a travel time distribution specific to the experimental site. The ensemble was also parameterized from the tracer test analyses, thus the travel time distribution should inherently reflect regional gradients and hydraulic characteristics of the site. The arrival time distribution was binned into seven streamtubes that represent a symmetric streamline network between the wells; every streamtube possesses a unique travel time to ensure that they each contribute $1/7^{th}$ of the total flux as determined from the tracer tests.

When considering transport, a streamtube ensemble was chosen to represent well-to-well transport at the VZRP. This ensemble not only depicts the flowfield between two wells, but may also be used with varying cell lengths to simulate variable velocity within each tube.

For this application, the streamtube ensemble was generated by first conducting and analyzing a tracer test. After performing the required tracer tests, the results were analyzed to provide necessary information about general field characteristics to be used in the modeling process. Tracer tests are primarily used to calculate breakthrough times, or the time it takes for a specific mass (tracer) to travel from one well (input) to another (output). After an overall travel time is obtained for each streamtube, the length of each streamtube is determined by associating each binned travel time with a streamtube length corresponding to the potential theory-based representation of the transport field according to Figure 3. Finally, each streamtube is divided into cells of an appropriate length to simulate variable velocity within the streamline.

Creation of the streamtube ensemble usually includes the most direct path between the wells, a straight line, as this is the simplest streamtube. The other streamtubes branch out from one well and reach back to the others along a circular arc. Figure 6 below depicts idealized streamlines in the present case ensemble. For this application, seven streamlines are chosen. These represent a symmetric streamline network between the wells. To determine the travel time along each path, the tracer test deconvolution is utilized. The mass flux that the output well received from the tracer test is balanced so that the flux in each streamtube would be $1/7^{th}$ of the total mass flux

4.2.1 Mathematical Background of Streamline Designation

Luo and Kitanidis (2004) provides an analytical solution for the fluid residence time in an injection-extraction well pair, or doublet. They explore the solutions in a variety of flow fields; for the VZRP a well doublet in the absence of regional flow is most applicable. In this case, Luo and Kitanidis (2004) present an analytical solution for all streamlines. They utilize complex potential theory to determine streamlines and equipotential lines. The equipotential lines are represented by Φ. By definition, the gradient of the potential field provides the aquifer flux:

$$\tilde{U} = -\nabla\Phi \qquad \text{(EQ 40)}$$

where $\tilde{U}$ is the aquifer flux (defined as the product of Darcy velocity and aquifer thickness) (Charbeneau, 2000). Lines of a constant potential value are termed equipotential lines. The common path of a flowing particle is a streamline. Streamlines are described by the stream function, Ψ. The function, $\Psi(x,y)$, is constant along a flow line (Charbeneau, 2000). The discharge passing between two flow lines is equal to the difference in their stream function values. The stream function and potential function are considered conjugate functions; streamlines and potential lines are orthogonal.

Theoretically, a well doublet in the absence of regional flow is a symmetric system as shown below in figure 6.

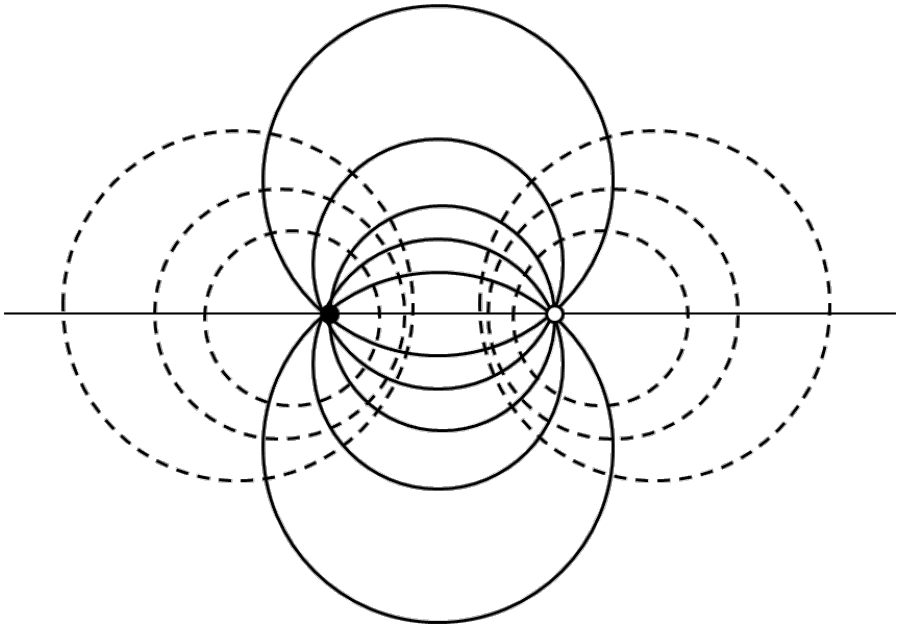

Figure 6: Streamlines (solid) and equipotential lines (dashed) between and injection well (dark circle) and extraction well (white circle). The horizontal line corresponds to Ψ = 0.

Charbeneau defines the potential function for the pair of wells as:

$$\Phi = \Phi_0 + \frac{Q}{2\pi}\ln(r_2) - \frac{Q}{2\pi}\ln(r_1) \quad \text{(EQ 41)}$$

where $\Phi_0$is a constant that determines the elevation of the potential surface, Q is the injection/extraction rare, r_2 is the distance from the extraction well, and r_1 is the distance from the injection well. As the distance between the wells (L) approaches 0 and if the following relationship in equation 42 is defined, equation 43 results (Charbeneau, 2000).

$$2L\left(\frac{Q}{2\pi}\right) = \lambda \quad \text{(EQ 42)}$$

$$\Phi = \Phi_0 + \frac{\lambda x}{x^2+y^2} \quad \text{(EQ 43)}$$

Here λ is a constant representing the dimensionless pumping rate, and x and y are Cartesian coordinates with each well along the x-axis and the origin at the midpoint between the wells. Similarly, the stream function can be defined as follows (Charbeneau, 2000):

$$\Psi = \Psi_0 - \frac{\lambda y}{x^2+y^2} \quad \text{(EQ 44)}$$

Luo and Kitanidis (2004) use a similar approach, but eliminate the need for a λ, Φ_0, or Ψ_0. The potential function is described with

$$[x + d\coth\left(\frac{2\pi\Phi}{Q_w}\right)]^2 + y^2 = \frac{d^2}{\sinh^2(\frac{2\pi\Phi}{Q_w})}\ if\ \Phi \neq 0$$
$$x = 0\ if\ \Phi = 0$$

(EQ 45)

and the stream function is described with

$$x^2 + [y - d\cot\left(\frac{2\pi\Psi}{Q_w}\right)]^2 = \frac{d^2}{\sin^2(\frac{2\pi\Psi}{Q_w})}\ if\ \Psi \neq 0, \pm\frac{Q_w}{2}$$
$$y = 0, x > d, x < -d\ if\ \Psi = 0$$
$$y = 0, d > x > -d\ if\ \Psi = \pm\frac{Q_w}{2}$$

(EQ 46)

where d is the distance between one well and the origin. For ease of calculation, Luo and Kitanidis (2004) opt to convert to radial coordinates via the following relationships:

$$x = x_c + r\cos(\beta) \quad \text{(EQ 47)}$$

$$y = y_c + r\sin(\beta) \quad \text{(EQ 48)}$$

where β is the angle beginning at the x-axis from one of the wells to the center of the streamline "circle. Figure 7 below depicts the naming convention for a generic streamline that is used in Luo and Kitanidis (2004) and amended for use in the VZRP application.

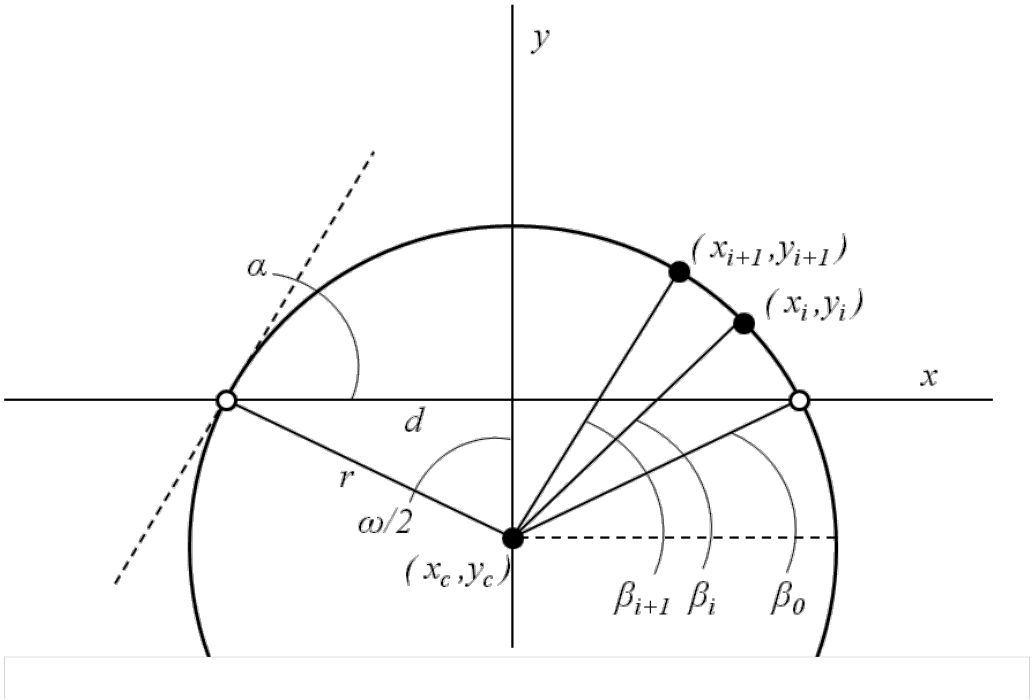

Figure 7: Definition of terms for a generic streamtube with the white circles representing the wells.

Luo and Kitanidis (2004) determine that the magnitude of the seepage velocity is only a function of y considering the above convention for each streamtube. They derive the travel time along a streamline between (x_1,y_1) and (x_2,y_2) as:

$$t = \int_{\beta_1}^{\beta_2} \frac{r|d\beta|}{|v|} = \frac{2\pi nbr^2}{Q_w d}[y_c|\Delta\beta| + (x_2 - x_1)] \quad \text{(EQ 49)}$$

where $\Delta\beta$ corresponds to the angle of the segment between (x_1,y_1) and (x_2,y_2).

4.2.2 Mathematical Background of Streamline Velocity

The velocity between an injection/extraction well pair has been defined in Luo and Kitanidis (2004). They also provide a function for travel time along a streamline between two points (x_1, y_1) and (x_2, y_2) as shown below:

$$t = \frac{2\pi nbr_s^2}{Q_w d}[y_c|\Delta\beta| + (x_2 - x_1)] \quad \text{(EQ 50)}$$

where t is the travel time (for this application it is not the overall travel time, but the predetermined time spent in each cell); n is effective porosity, b is aquifer thickness, r_s is the radius of the streamline circle, Q_w is the pumping rate, d is the distance between one well and the centerline between the wells, y_c is the y coordinate of the center of the

streamline circle, and Δβ is the streamline arc angle corresponding to the segment between (x_1, y_1) and (x_2, y_2) (Luo and Kitanidis, 2004). Reference to figure 7 may be helpful. In this case, the porosity and aquifer thickness are unknown or estimated with little confidence. This quantity is adjusted to equal a constant that is easily as the desired velocity is already known. The velocity curve specified by Luo and Kitanidis (2004) in Cartesian coordinates is shown below:

$$v(x,y) = \frac{-Q}{4\pi}\left[\frac{2(x-L)}{(x-L)^2+y^2} - \frac{2(x+L)}{(x+L)^2+y^2}\right] \quad \text{(EQ 51)}$$

where Q is injection/extraction rate, x and y are the coordinates along the streamline, and L is the distance between the wells. Figure 8 depicts this velocity function along the x-axis, or the first streamtube. Figure 9 is a three-dimensional representation of the velocity field for the VZRP as a two-well system with the same injection and extraction rates.

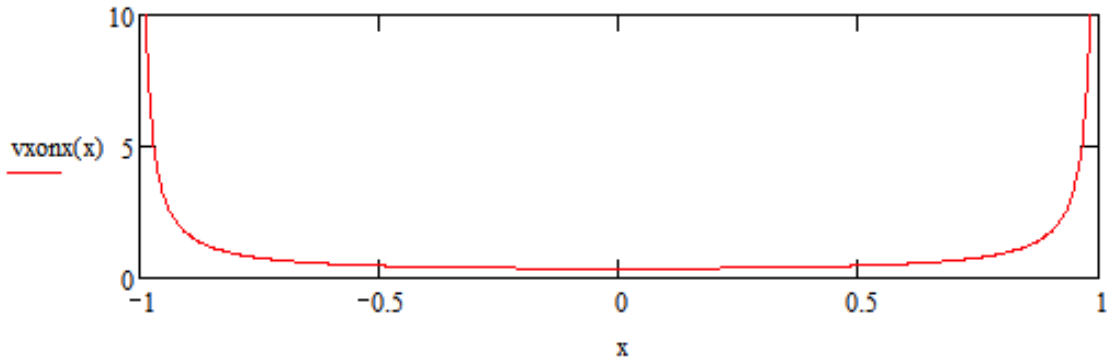

Figure 8: Velocity profile along the x-axis

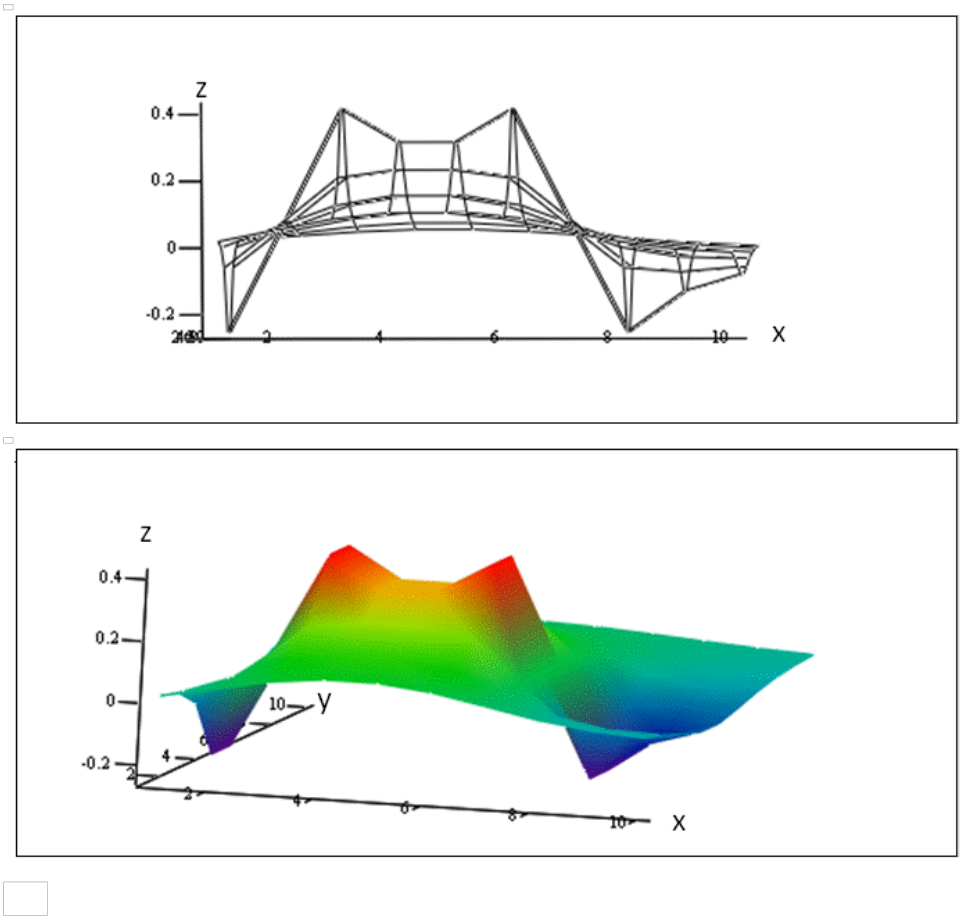

Figure 9: 3D velocity field. Top: Wire mesh looking along the y-axis. Bottom: Contour plot with all three axes

These fundamental equations are manipulated within MathCAD to develop varying lengths of cells that coincide with the expected velocity at that position along the streamline. Development of the cell lengths is described in section 4.2.4b.

4.2.3 Deconvolution

When the flow system is heterogeneous, highly complex, or unknown, as is the case for the VZRP, the residence time distribution theory may be utilized. This theory relates tracer migration between sources and sinks such that subsurface transport can be classified (Charbeneau, 2000). This method will not describe the actual location of the constituents, only the arrival time (Ginn, 2001). Tracer tests can be utilized as a way to observe effluent concentrations; these concentrations represent a distribution of travel times, or a residence time distribution function (Charbeneau, 2000).

For solute flux averaging of a breakthrough curve, the mass flux in the output well can be described by:

$$C_{out}(\tau) = \frac{1}{\sum_i Q_i} \sum_i Q_i \, C_{out,i}(\tau) \quad \text{(EQ 52)}$$

where τ is the travel time, i refers to a particle streamtube within the ensemble, $C_{out}(\tau)$ is the total concentration observed in the extraction well, and Q_i is the flow per streamtube i (Ginn, 2001). The residence time density function, (or probability density function, PDF) is the fraction of flux with the travel time τ, and is defined as (Ginn, 2001):

$$E(\tau) = \frac{C(\tau)}{\int_0^\infty C(\tau) d\tau} \quad \text{(EQ 53)}$$

and the solute flux average can be alternately defined as (Ginn, 2001):

$$C_{out}(\tau) = \int_0^\infty C(t, \tau) E(\tau) d\tau \quad \text{(EQ 54)}$$

The form of the PDF will vary depending on the type of injection scheme. For the VZRP, an inverse-Gaussian distribution is used (see section 4.2.3b). The relationship between the PDF and the fractional breakthrough curve is as follows (Ginn et al., 1995; Charbeneau, 2000):

$$F(\tau) = \int_0^\tau E(\tau) d\tau \quad \text{(EQ 55)}$$

This is also known as a cumulative density function, or CDF. This represents the fraction of mass that has arrived at the extraction well by the specific time. For a passive tracer injected as a pulse over a time, Δt, the observed concentration can be described by:

$$C_{out}(t) = C_0[F(t) - F(t - \Delta t)] \quad \text{(EQ 56)}$$

Note that equation 56 is in terms of t which represents time elapsed, not travel time. This equation results from solution of the advection transport equation by the Method of Characteristics (Ginn, 2009b; Charbeneau, 2000).

This deconvolution method is applied to the tracer tests performed at the VZRP. The output from the CDF is divided into 7 equal percents (for 7 streamtubes) with each percent segment corresponding to a specific travel time. A detailed description of this analysis is provided in the following sections.

4.2.3.a Tracer Tests

The tracer test at the VZRP was conducted as described in section 2.1.1. An injection solution containing urea and potassium-bromide was injected into well 2025 for 230 minutes at 2 gpm. Extraction occurred in wells 2024 and 2026 at 1.25 gpm each. Figure 10 below depicts the fractional breakthrough curves at both wells.

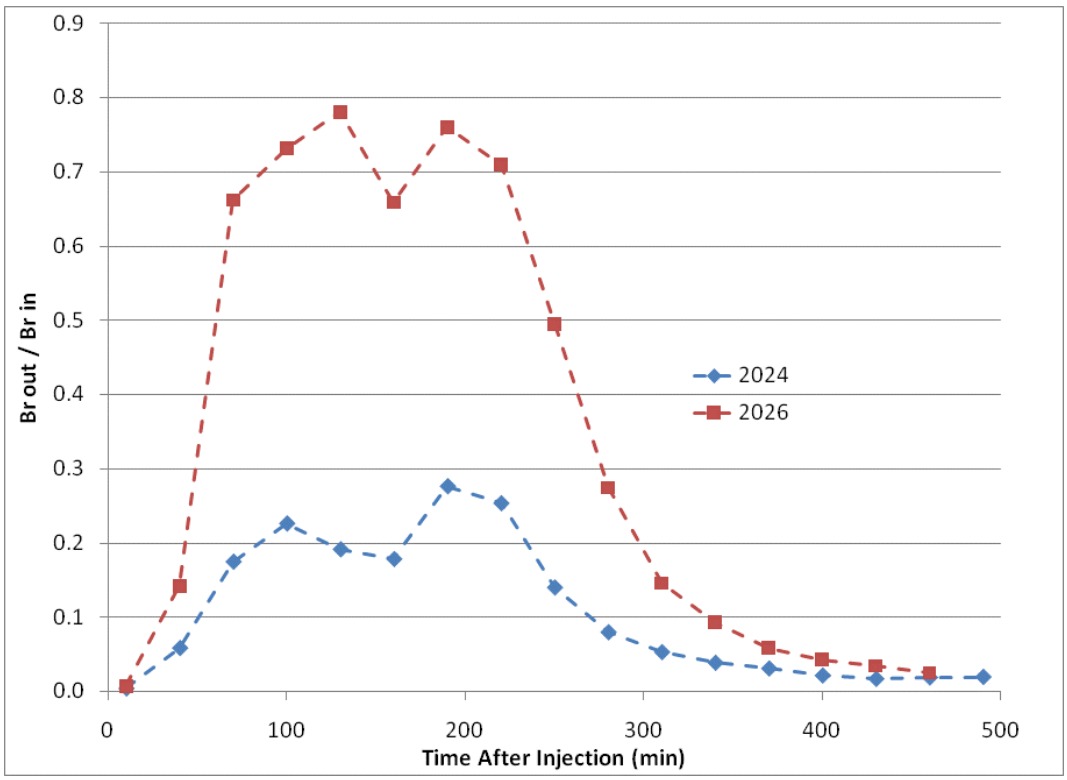

Figure 10: Fractional bromide breakthrough curves

The next step in finding streamtube travel times is to assign a PDF curve to the tracer tests. For this particular injection scheme, an Inverse Gaussian distribution was shown to provide an adequate fit at the front of the breakthrough curve.

4.2.3.b Inverse Gaussian

The Inverse Gaussian Distribution is a useful tool in many fields. The Inverse Gaussian Distribution has been used to describe Brownian Motion, as a reproduction function for a biological population, analysis of hydrologic data, stock market behavior, or for groundwater age. The Inverse Gaussian equation that follows is the density function for μ when λ is greater than 0 (Seshadri, 1993).

$$pdfc(\tau) = \left(\frac{\lambda}{2\pi\tau^3}\right)^{\frac{1}{2}} \exp\left(\frac{-\lambda(\tau-\mu)^2}{2\mu^2\tau}\right) \quad \text{(EQ 57)}$$

Alternatively, this function can be written as the following

$$pdfc(\tau) = \left(\frac{\mu^3}{2\pi\tau^3\sigma^2}\right)^{\frac{1}{2}} \exp\left(-\mu\frac{(\tau-\mu)^2}{2\sigma^2\tau}\right) \quad \text{(EQ 58)}$$

To convert between the two equations, the following transformation can be applied to Equation 58:

$$\sigma = \left(\frac{\mu^3}{\lambda}\right)^{\frac{1}{2}}$$

(EQ 59)

The format of equation 57 is preferable as it includes the common statistical values μ as a mean and λ as a shape parameter.

4.2.4 Implementation

The implementation of potential theory outlined in section 4.2.1, the results from the bromide tracer test in section 4.2.3a and their respective fit with the Inverse Gaussian Distribution are all described herein. The mathematics were programmed in MathCAD, as well as the graphics.

4.2.4.a Travel Times and Number of Cells

To determine the travel times for each streamtube, the following actions are implemented:

1. Fit the tracer test to a distribution, in this case an Inverse Gaussian
2. Convert distribution to a PDF
3. Convert PDF to a CDF
4. Divide the CDF into "n" equal percentages for "n" streamtubes of equal flux
5. Assign the arrival time for the midpoint of each "n" percentage as the travel time for that streamtube.

This concept is described graphically in image 11:

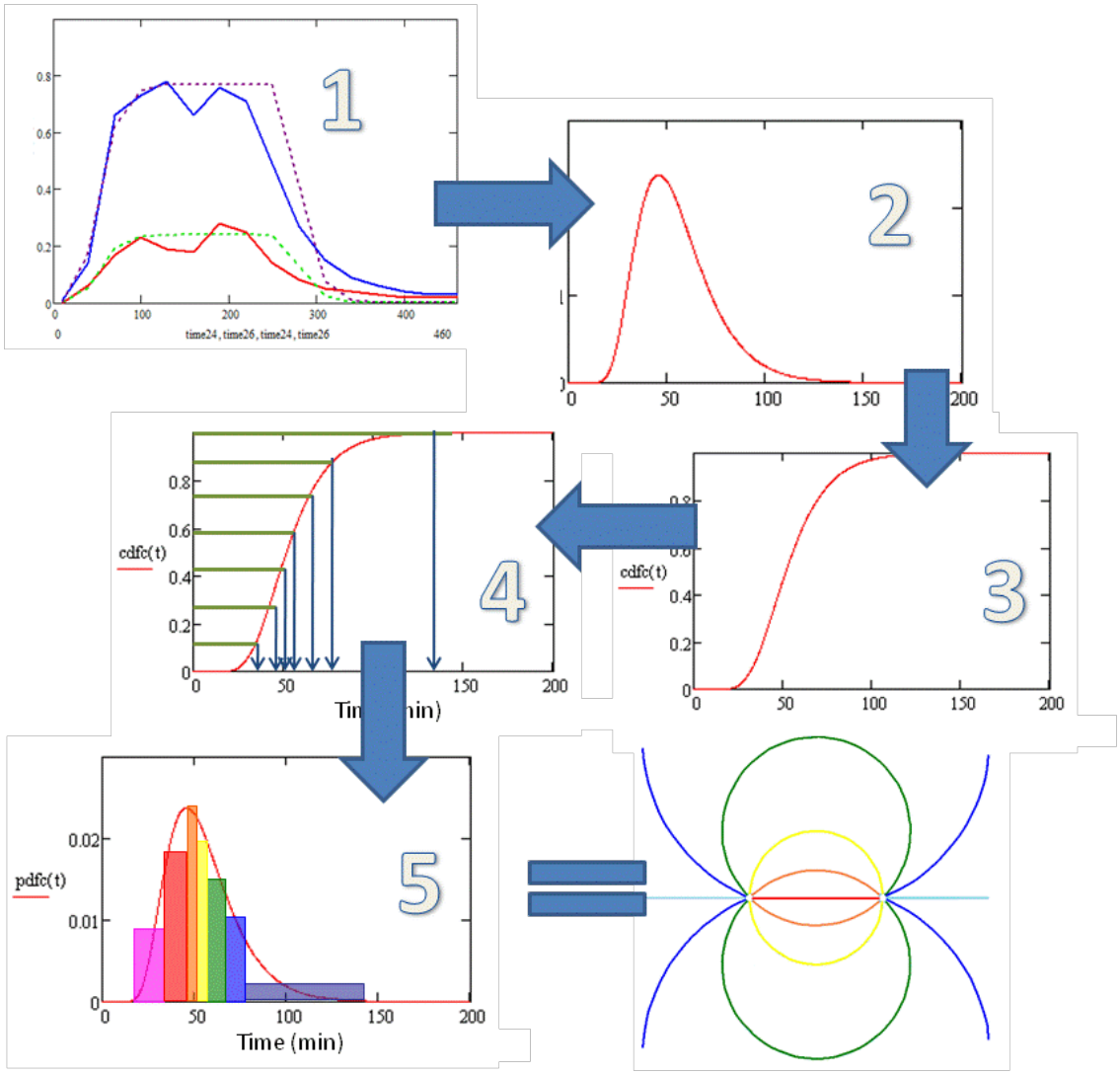

Figure 11: Graphic image of the 5 steps to obtain travel times for a tracer test

Utilizing the results from the bromide tracer test from figure 10, an Inverse Gaussian Distribution PDF is fit to match the front of the breakthrough curve. The resulting match is shown below in figure 12:

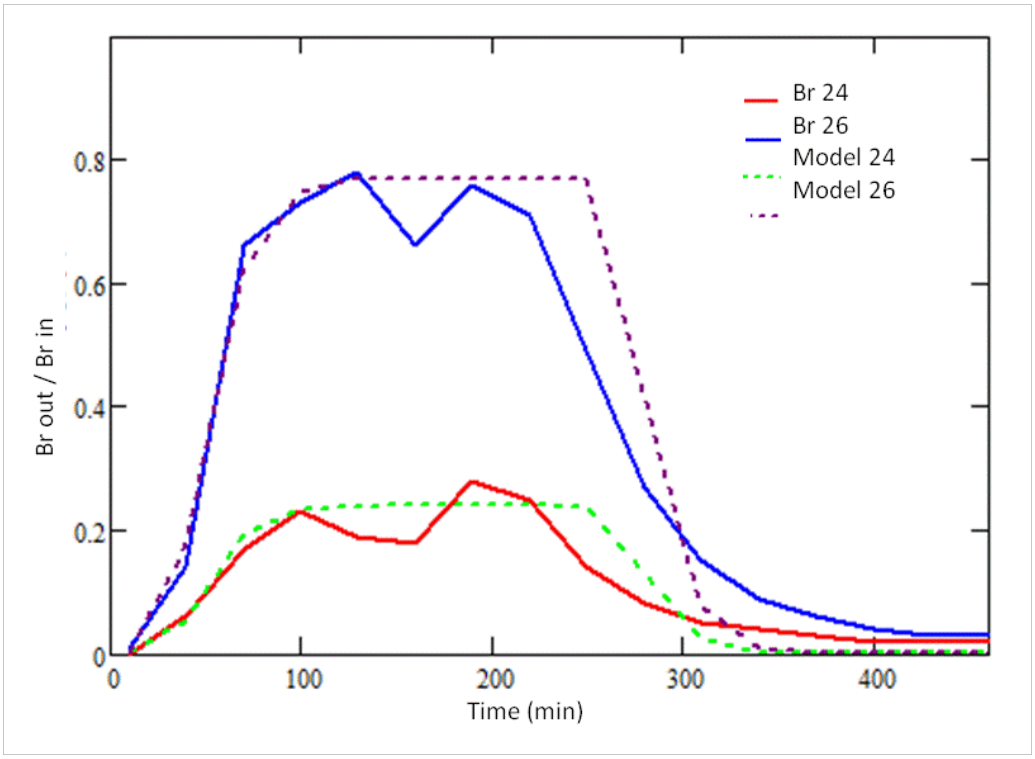

Figure 12: Breakthrough curves and corresponding Inverse Gaussian Distributions fits

The formulation for this Inverse Gaussian is that of equation 57, with $\lambda = 450$ and $\mu = 55$. The PDF in equation 57 is shown below in figure 13.

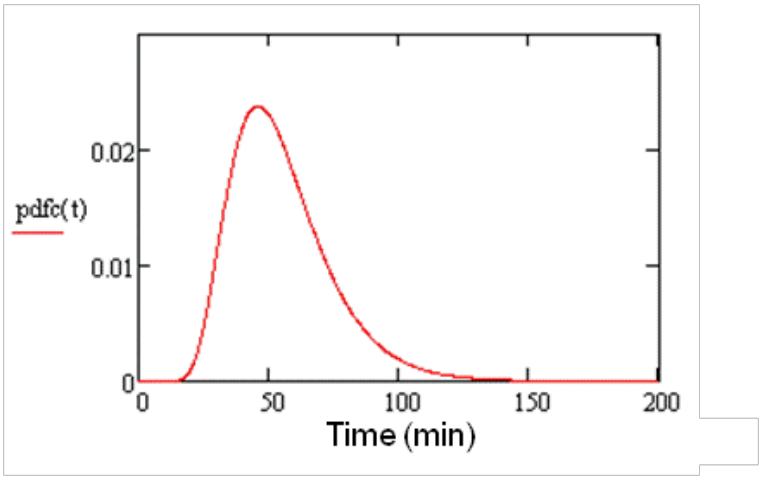

Figure 13: Inverse Gaussian Distribution PDF

The PDF is converted to a CDF by integration and is shown in figure 14:

$$cdfc(t) = \int_0^{\tau} pdfc(t)dt$$

(EQ 60)

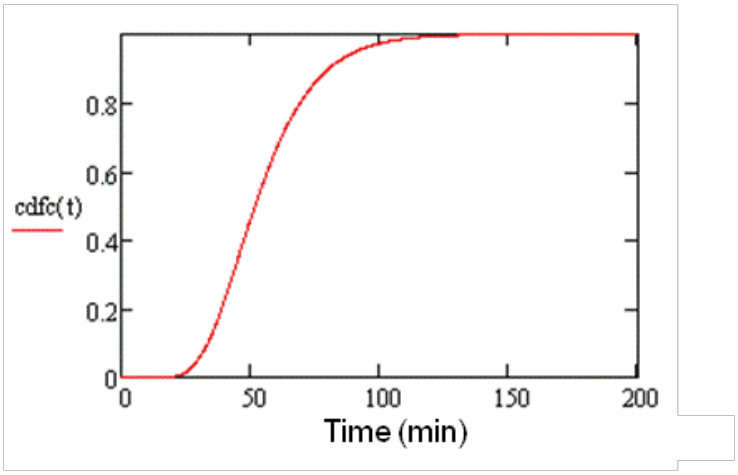

Figure 14: CDF curve derived from an Inverse Gaussian Distribution

The CDF curve represents the total percentage of mass that has arrived at each time. In MathCAD, the actual CDF is defined by the following statement:

$$cdf(t) = \begin{cases} 0 \; if \; \tau < \tau_0 \\ cdfc(t) if \; \tau \geq \tau_0 \end{cases} \quad \text{(EQ 61)}$$

where τ_0 in this case is 0 minutes. As per equation 61, the discharge concentration is defined within MathCAD as follows:

$$C_{out,w}(t) = k_w \begin{cases} cdf(t) if \; t < \Delta t \\ cdf(t) - cdf(t - \Delta t) if \; t \geq \Delta t \end{cases} \quad \text{(EQ 62)}$$

where the subscript w implies that it represents either well 2024 or 2026, k_w is the factor to account for loss in recovery (matched by visual inspection, 0.77 for well 2026 and 0.24 for well 2024), and Δt is the injection time (230 minutes). It is equation 62 that generates the curve that is fit to the breakthrough curves in figure 12.

Once the correct output concentration function has been obtained, the CDF is again brought to the forefront. The CDF is divided into seven equal percents, or chunks; one chunk for each streamtube. For each of those percent values (which are on the y-axis) the corresponding x-value is found. Because the highest percent is 100%, it provides an unrealistic x-value in terms of what would be observed in the field. An x-value of 154.461 minutes is chosen as it provides 100% within the desired degree of accuracy. The travel times of a streamtube should correspond to the average of the mass flux's arrival; the numbers at this point in the calculation correspond to the end of each chunk's arrival. The average time is found between the initial and last arrivals of each chunk; these are the travel times for each streamtube. The travel times and corresponding percent-chunks-turned-sreamtube that have arrived at that time are shown in table 7. The next step is to determine the number of cells in each streamtube that is required to achieve the maintain the overall travel time. The first streamtube is chosen to begin with

17 cells. This number is selected so as to maintain the Representative Elementary Volume (REV) for this cell and all following (Charbeneau, 2000). The timestep for each cell length (for transport calculations) can now be easily calculated as follows:

$$dt = \frac{\tau}{N} \quad \text{(EQ 63)}$$

where dt is the timestep per cell, τ is the travel time for this streamtube (18.011 minutes) and N is 17, the number of cells. This results in a timestep of 1.059 minutes. For the variable velocity calculations discussed in section 5.4 the timestep will remain constant for every single cell in the simulation while the length of the cell will change to accommodate changes in velocity. This timestep is now used to calculate the number of cells in all of the following columns. Error is introduced in this step, however, as the number of cells must be an integer. As a check, once an integer is selected, the travel time is back-calculated to verify that it is not unreasonably different from the originally selected travel time of 1.059 seconds. Table 7 includes the important streamtube parameters calculated herein: travel time and number of cells.

Table 7: Streamtube parameters (travel time in minutes)

Streamtube	Travel Time	Number of Cells
1	18.011	17
2	39.363	37
3	45.725	43
4	51.961	49
5	59.098	56
6	68.931	65
7	114.652	108

Traditional streamtube ensemble methods ordinarily stop at this step. For this study, however, a variable velocity ensemble is predicted to provide a more accurate representation of the reactive transport.

4.2.4.b Variable Velocity within Tube

In the field, the velocity between and injection and extraction well is not constant. It is very fast at the input well, gradually slows as it approaches the midpoint between the wells, and finally speeds up as it is exiting. This velocity variability can be of significance if kinetic reactions are velocity dependent or if they impact physical characteristics, as does ureolytic calcite precipitation. To replicate non-uniform velocity, a non-uniform spatial discretization is implemented that honors the travel times as specified from the tracer tests. To preserve travel times along each streamtube, the streamtubes must maintain the same average velocity as would be expected for that streamline in the field. Each streamtube is separated into a specified number of cells (formulation discussed in section 4.2.4); average velocities within the streamtube can be

determined by varying the length of each cell while keeping the time spent within each cell constant. The travel time for that streamtube is equal to the summation of the time spent in each cell; similarly, the summation of each cell's length must equal the actual length of the streamtube. PHREEQC2 processes advective transport using a SHIFT operator. This is equivalent to a direct shift of matter (mass, water, chemical solutions, etc.) that move from one cell to another. The use of PHREEQC2's transport function is convenient because it treats each increment as a shift, and holds no requirement for mass balance within shifts. The mass balance constraint will be met overall, however, as long as total travel times are honored. An evaluation of the differences between a constant velocity ensemble and a variable velocity ensemble is included in section 5.4.

As described in equation 51, the velocity between two wells is shown below (reprinted here for convenience):

$$v(x,y) = \frac{-Q}{4\pi}\left[\frac{2(x-L)}{(x-L)^2+y^2} - \frac{2(x+L)}{(x+L)^2+y^2}\right] \quad \text{(EQ 64)}$$

Additionally, the travel time along a streamline between two points (x_1, y_1) and (x_2, y_2) as shown below (reprinted for convenience):

$$t = \frac{2\pi n b r_s^2}{Q_w d}\left[y_c|\Delta\beta| + (x_2 - x_1)\right] \quad \text{(EQ 65)}$$

To solve for the length of each cell, and thus velocity along the streamline, t is known while $\Delta\beta$ and x_2 are unknown yet dependent via the relationship:

$$x_2 = r_s \cos(\beta_2) \quad \text{(EQ 66)}$$

where β_2 is the polar angle at x_2. Equation 65 must be solved for a new β_2 for every cell, thus providing the desired lengths for each cell within a specific streamtube. The first step is to establish which streamtube we are working with. For mathematical ease and for adherence to an idealized ensemble, streamtubes are chosen to be evenly spaced; their origin at the well is π/7 from the next streamtube. This is the angle between the x-axis and the tangent of the streamline at the well is considered α. The next step is to determine β_1 which is an inherent quantity in $\Delta\beta$. This is the angle from the center of the stream function circle to the point where the streamline intersects the radius of the well. It is critical to note that this intersection point is not actually along the x-axis; that would denote the center of the well, a difference in distance of 0.25 feet.
To calculate the length of the first cell, MathCAD implements a root solver to solve the following equation for β_2:

$$dt = \int_{\beta_1}^{\beta_2} \frac{r}{v(\beta)} d\beta$$

(EQ 67)

where dt, β_2, β_1, and r are all previously defined. The velocity as a function of β is described below:

$$v(\beta) = \frac{Qd}{2\pi nbr(r\sin(\beta) + y_c)}$$

(EQ 68)

The angle that results from this solver is plugged back into $\Delta\beta$ to determine the length of the arc segment corresponding to that angle.

It is important to note here that to utilize MathCAD's root solver, a guess value needs to be supplied. Checking that the roots provided are the roots applicable to the system at hand is a worthwhile exercise. Figure 15 below depicts equation 68.

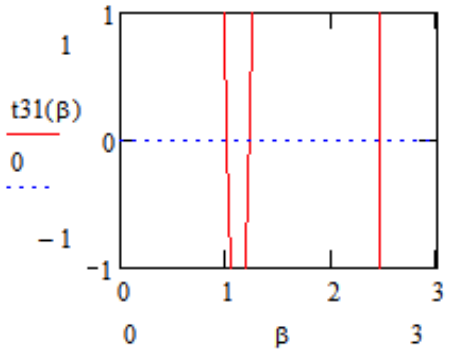

Figure 15: Multiple roots of equation 68

As is evident, there are three roots within a small range. For this calculation, the upper and lower roots can be eliminated as they are not feasible given the physical constraints of our system.

This calculation pattern is iterated with a loop in MathCAD. It automatically calculates and records the appropriate length of each segment along the velocity curve. The cell lengths and values of the velocity for each cell are shown in table 8 below. This is for the first streamtube as an example. Note that the velocities symmetric; they are larger at the end cells and smaller in the middle. The Total and Actual values are calculated as a check: the total length matches the measured length, and the velocity is the overall velocity determined by the total length over the travel time.

Table 8: Cell lengths and velocities for the first streamtube

Cell Number	Cell Length (ft)	Velocity (ft/min)
1	0.29598	0.27949
2	0.19870	0.18763
3	0.16623	0.15697
4	0.14912	0.14081
5	0.13875	0.13102
6	0.13214	0.12478
7	0.12802	0.12089
8	0.12574	0.11874
9	0.12501	0.11805
10	0.12574	0.11874
11	0.12802	0.12089
12	0.13214	0.12478
13	0.13875	0.13102
14	0.14912	0.14081
15	0.16623	0.15697
16	0.19870	0.18763
17	0.29598	0.27949
Total	2.79439	0.15522
Actual	2.79439	0.15515

These lengths are applied directly to the transport block of PHREEQC2. PHREEQC2 is run once for every streamtube; the results for all seven runs simulate the reactive transport processes that exist in the subsurface of the VZRP.

An alternate method for developing cell lengths is to utilize the particle tracking programs, such as Pumpit (AquaLogic, Berkeley, CA, 1995). Application of the tracer test data in Pumpit will provide particle locations over time that can be used to develop a customized velocity function that reflects specific site characteristics that may not be captured with a classical mathematical model.

5. Results and Discussion

To verify that the streamtube ensemble and reaction network are properly functioning and are capable of predicting future events, a variety of steps can be taken. First, a kinetic rate is calculated based on the experimental data and is followed by the same calculation performed for the model. To determine the effect of varying numbers of streamtubes, a sensitivity exercise is performed that evaluates the system with 1 and with 17 streamtubes. Next, the bromide tracer tests are compared with the model results. If these tests are sufficient, the model can be used to replicate other sets of known data or to predict future experimental behavior.

5.1 Kinetic rate verification

The kinetic rate is calculated based on the experimental data and on the model data. To calculate this rate, the well system is treated as a Continuously Stirred Tank Reactor (CSTR). For this approximation to apply, we assume that we are working with a well mixed, steady state system (accumulation, dN/dt = 0). The mass balance on a CSTR is

In – Out +/- Reactions = Accumulation (EQ 69)

Algebraically this is defined as:

$$F_{in} - F_{out} + rV = dN/dt \quad \text{(EQ 70)}$$

where F is a flow rate in or out and is defined as:

$$F = vC \quad \text{(EQ 71)}$$

Here, v is the volumetric flow rate and C is a concentration. The term dN/dt is equal to zero for steady state systems. Rearranging terms provides the following:

$$\frac{v_{in}C_{in} - v_{out}C_{out}}{V} = -r \quad \text{(EQ 72)}$$

The reaction term r can be rewritten as kC. A new term in this calculation, τ, is the average time spent in the volume of the reactor and is defined as:

$$\tau = V/v \quad \text{(EQ 73)}$$

In general terms, the equation can now be written as:

$$\frac{C_{in} - C_{out}}{\tau} = -kC_{in} \quad \text{(EQ 74)}$$

To evaluate this equation in terms of VZRP chemistry, the concentrations are written as a fraction of observed bromide. This mitigates any unknown transport effects that may have occurred throughout the well-to-well zone.

$$\frac{\frac{[Urea]_{in}}{[Br]_{in}} - \left(\frac{[Urea]_{in}}{[Br]_{in}} - \frac{[NH4]_{ss}}{2[Br]_{ss}}\right)}{\tau} = -k\frac{[Urea]_{in}}{[Br]_{in}} \quad \text{(EQ 75)}$$

The previous equation can be further simplified to:

$$\frac{\frac{[NH4]_{ss}}{2[Br]_{ss}}}{\tau} = -k\frac{[Urea]_{in}}{[Br]_{in}} \quad \text{(EQ 76)}$$

This calculation was performed by Bob Smith (Taylor, 2008) for the experimental results. Well 2024 exhibited a kinetic rate of k = 0.034/day; well 2026 was calculated to as k = 0.032/day.

The model rates were determined with the following values:

Table 9: Parameter values for kinetic rate calculations

	2024	**2026**
$[Urea]_{in}$	16.46 mM	16.46 mM
$[Br]_{in}$	1.81 mM	1.81 mM
$[NH4]_{ss}$	0.315 mM	1.01 mM
$[Br]_{ss}$	0.434 mM	1.39 mM
τ	75 minutes	75 minutes

Substituting these values into the final equation, the modeled reaction rate for well 2024 is 0.766/day; for well 2026 the rate is 0.767/day. These results should be similar, the only difference between the two in the model is initial calculations, and that difference is not significant.

The modeled rates are much greater than the experimental rates. Evaluation of the breakthrough curves (see next section) will not only support this claim, but provide further evidence that ureolysis is not happening, or is occurring at a very small scale, within the field.

5.2 Number of streamtubes

In section 4.2.4a, the CDF is divided into seven equal parts, each representing a streamtube. The number of streamtubes is a parameter that can be chosen to affect the degree of mixing (Luo, 2008). To establish that seven streamtubes is an appropriate selection to match tracer test data, the simulation is run with only one streamtube and also

with 17 streamtubes. The process to create the streamtubes (travel time, timesteps, and length segments) is the same as discussed in section 4.2.3. This evaluation was only compared to the results of 2024, assuming the behavior and trends will be the same for well 2026.

For the single streamtube simulation, the direct path streamtube is utilized with a length of 2.794 feet. Again, 17 cells are used. This provides a timestep of 4.543 minutes with a total travel time of 77.231 minutes. The cell lengths and velocities for the single streamtube follow in table 10. The cell lengths are the same as found in the first straight path streamtube of the 7 and 17 tube simulations, however the velocity in each cell will be different to reflect an overall travel time of 100% of the mass.

Table 10: Cell lengths and velocities for the single streamtube simulation

Cell Number	Cell Length (ft)	Velocity (ft/min)
1	0.29598	0.06515
2	0.19870	0.04374
3	0.16623	0.03659
4	0.14912	0.03282
5	0.13875	0.03054
6	0.13214	0.02909
7	0.12802	0.02818
8	0.12574	0.02768
9	0.12501	0.02752
10	0.12574	0.02768
11	0.12802	0.02818
12	0.13214	0.02909
13	0.13875	0.03054
14	0.14912	0.03282
15	0.16623	0.03659
16	0.19870	0.04374
17	0.29598	0.06515
Total	2.79439	0.03618
Actual	2.79439	0.03618

Travel times and numbers of cells per streamtube for the 17 steamtube simulation are shown in table 11 below. The timestep used for the simulation of each streamtube is 0.898 minutes. Tables of each streamtube cell length and corresponding cell velocity can be found in the appendix.

Table 11: Streamtube travel times and cell quantities for the 17-tube ensemble

Streamtube	Travel Time	Number of Cells
1	15.26	17
2	32.564	36
3	36.177	40
4	39.123	44
5	41.782	47
6	44.308	49
7	46.79	52
8	49.294	55
9	51.876	58
10	54.597	61
11	57.53	64
12	60.775	68
13	64.486	72
14	68.93	77
15	74.662	83
16	83.258	93
17	121.516	135

The urea breakthrough curves for the single streamtube, seven streamtube, and seventeen streamtube ensembles are shown in figure 16.

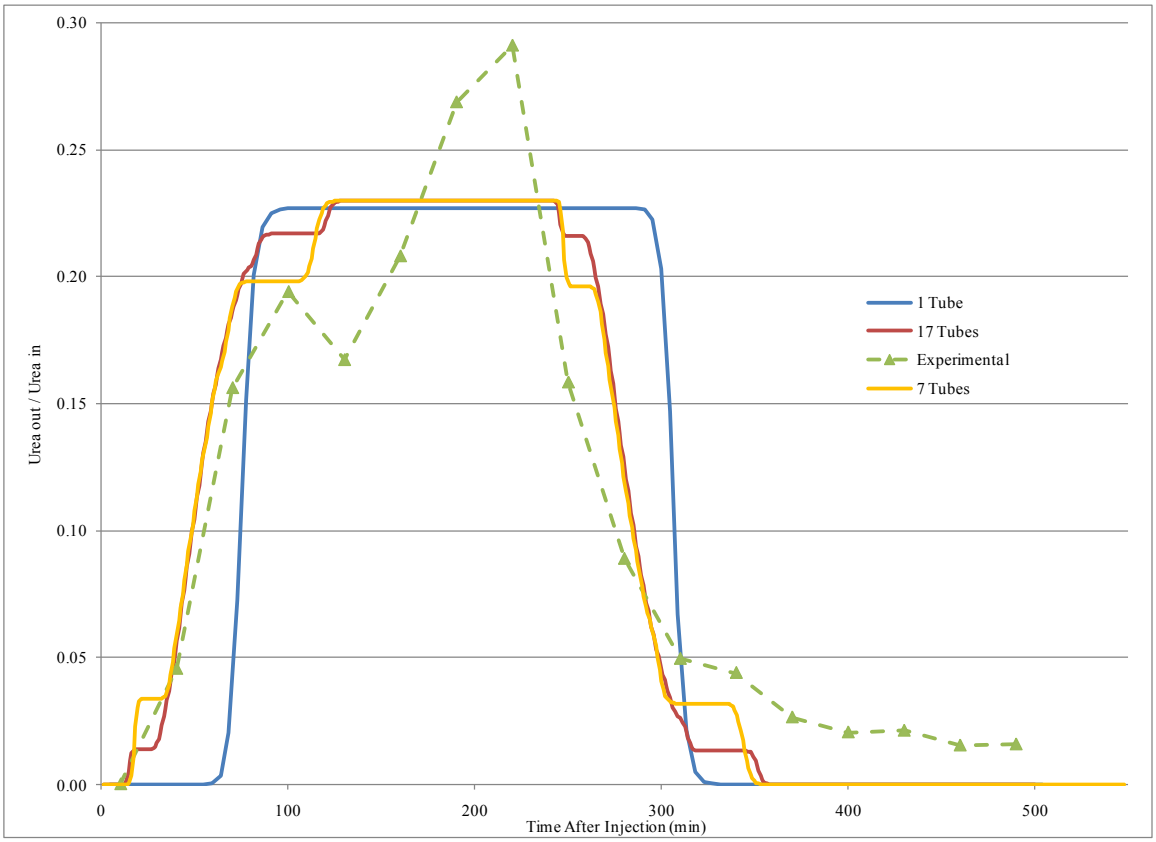

Figure 16: Fractional urea breakthrough curves for varying numbers of streamtubes

The single streamtube (blue) has the steepest front and steepest tail. The spike in urea begins at approximately 70 minutes after injection began, and escalates quickly to the maximum fractional breakthrough modeled value of 0.227 after nearly 100 minutes. Note that the maximum possible modeled value of fractional breakthrough would be equal to 0.24, the fitting parameter from the deconvolution for this particular well. The spike is expected to appear at this time because the travel time along the entire streamtube is 77.231 minutes; the front would begin at exactly that time for a case with only advection. At approximately 300 minutes after injection, the observed urea begins to sharply decrease. Out of all of the ensemble options, the single streamtube begins to decrease in the shortest amount of time for after the injection stops at 230 minutes. The simulation with seventeen streamtubes (red) more closely fits the results from the seven streamtube model. This simulation boasts the smoothest breakthrough curves, as would be expected with increasing quantities of streamtubes. Urea is reported at an earlier time (and at later times) than in the single streamtube simulation. This deviates from the nearly advection-only scheme evident in the single streamtube, demonstrating greater longitudinal mixing as a result of increased dispersivity.

The simulation with seven streamtubes (yellow) nearly matches the front and tail of the seventeen streamtube ensemble. This curve appears to be less accurate than the seventeen streamtube ensemble. This is evidenced by the step-like behavior as the results approach the peak and as they begin to descend. Graphically, it appears the step-like behavior fits the experimentally observed data better than the supposedly more accurate

seventeen streamtube model. However, this is most likely a result of unreliable data within the experimental results (see section 5.3) and not a projection of appropriate model fit.

All simulations match the front data better than the tail. This is expected considering the Inverse Gaussian deconvolution was selected and parameterized to fit the front specifically. Each simulation under predicts the peak observed values, however the simulations seem to peak at the approximate average value during the 230 minutes of injection.

A balance between computational time and model acuity is critical to achieve in any modeling framework; the appropriate caliber of result must be produced within a feasible quantity of computational effort. It is apparent that an increase in number of streamtubes greatly adds to computational time (in terms of computer capacity, run time, and human computation time) but the increase in quality of results is only marginal. The seven streamtube model was chosen because it most effectively balances the accuracy of the seventeen streamtube ensemble with the computational effort of the single streamtube simulation.

5.3 Comparison with experimental results

The simulation with seven streamtubes provides breakthrough curve data for wells 2024 and 2026. This data is compared with theory and experimental data to assess the quality of the model. Each streamtube for each well is run separately. The results of each streamtube is multiplied by its weighting factor. In this case, each simulation is 1/7 of the total mass flux, so each simulation is multiplied by a factor of 1/7. Figure 17 below depicts each of the breakthrough curve results in 2024 for each streamtube.

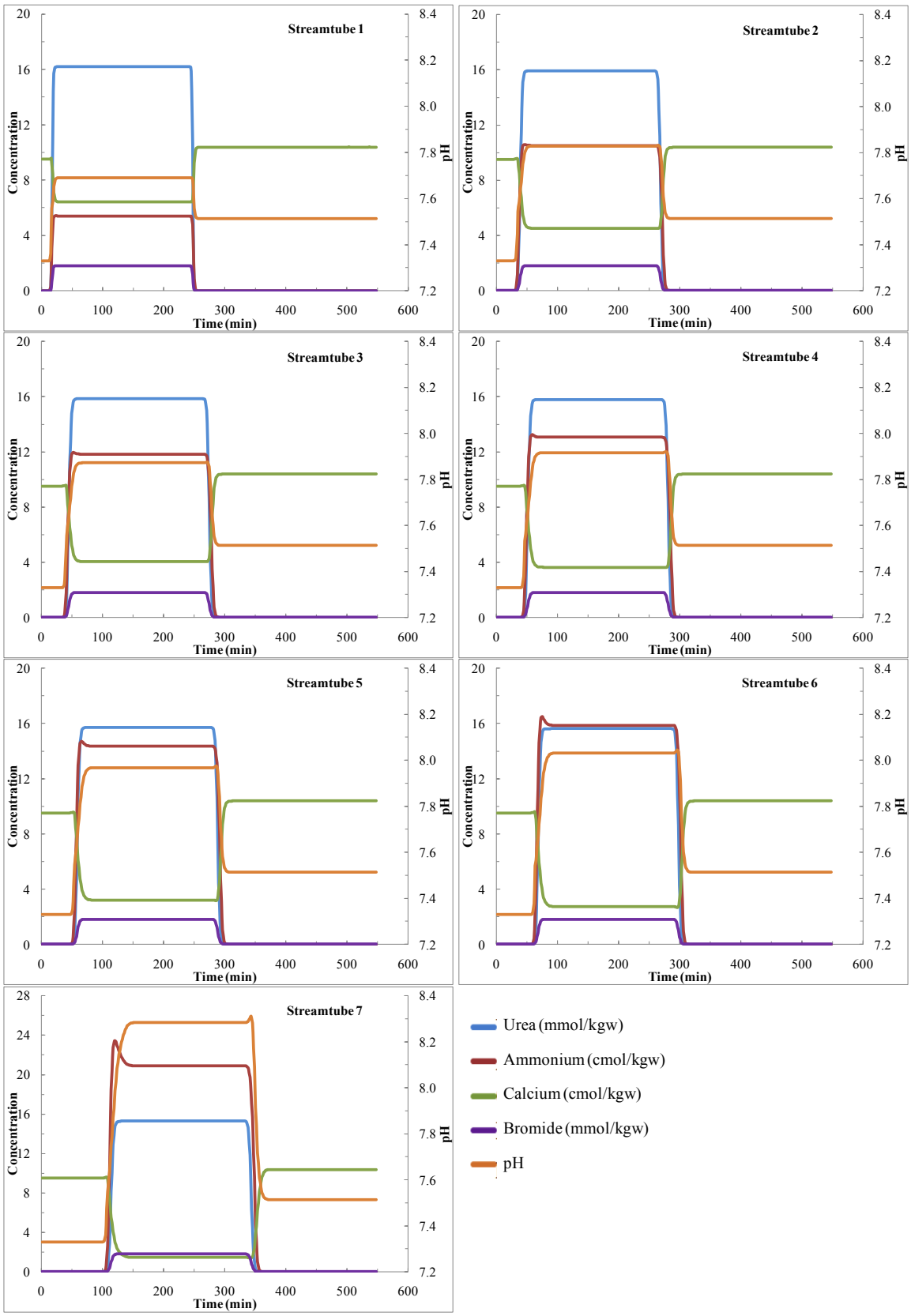

Figure 17: Single BTC's for each streamtube in well 2024

The breakthrough curves for each streamtube on well 2026 are identical in trend to those shown in Figure 17. Note in the graphs above the varied units: urea and bromide are in mmol/kgw (mol/kgw x 10^{-3}); ammonium and calcium are in cmol/kgw (mol/kgw x 10^{-2}). With each breakthrough curve displaying the primary reaction species, it is clear to see the trends within the reaction network.

Every graph of the seven streamtubes begins with urea, calcium, ammonium, bromide, and pH at the initial injectate values. The residence time for the first streamtube is 18.02 minutes. As expected, the first trace of the nonreactive bromide occurs near this time. The urea begins to spike earlier, ten minutes after pumping. The introduction of urea to the system is the catalyst for the ureolysis reaction; when urea arrives in the system, ammonium does as well and the pH increases. The presence of ammonium is proof that the urea has been hydrolyzed as it is a product of the kinetic reaction.

In Streamtube 1, the urea plateaus at 16.2 mmol/kgw. The injection quantity is 16.46 mmol/kgw. Similarly, ammonium reaches a plateau of 0.54 mmol/kgw (the injectate solution contains 0.015 mmol/kgw). Because none of the primary species are fully depleted in this simulation, Streamtube 1 appears to be rate dependent (as do Streamtubes 2 through 7). The reaction does not continue hydrolyzing urea and producing ammonium exponentially because the kinetic rate is not fast enough to deplete the surplus of reactants. Urea, ammonium, pH, and bromide all begin to drop around 250 minutes. This corresponds to the shutoff of the injection system at 230 minutes, plus the 18.02 minutes of travel time through the streamtube. Once injection is terminated, urea is no longer introduced to the system and a decrease in ureolysis is observed. Bromide, as a nonreactive tracer, is the first to descend. Urea exhibits more tailing behavior, though it is difficult to see in Streamtube 1. Calcium is the only species of interest that begins to appear in the effluent as ureolysis ceases. This is expected; the introduction of urea catalyzed calcite precipitation which removed Ca^{2+} from solution. After the urea injection, calcium was re-introduced to the system through the ambient conditions and was not utilized for calcite precipitation. After time, the system reaches steady state with the initial solution.

Streamtubes 2 through 7 share the same general trends as discussed with Streamtube 1. Because the length of the streamtubes are increasing, the total travel times are increasing. This will lead to a later initial breakthrough of urea, ammonium, pH, and bromide, as well as a later tail. The plateau levels for urea and ammonium decrease with increasing streamtube length. This may be attributed to the increased distance that provides the urea more time to degrade within the streamtube before it begins to reach the extraction well. With the longer streamtubes, more urea is utilized, more ammonium is produced, and the pH reaches larger values. In Streamtube 7, the maximum observed urea concentration is 15.3 mmol/kgw, the maximum ammonium concentration is 2.35 mmol/kgw, and maximum pH is 8.31.

An interesting pattern begins to appear in Streamtube 2 and is the most apparent in Streamtube 7. In Streamtube 7 we see a spike in ammonium and calcium at the front before the plateau and a spike in pH and the end of the plateau, immediately before the

final drop. This curious behavior may be linked to the cation exchange that programmed as an equilibrium process. The spike in calcium seems to be a sudden "dump" of calcium – aqueous calcium enters the system, presumably because it was released from the exchange material as the initial batch of ammonium was produced by ureolysis. Soon after the calcium is released it begins to precipitate, also as an equilibrium reaction, as calcite. The ammonium, however, has been generated very suddenly. Not only has it begun to remove calcium from the exchange material, but it is accumulating. It is not until enough timesteps have passed that more ammonium begins to sorb to the exchange material than is being produced. Eventually this relationship stabilizes at the plateau value. This spiking is more prevalent in the longer streamtubes because of the extended duration available for reactions.

To create the cumulative breakthrough curves for each well, the results from each separate streamtube are multiplied by each streamtubes mass fraction, are summed together, and the final result is multiplied by the well factor. For this simulation, the mass fraction for each streamtube is equal: $1/7^{th}$ of the total flux. After combining each streamtube, the results are compared against the bromide observations in each well. We expect this to be a sufficient fit, as bromide was the tracer used to create the streamtube ensemble. Figure 18 below depicts the fractional bromide breakthrough in well 2024 for both the model and the experimental data. Figure 19 is the fractional bromide breakthrough for well 2026.

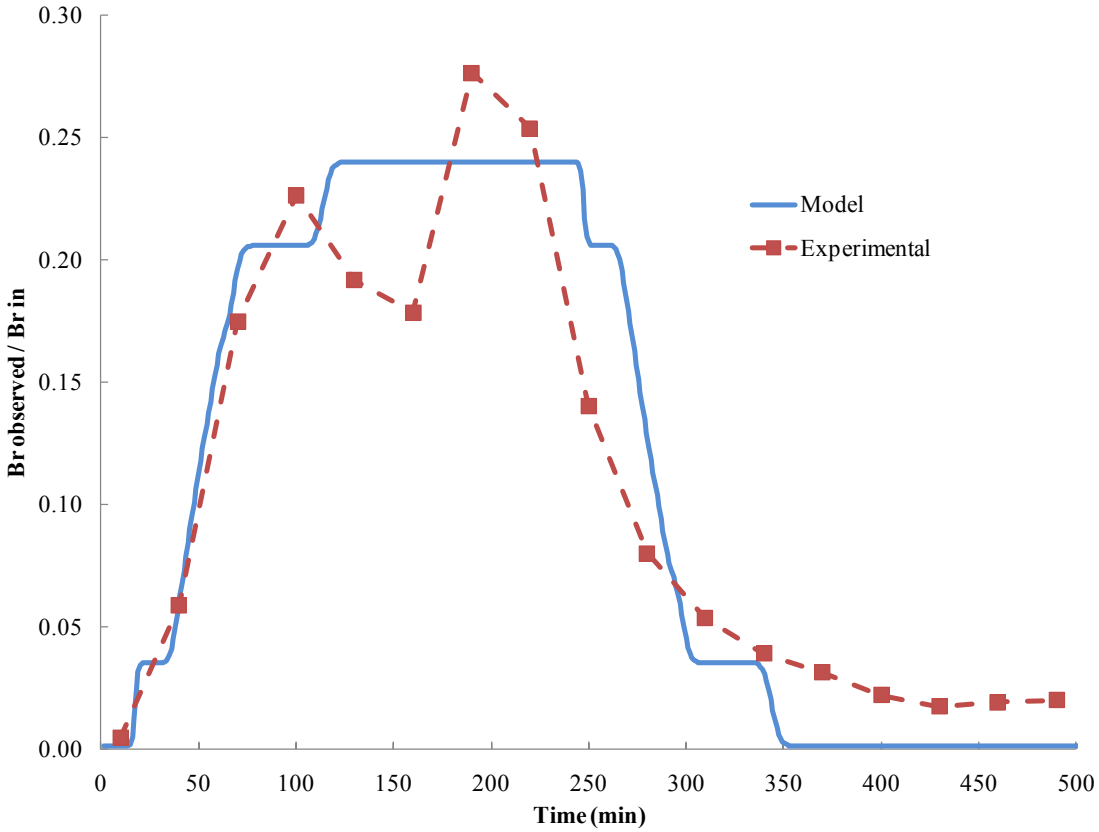

Figure 18: Fractional breakthrough for bromide in well 2024

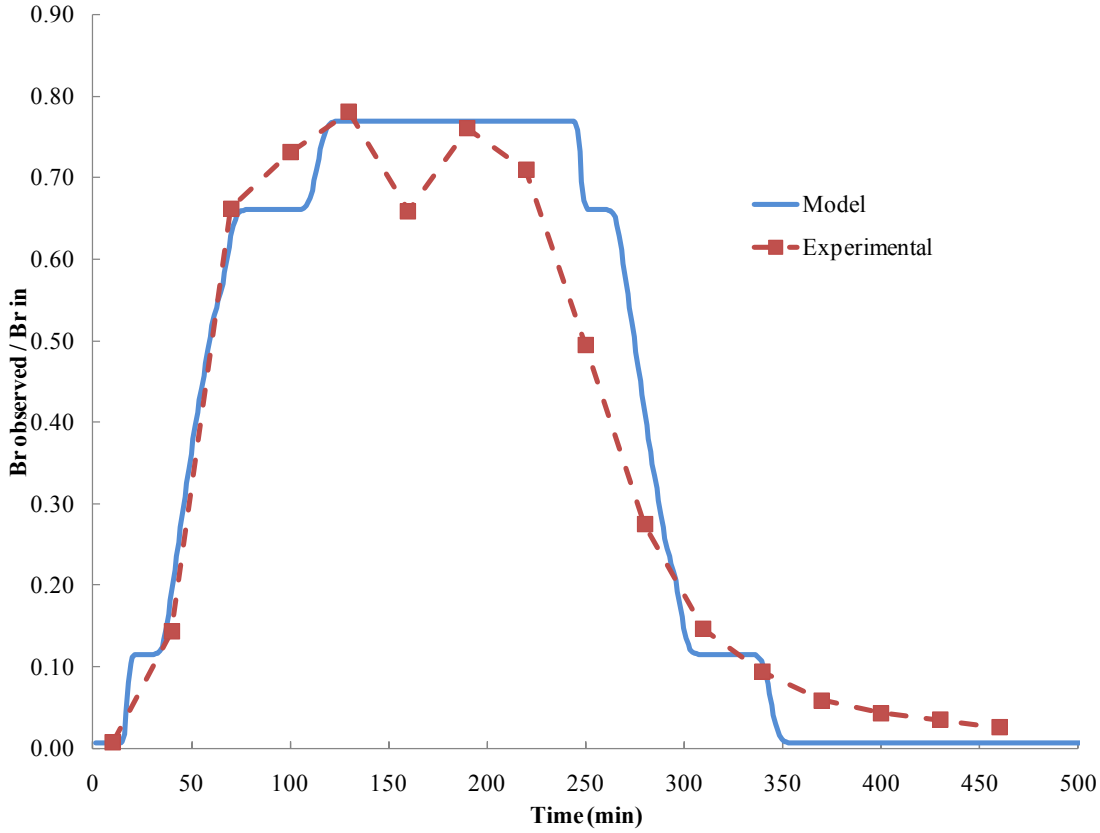

Figure 19: Fractional breakthrough for bromide in well 2026

The fronts of the modeled curves fit the experimental fronts the best (relative to the tails) for both of these wells. The fit in well 2026 is better than 2024. This because the same parameters (λ, μ) must be used for each well during the same simulation. The Inverse Gaussian fit the data better in 2026, thus we can expect a better model fit in well 2026. The Inverse Gaussian fit can be seen in Figure 12. The tails do not fit by the same reasoning: the deconvolution was performed with the objective of fitting the front. Because the Inverse Gaussian does not fit the tail as well as the front, the same behavior can be expected in the model. Additionally, the model does not fit the concentration drop that occurs in both wells at 130 and 160 minutes in well 2024 and at 160 minutes in well 2026. This behavior is not expected in a nonreactive tracer in a test with a constant pumping rate, therefore is not included in the model. The "steps" apparent in the model curves are a result of the streamtube averaging. Elimination or minimization of these steps can occur with an increase in number of streamtubes. The sensitivity and appropriateness of streamtube selection is discussed in section 5.2. Comparison of the experimental results with the model for the bromide tracer test provides a metric for establishing the suitability of the streamtube ensemble. Because the simulation matches the results appropriately, the model is determined to be self-consistent and can be confidently applied to the other constituents.

The first reactive component compared to the experimental results is urea. The fractional breakthrough curve for urea in well 2024 is shown in Figure 20; well 2026 is depicted in

Figure 21. For well 2024, the peak modeled value seems to be approximately the average of the plateau region of the experimental data. As in the bromide curves, the front fits better than the tail, with the front of 2026 fitting better than 2024 for the same reasons as discussed previously. The experimental data for urea exhibits a drop at 130 minutes in both wells. Although this could potentially be attributed to changes in the chemical conditions that affect ureolysis, it is most likely related to the same anomaly that caused the drop in bromide data. Like the bromide data, the model is not expected to replicate any drops in urea production at that point in the simulation, and thus the model is consistent with theory. These drops may be attributed to experimental error, such as malfunction of the injection or extraction pumps or of the data collector. Because the non-reactive bromide exhibits the same drops in concentration, we can deduce that the drops in concentration of urea are not a result of ureolysis or a different undefined reaction system.

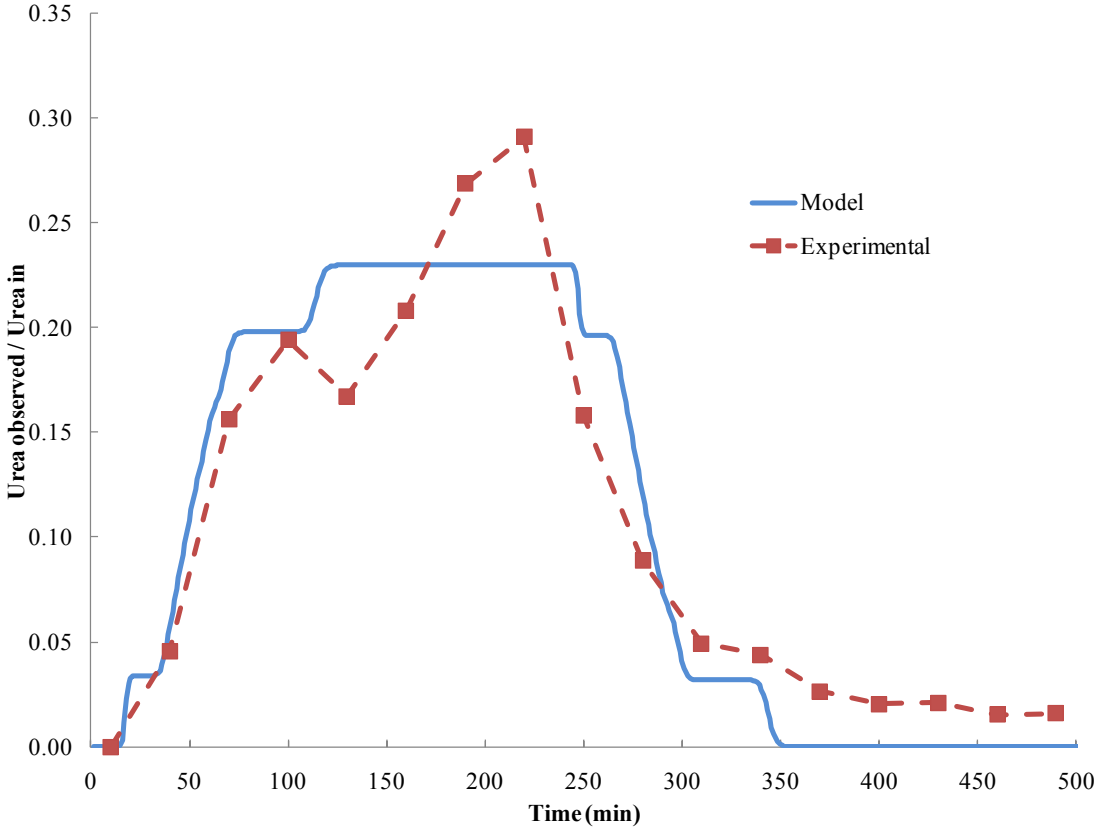

Figure 20: Fractional breakthrough for urea in well 2024

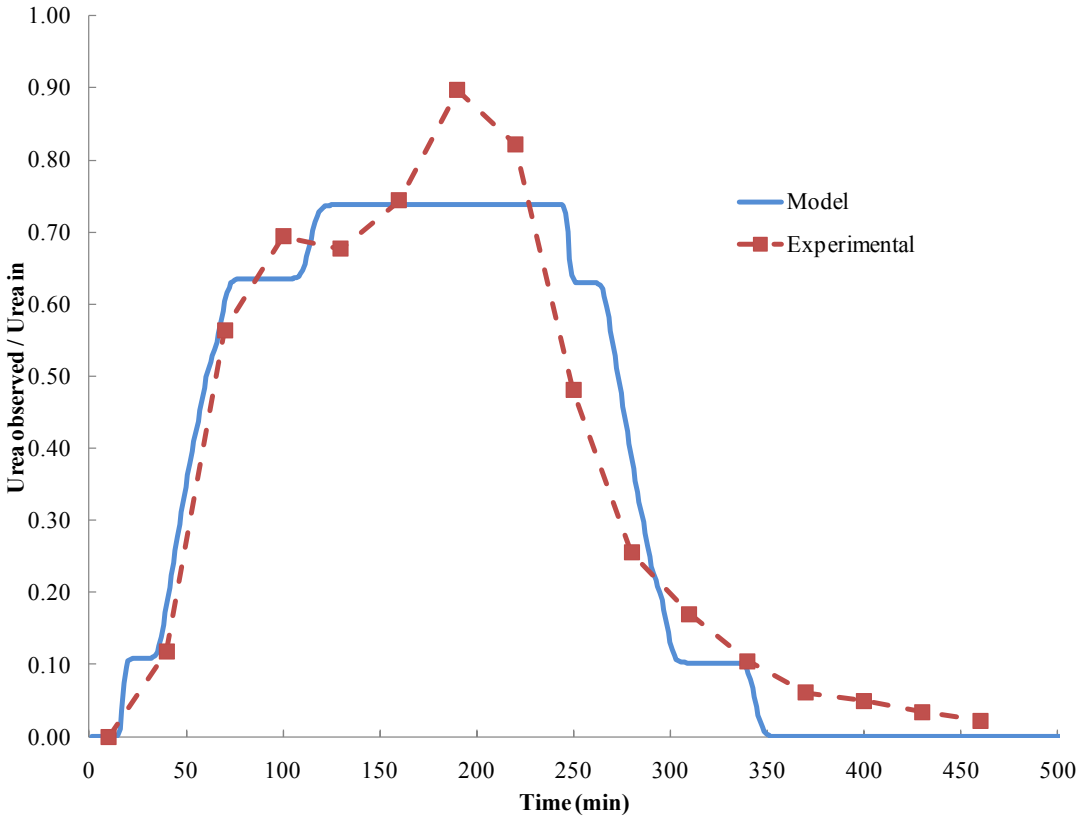

Figure 21: Fractional breakthrough for urea in well 2026

The next component to analyze is ammonium. Ammonium production can represent the extent of urea hydrolysis. Figure 22 depicts the breakthrough curve for ammonium in well 2024. Note the difference in units between the model values and the experimental values: the model is in mmol/kgw and the experimental data is in cmol/kgw. This is to further illustrate the difference between the two sets for this particular test. It is apparent that the model does not fit the experimental data very well; every single modeled value is significantly greater than the experimental findings. The model behaves according to theory: because urea is degraded and pH increases, it seems that ammonium must be produced! However, the experimental data shows only 2 different times where any ammonium was detected. The ammonium breakthroughs for 2026 are marginally better than those of 2024. In 2026, seen in figure 23, there are 10 different times when ammonium was detected. Again, note the units, and note that even though ammonium was detected in the experimental results, it is still in a significantly smaller quantity. The ammonium trends in 2026 are more representative of theory, there is essentially a front, a plateau, and a tail, however the front and tails are both short (due to the small size of the recorded data) and the plateau includes three data points that drop below the plateau value.

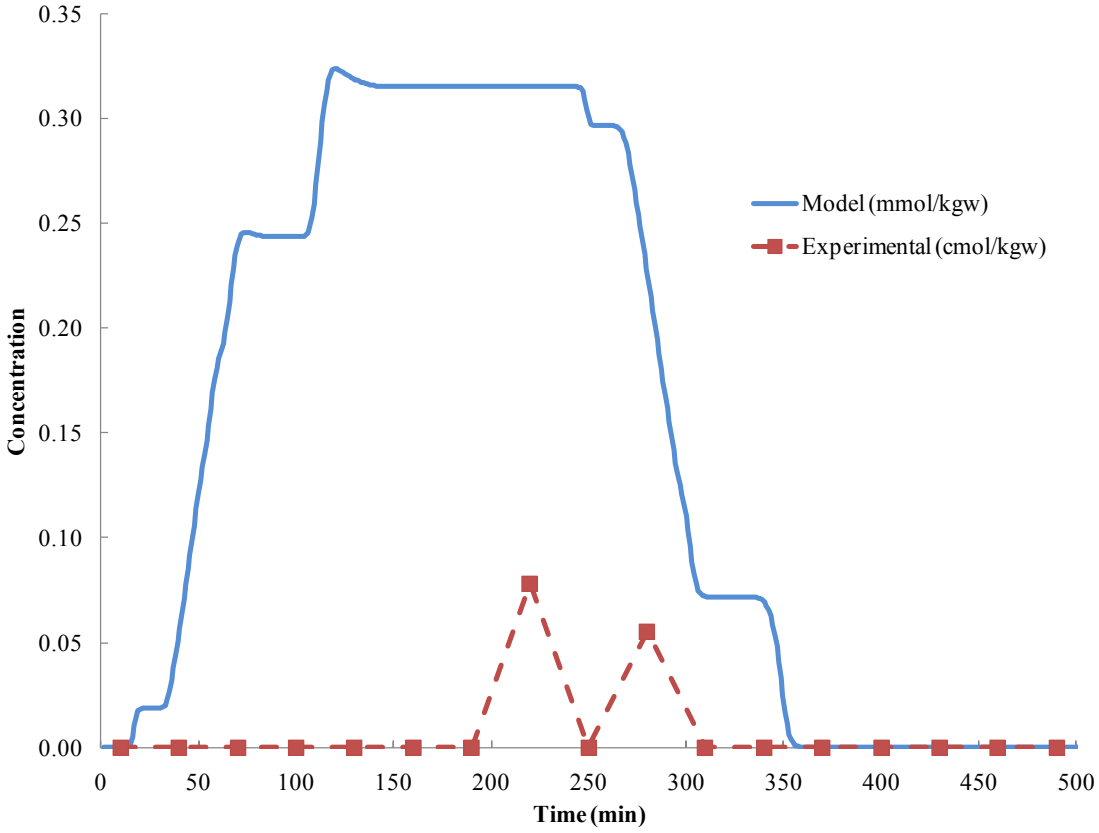

Figure 22: Ammonium breakthrough for well 2024

The values of ammonium observed in both wells is nearly insignificant. Based on the reaction network, for ureolysis to be occurring, we expect much greater concentrations of ammonium. The small ammonium concentrations may be a result of experimental and/or measurement error, or may signify that ureolysis is in fact *not* occurring within the well field, or is occurring at a much smaller magnitude than expected. An alternative explanation for this behavior may be the presence of nitrification within the system; in this case, ammonium is being oxidized to nitrate.

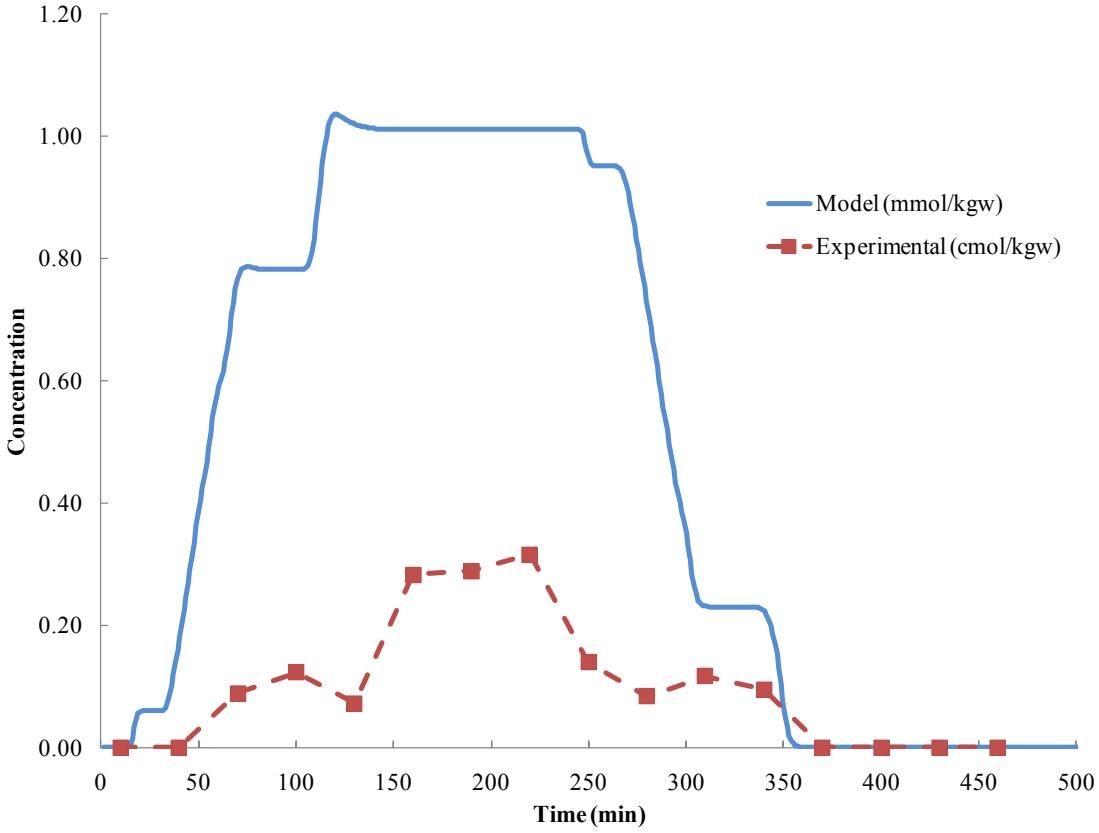

Figure 23: Ammonium breakthrough in well 2026

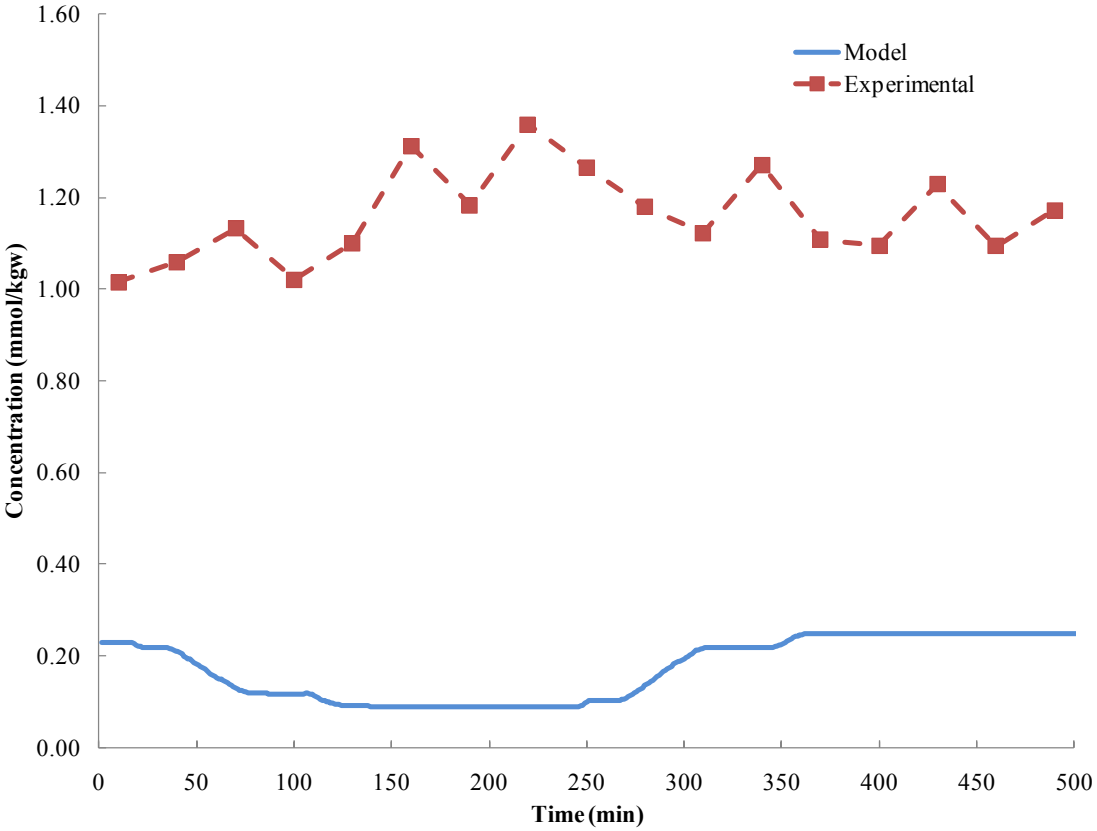

Figure 24: Calcium breakthrough in well 2024

Figure 24 provides the breakthrough curves for calcium in well 2024. This constituent presents the opposite trend to that discussed for the ammonium breakthrough. Here, the model values are less than the experimental values. This is logical, if less ammonium is actually being produced, less ureolysis is occurring, thus less calcite can precipitate and more calcite will be found in the aqueous solution. In figure 2024, modeled calcium begins to drop around 50 minutes. This is consistent with theory: calcite is precipitating during the experiment, so there should be a drop in calcium (not a plateau as seen with bromide or urea). After the urea injection, ureolysis slows and calcium is able to regenerate within the aquifer. The experimental results for well 2024, however, do not show a clear drop in values around 50 minutes, in fact the general curve seems to be concave. The same trends are seen below in figure 25. The model and experimental results are a better match in 2026; the difference ranges between 0.4 and 1.0 mmol/kgw, whereas 2024 differs between 0.8 to 1.3 mmol/kgw.

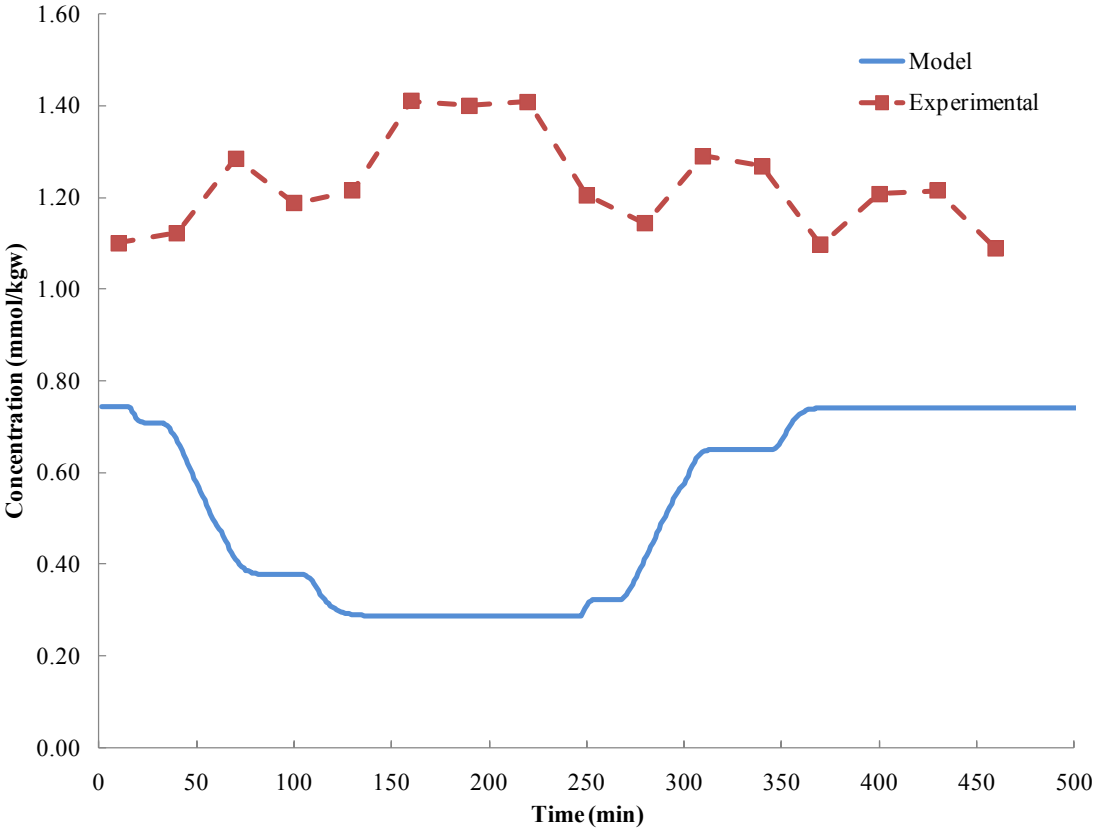

Figure 25: Calcium breakthrough in 2026

If urea is not degraded, results would demonstrate little or no ammonium values, as well as no degradation in calcium. The experimental results for both wells demonstrate those two trends. Although the questionable observations for both ammonium and calcite may be a result of experimental or measurement error, they also point to little or no ureolysis.

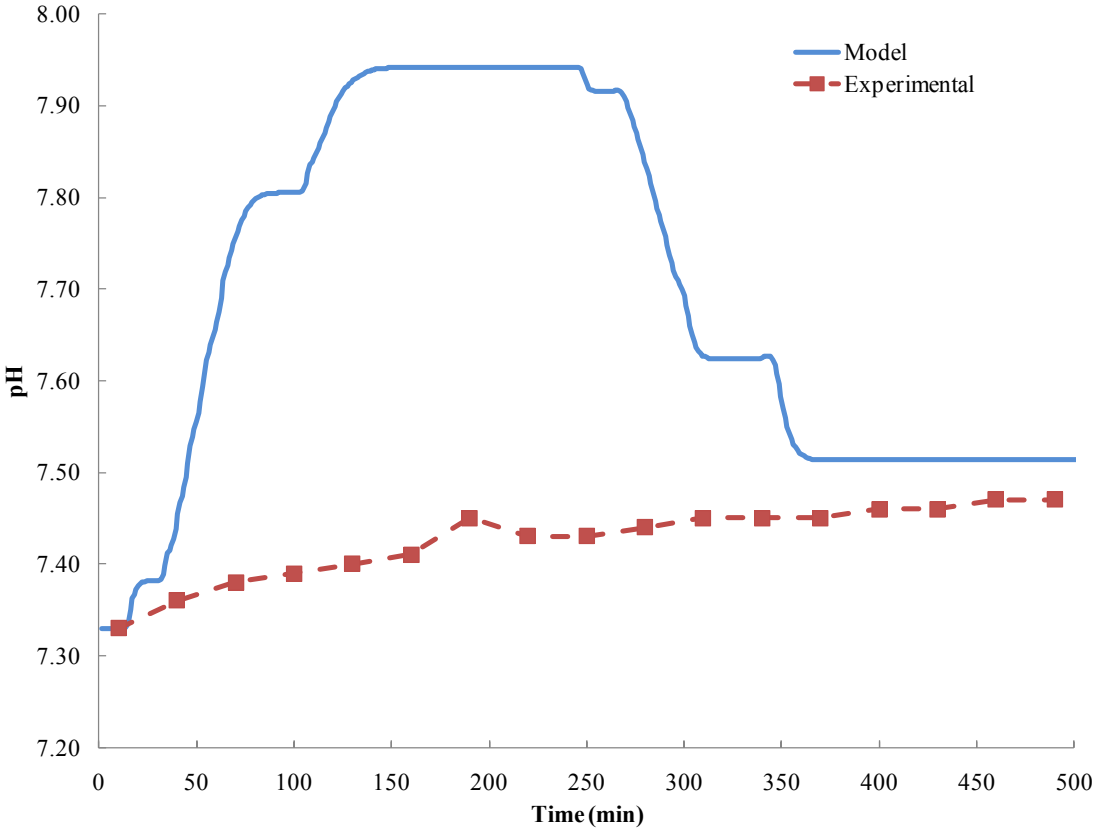

Figure 26: pH in well 2024

The pH in each well is also measured and modeled. Theoretically, pH will increase as ureolysis progress. The model and experimental data in both wells all at least begin with an increase. In well 2024, the observed pH steadily rises throughout the simulation. The modeled pH represents the average pH contributed from each streamtube at that particular time. Modeled pH in 2024 increases at approximately the same time ammonium is detected in the effluent. This is expected as they are both consequences of the ureolysis reaction. The modeled pH climbs steeply to a value of 8.31, plateaus, and begins to drop after the injection cycle ends. This is presumably when ureolysis would begin to slow as urea is no longer being introduced to the system. The pH drops more slowly than it rises as the ureolysis reaction experiences tailing behavior. The experimental pH in 2024 slowly rises at an approximately steady rate throughout the entire observation period. In well 2026, the maximum modeled pH reaches 7.94. This is less than the maximum in 2024 due to initial aqueous conditions that effect the progression of the entire reaction. The general model trends for pH, however, are similar in both wells. The experimental pH values rise early, up to 7.84, but begin to decrease after about 100 minutes.

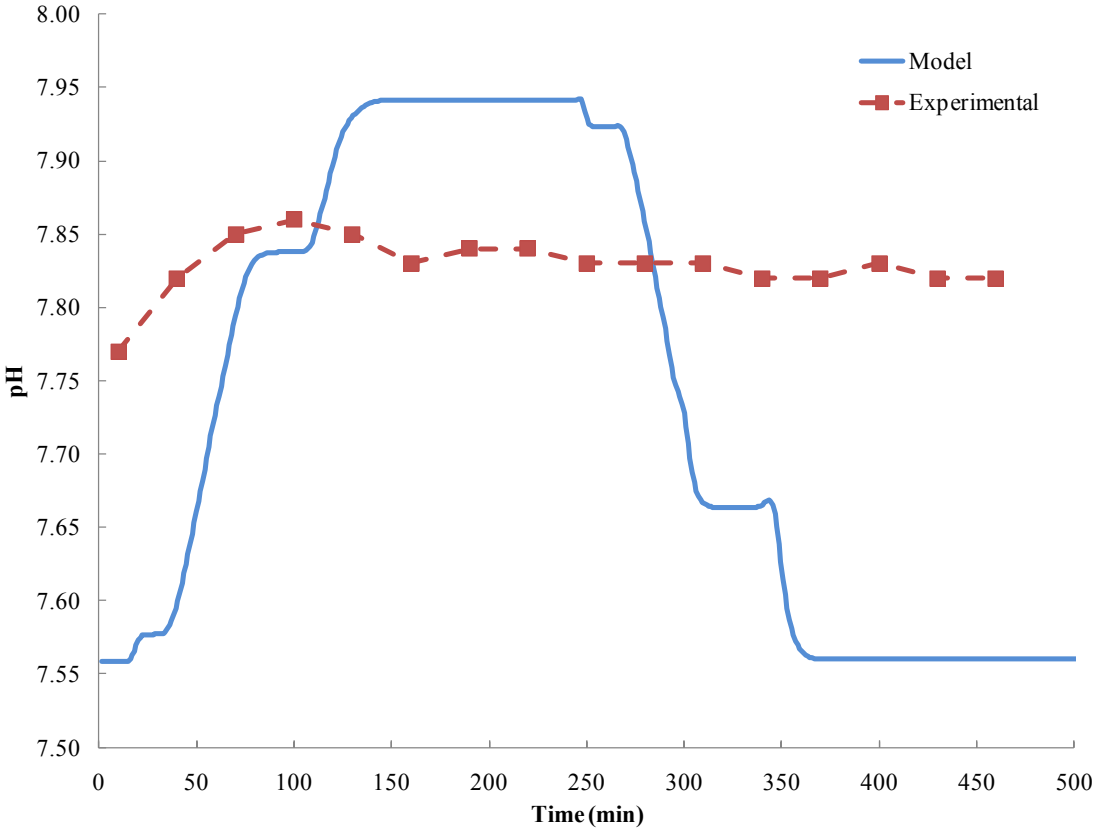

Figure 27: pH in well 2026

The experimental pH trends seem to further suggest that ureolysis is not occurring at a rate close to what is expected. The steady pH rise in well 2024 may suggest minor ureolysis, however the pH behavior in well 2026 suggests no ureolysis. The increase at early time in pH in well 2026 may simply be a reflection of the higher pH in the injectate solution.

Although the model performs as expected according to theory, it does not fit the experimental data. The modeling has, however, provided us with a tool to evaluate the behavior of the experimental data. Comparison of the model with the field data demonstrates that urea hydrolysis was occurring at a very small scale, if at all. The possibility still exists for measurement or experimental error, however every observed constituent is consistently unexpected which may suggest a lack of ureolysis.

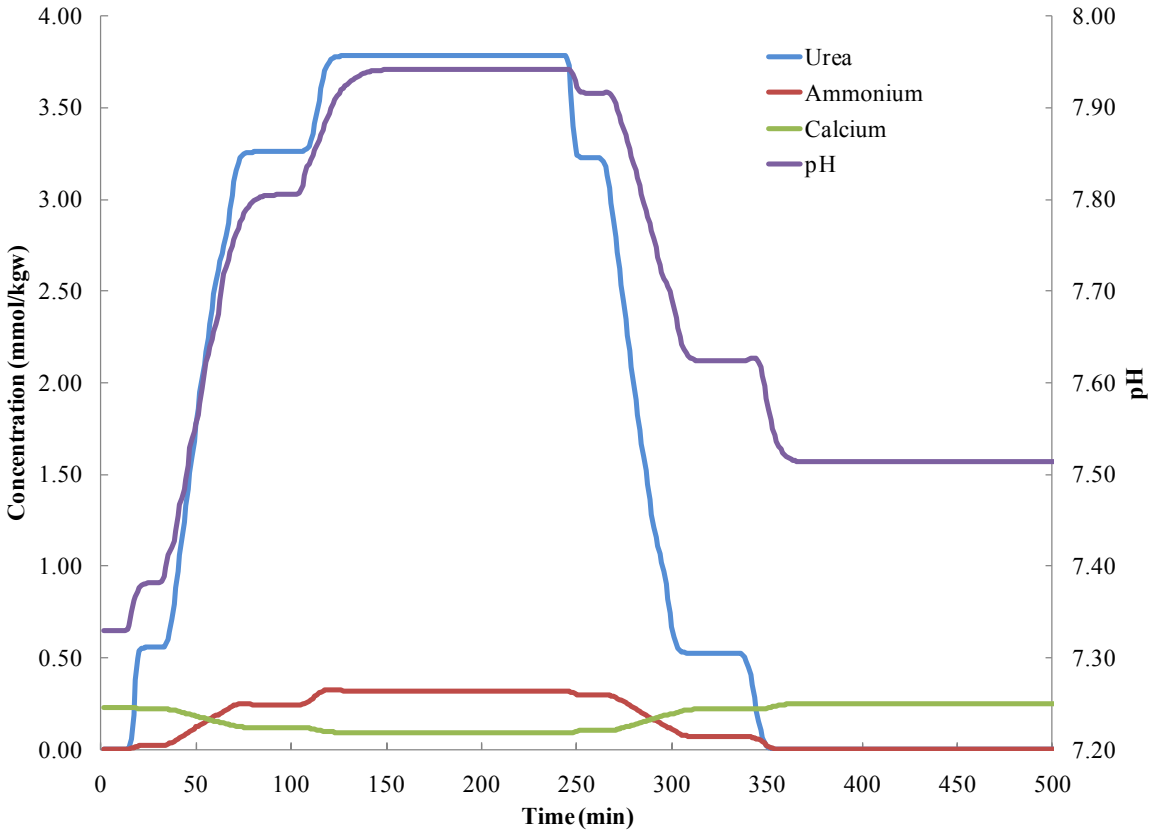

Figure 28: Breakthrough curves of critical species in well 2024

A useful technique to evaluate the effectiveness of a model is to analyze the overall results together. Figure 28 above demonstrates all of the breakthrough curves of the critical species (urea, ammonium, calcium, and pH) in well 2024. This graphic represents the cumulative breakthrough curves from the individual curves shown in figure 17. For urea (blue), the front begins to rise around ten minutes, corresponding to the quickest arrival time inherent in the first streamtube. The plateau is reached around 130 minutes, corresponding to the slowest arrival times found in the seventh streamtube. The urea concentrations begin to drop after around 250 minutes, with about 150 minutes at the plateau. The injection is stopped at 230 minutes, so the first drop corresponds to the shortest distance between the wells that is described by the first streamtube. Ammonium (red) follows the same behavior as expected from the individual breakthrough curves: initial rise near 10 minutes, maximum value reached at 130 minutes, and a decrease beginning near 250 minutes. After 350 minutes, ammonium values are essentially zero, as are the urea values. This is also near the point where calcium (green) reaches its initial concentration representative of the ambient conditions. Calcium decreases during the injection period: it is being precipitated as calcite. The calcium reduction occurs when both urea and ammonium begin to rise, and begins to rebound as urea and ammonium decreases. pH (purple) begins at 7.33 and begins to rise after about 15 minutes and increases until 150 minutes. There is a small lag in pH rise compared to urea and ammonium production. pH does, however, begin to drop at the same time as urea and ammonium, but does not drop as steeply as the others. Unlike

urea, ammonium, and calcium, after injection pH does not return to the approximate initial value, but instead stays around 7.51.

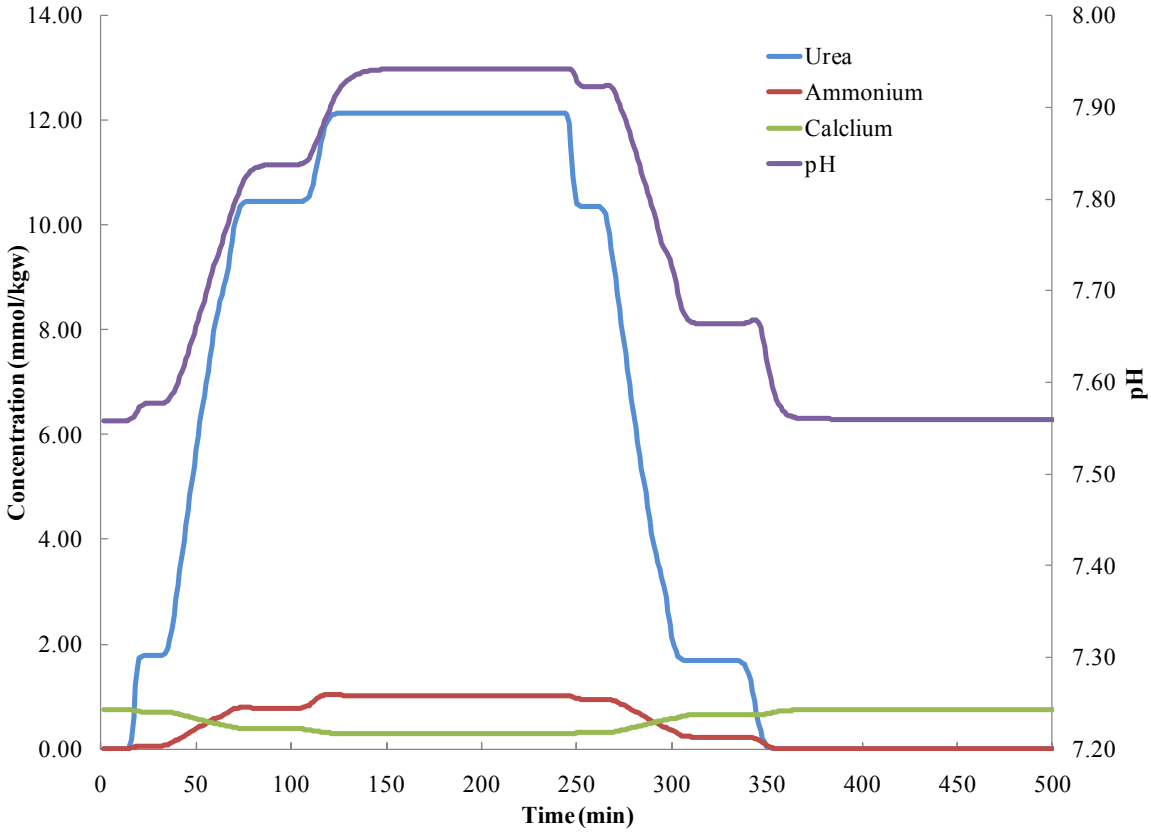

Figure 29: Breakthrough curves of critical species in well 2026

Many of the trends observed in well 2024 are also seen in well 2026, pictured above in figure 29. The urea and ammonium begin around the time corresponding to the travel time of the first streamtube, and they begin to drop at the time of the first streamtube's drop. Calcium behaves similarly: it begins to drop with the first streamtube and rises after the first streamtube's influence has passed. The plateaus last about 150 minutes in both wells, which further demonstrates that the overall travel time between the wells is longer than the injection period of 230 minutes. pH in well 2026 begins at 7.56, begins to rise as urea and ammonium are introduced, and slowly rises to the maximum of 7.94 at 135 minutes. Unlike well 2024, the pH eventually returns to the initial value of 7.56.

5.4 Constant velocity vs variable velocity

To validate the use of variable velocity streamtubes, PHREEQC was run with constant velocity and variable velocity transport simulations. Both runs entail the same chemistry and background components. The only difference occurs within the transport block, in particular, with the lengths of each cell. Constant velocity streamtubes were implemented with each cell being the same length. Variable velocity cells are of varying lengths.

Each particular streamtube has the same required travel time as predicted from deconvolutions. This ensures that the flux between the wells is constant and consistent with experimental data. Once dependence on variable streamtube velocity is exhibited, model results are ready to be implemented with practical applications. To verify model accuracy, the simulations with variable velocity are performed to replicate urea data derived from the extraction well.

The new lengths are listed below in table 12. These lengths are calculated by the direct quotient of the length over the pre-determined number of cells. By utilizing a constant cell length throughout the streamtube, the velocity in each cell and thus throughout each streamtube, will be constant.

Table 12: Constant length values for constant velocity simulations

Streamtube	Constant Length
1	0.05
2	0.024
3	0.023
4	0.025
5	0.03
6	0.042
7	0.056

To determine the effects of a variable velocity ensemble, PHREEQC is run with the constant cell lengths above and is graphically compared to the results from the variable velocity simulations. Breakthrough curves in well 2026 for these two types of simulations are shown below in figure 30. Similarly, well 2024 exhibits the same trends, but is not shown here.

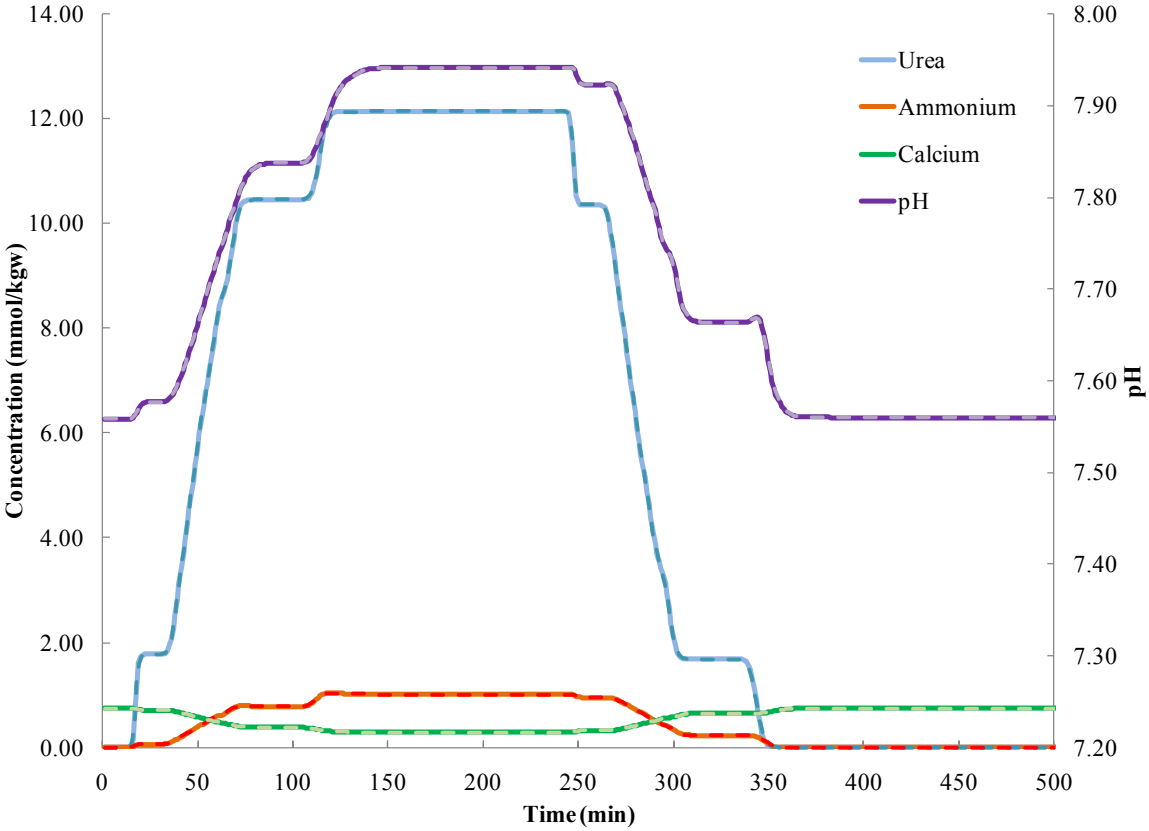

Figure 30: Variable vs. constant velocity breakthrough curves of significant species in well 2026. Constant velocity series are dashed lines corresponding to the same color species as described in the legend. Variable velocity simulations are solid lines (beneath the dashed constant velocity lines)

It is evident that the effect of a variable velocity ensemble is negligible for this reaction network upon evaluation of breakthrough curves. The solid lines representing variable velocity above match so well with the constant velocity curves that it is impossible to note that the lines are actually solid. However, the simulations are not completely identical; application of a variable velocity ensemble may have more of an effect on reaction constituents that are heavily reliant on kinetic behavior. Calcite precipitation in this experiment, for example, is dependent on kinetic ureolysis and may exhibit an impact from a variable velocity ensemble. Figure 31 below demonstrates the quantity of calcite precipitated over the length of the seventh streamtube at 223 minutes (the peak of injection). Streamtube 7 should have the greatest reliance on the velocity within cells, and due to its length there is more observational space. Well 2026 reflects the same trends and is not shown here to avoid redundancy.

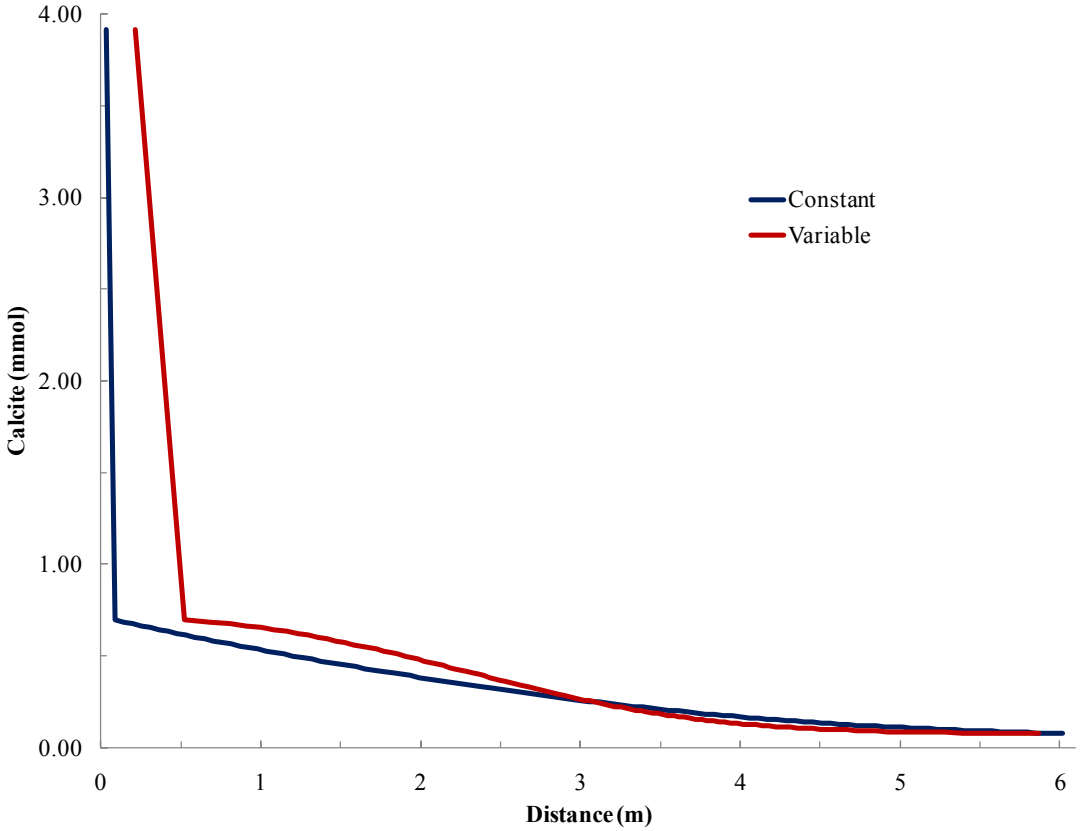

Figure 31: Constant velocity vs. variable velocity for calcite over length in well 2024 at 223 minutes

In the figure above, the constant velocity ensemble (blue) behaves in a significantly different way compared the the variable velocity ensemble (red). The first cell for both simulations begin at the same value. They occur at different distances because the center of each cell will be in different locations. The constant velocity ensemble quickly drops by about 0.65 mmol in the 0.056 meters between the first two cells. The variable velocity ensemble drops about the same amount, but it occurs over 0.43 meters. Until about halfway between the injection and extraction wells, the constant velocity ensemble predicts less calcite precipitation than the variable velocity ensemble. Past 3 meters, the two simulations are very close, but the variable velocity ensemble does simulate less calcite than the constant velocity ensemble. In general, the variable velocity ensemble produces a calcite profile that is less linear that the constant velocity ensemble.

In the first half of the column, this exercise supports the theory that the longer the reactions occur within a cell, the more calcite will precipitate. For example, between 0.5 and 1.5 meters, the velocity ranges from 0.05 to 0.1 m/s. There is more calcite precipitation here than between 2 and 3 meters, where the velocity ranges from 0.03 to 0.04 m/s. However, this correlation does not continue after about 3 meters. This may be because the greater quantities of calcite precipitation nearer to the extraction well depleted the calcium by the time the injectate solution reached midway through the column.

Although the breakthrough curves do not reflect any dependency on a variable velocity versus a constant velocity ensemble, the calcite precipitation profile is affected. Considering the purpose of this study is to promote calcite precipitation, it is logical that a variable velocity ensemble be implemented.

5.5 Calcite precipitation predictions

To analyze calcite precipitation, PHREEQC is instructed to tabulate precipitation along the length of the streamtube at every timestep. The output provides the cumulative millimoles of calcite precipitate in each cell at every ten timesteps. This data is visualized in MathCAD with the three-dimensional plots below (figures 32-38). Unlike the breakthrough curves for each streamtube, the precipitation results cannot be summed for every streamtube to create a single cumulative dataset. Instead, the results demonstrate where along each streamtube's path calcite precipitation will occur. Each figure is shown with two different angles to provide an alternative perspective. The data does not visibly change from one streamtube to the next; changes are more evident upon comparison of the first and seventh streamtubes.

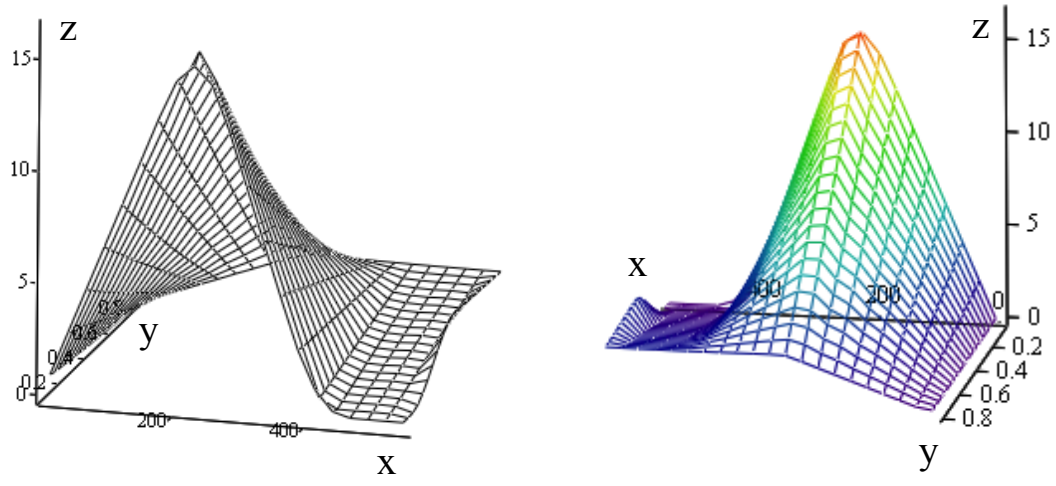

Figure 32: Three dimensional plots shown from different angles of calcite precipitation (z, mmol/cell) over time (x, minutes) and distance along the streamtube (y, meters) for streamtube 1, well 2024

Figure 32 above depicts a set of trends that can also be found in figures 33-38 representing the behavior in streamtubes 2-7. Initially, there is no calcite present along the length of each streamtube. Each movement along the x-axis represents increasing time. Focusing the first cell (y = 0.026 m) for Streamtube 1, calcite precipitation steadily increases with time, reaching a maximum of 16.3 mmol/cell after 223 minutes. At this point, it appears the calcium in the system is depleted or transported to the next cell and

precipitation no longer occurs at this location. It appears that the quantity of calcite actually decreases, which infers dissolution. It is difficult to visualize in figures 32-38 but there is calcite present in each cell throughout the simulation; after about 410 minutes, however, no more calcite is dissolved or precipitated. This first cell is where the most calcite is documented. Each following cell has less calcite in it than the previous cell at the same time. This means calcite precipitation is not occurring uniformly and is largely happening at the entrance of the streamtube. Less dissolution occurs as distance along the streamtube increases, presumably by the same mechanism that causes the precipitation nonuniformity. For a discussion of the dissolution potential, see section 5.6. The calcite precipitation front becomes increasingly steep with streamtube number, as does the tail.

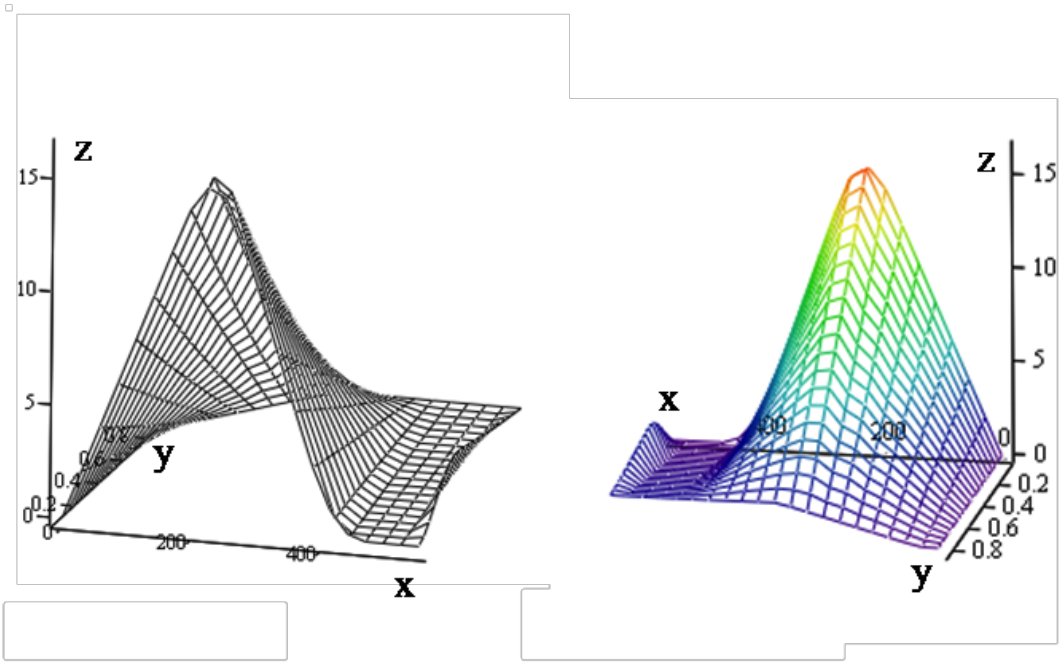

Figure 33: Three dimensional plots shown from different angles of calcite precipitation (z, mmol/cell) over time (x, minutes) and distance along the streamtube (y, meters) for streamtube 2, well 2024

Streamtube 2 (figure 33) depicts the same trends as seen in Streamtube 1. The maximum value is again 16.3 mmol/cell, however in general, there is less precipitation per cell. In Streamtube 3 (figure 34) there is more precipitation near the injection site when compared to precipitation near the injection site in Streamtube 1. These differences may be attributed to the varied cell sizes and PHREEQC's calculation mechanisms that sum precipitates per cell. The maximum amount of calcite in Streamtube 3 is slightly larger than Streamtubes 1 and 2 at 16.317 mmol/cell.

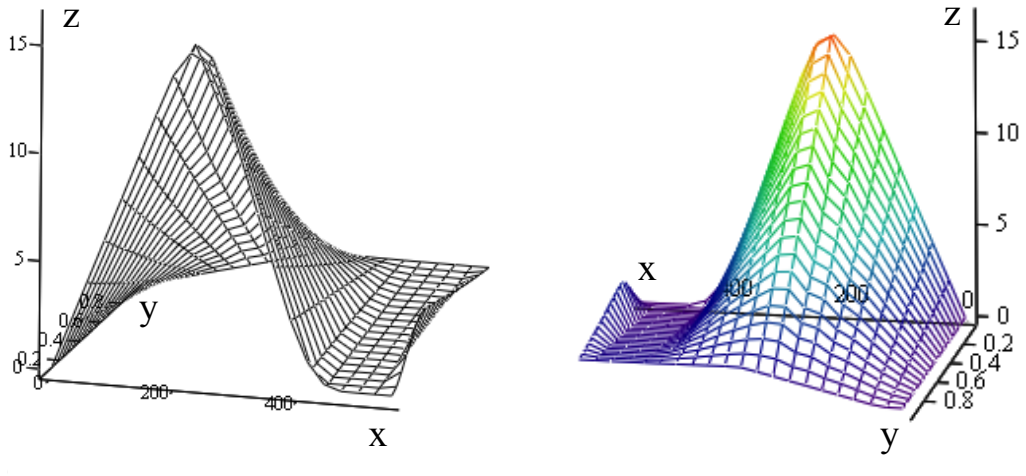

Figure 34: Three dimensional plots shown from different angles of calcite precipitation (z, mmol/cell) over time (x, minutes) and distance along the streamtube (y, meters) for streamtube 3, well 2024

The maximum calcite quantity in Streamtube 4 is 16.318. As witnessed in the comparison between Streamtubes 2 and 3, there is less calcite precipitation at a particular time at cells near the extraction well in Streamtube 4 (compared to 3) and more calcite in cells near the injection well.

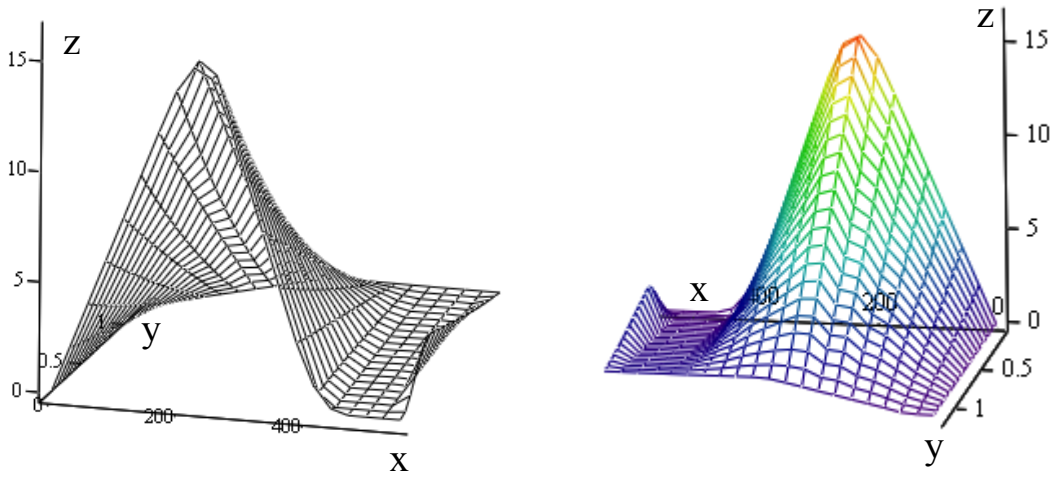

Figure 35: Three dimensional plots shown from different angles of calcite precipitation (z, mmol/cell) over time (x, minutes) and distance along the streamtube (y, meters) for streamtube 4, well 2024

In Streamtube 5, the maximum amount of calcite is again marginally increased to 16.32 mmol/cell. There is more precipitation in the first cells as compared to the first cells of Streamtube 4, and less at later cells.

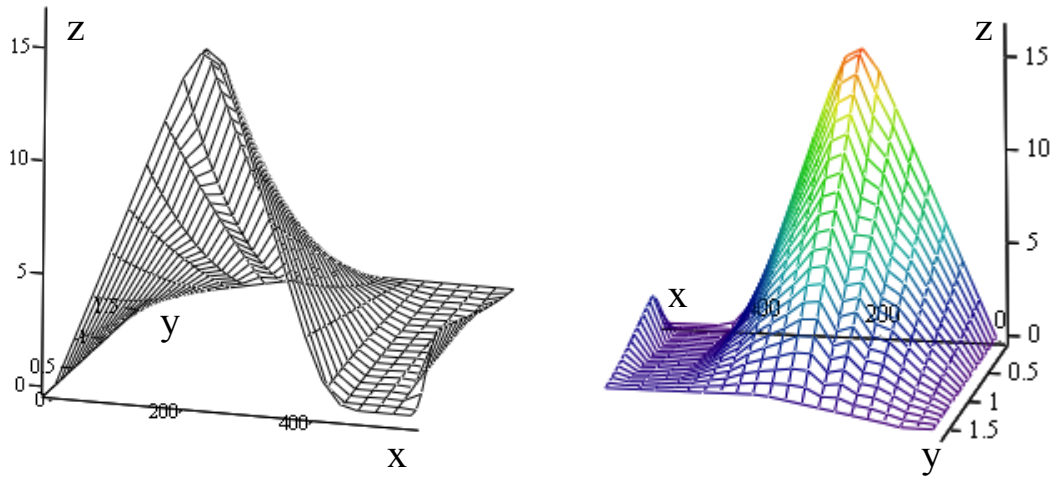

Figure 36: Three dimensional plots shown from different angles of calcite precipitation (z, mmol/cell) over time (x, minutes) and distance along the streamtube (y, meters) for streamtube 5, well 2024

The maximum calcite value in Streamtube 6, 16.321 mmol/cell, can be seen in figure 37. In this streamtube, an interesting pattern begins to appear: the calcite values fluctuate over time. They do not progress steadily in an increasing or decreasing fashion, instead they exhibit instability. This is even more apparent in Streamtube 7 (Figure 38).

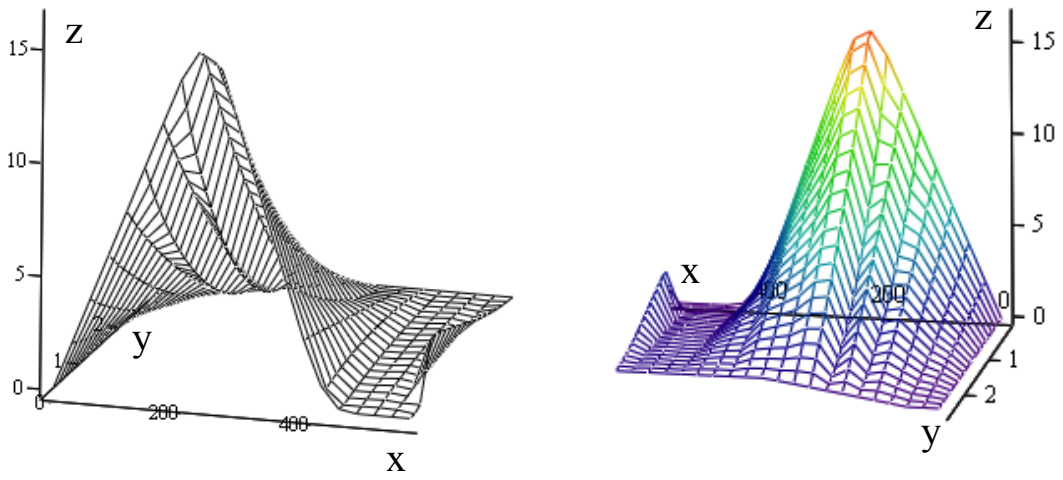

Figure 37: Three dimensional plots shown from different angles of calcite precipitation (z, mmol/cell) over time (x, minutes) and distance along the streamtube (y, meters) for streamtube 6, well 2024

Streamtube 7 exhibits the maximum calcite value of all of the streamtubes: 16.322 mmol/cell. Again, there is more precipitation near well the injection site than in Streamtube 6, and less near the extraction well.

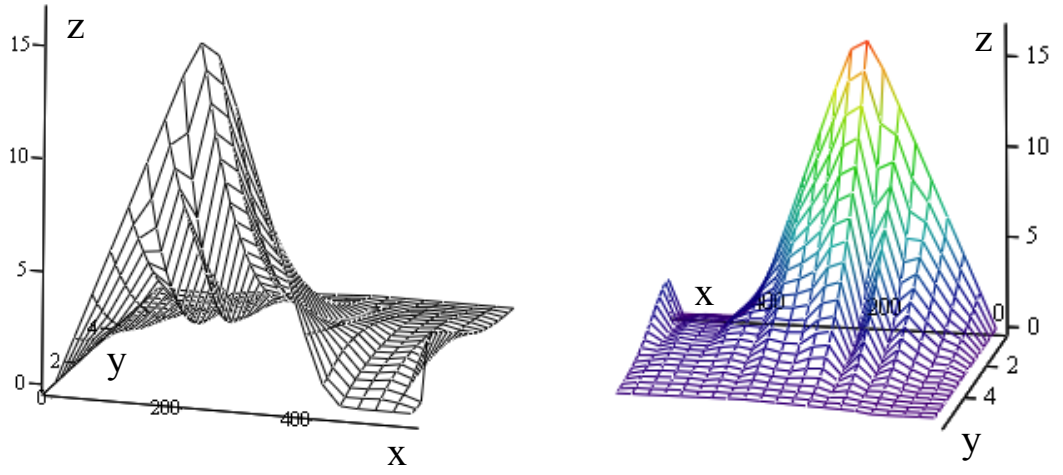

Figure 38: Three dimensional plots shown from different angles of calcite precipitation (z, mmol/cell) over time (x, minutes) and distance along the streamtube (y, meters) for streamtube 7, well 2024

Figures 39 and 40 below depicts Streamtubes 1 and 7 for the results in well 2026. Due to similarity of trends between each streamtube and to the results observed in well 2024, Streamtubes 2 through 6 are omitted.

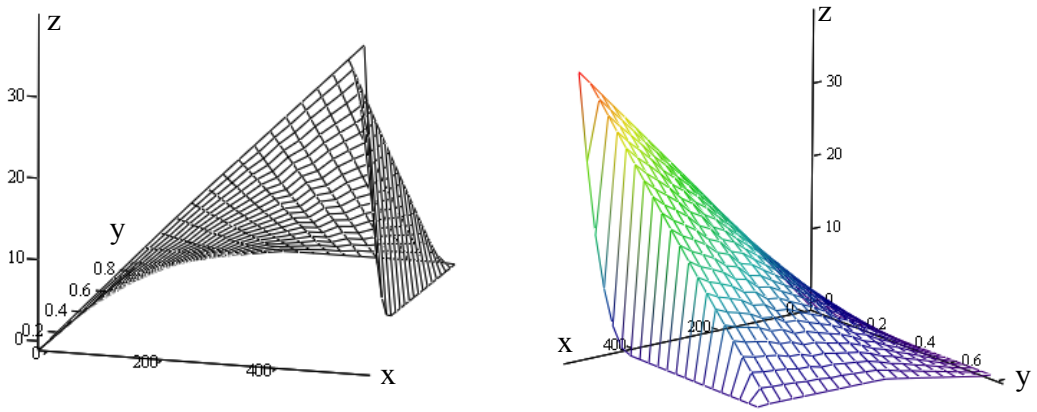

Figure 39: Three dimensional plots shown from different angles of calcite precipitation (z, mmol/cell) over time (x, minutes) and distance along the streamtube (y, meters) for streamtube 1, well 2026

Due to the animation capacity of Mathcad13, Figures 39 and 40 show zero values for calcite at the latest time in each cell. This is a Mathcad13 quirk, the actual values for calcite never decrease (let alone to a value of zero) in well 2026. The maximum value for each streamtube is 38.97 mmol/cell, however Streamtube 1 exhibits a more smooth gradient as distance along the streamtube increases.

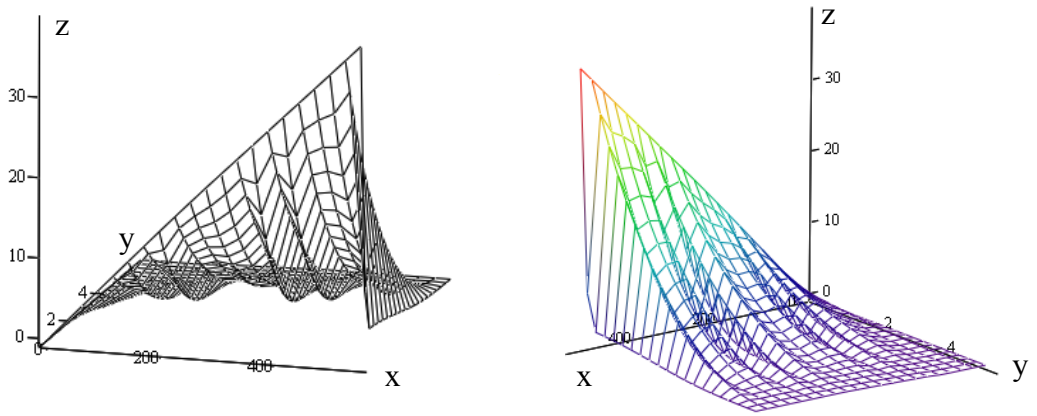

Figure 40: Three dimensional plots shown from different angles of calcite precipitation (z, mmol/cell) over time (x, minutes) and distance along the streamtube (y, meters) for streamtube 7, well 2026

In Streamtube 7, the minimum values (>1 mmol/cell) along the length of the streamtube occurs after about 3.5 meters, while the minimum value in Streamtube 1 occurs in the cell nearest the extraction well at about 2.55 mmol/cell at later times and >1 mmol/cell at earlier times. This difference can be explained by considering the actual distance. There is more calcium available to be precipitated in Streamtube 1 by the time the end of the streamtube is reached; in Streamtube 7, most of the calcium is exhausted before it reaches the end of the streamtube.

The behavior in well 2026 is markedly different than that observed in well 2024. Namely, there is no dissolution in well 2026. This corresponds to the initial speciation evaluation; the ambient water (the solution permeating the system after injection) is supersaturated with respect to calcite, calcite will not dissolve. Well 2024 exhibits dissolution potential; if this site is desired for a long-term remediation strategy, it is necessary to establish that the saturation index in the soil is within the tolerable limits for permanent precipitation.

Analytically, both wells exhibit instabilities in longer streamtubes. This may be due to difficulties within the PHREEQC solver as it attempts to solve for a set of reactions within an extremely small length segment.

5.6 Future Work

One of the most valuable insights gained from creation and operation of this model is the concept that much more work can be done to improve the simulations. A few of the more critical issues, such as inclusion of strontium and solid solutions, temperature variance, the inclusion of microbial behavior coupled with improvements to the Fidaleo and Lavecchia kinetics, and model validation with other codes are all viable options to improve the model's functionality in the future. This list is not all-inclusive, there is a plethora of options available to improve the model development and execution.

Currently, the model does not predict strontium incorporation. To build a knowledge base suitable to determine the effectiveness of this remediation strategy, strontium needs to be added. Preferably, strontium could be modeled within PHREEQC as a solid solution, which is ordinarily observed in the field (Pingitore, 1992; Fujita, 2004, 2008). This solid solution is assumed to very stable and efficient at immobilizing strontium-90. Addition of strontium will also affect the general reaction network. If strontium is present within the system, a higher saturation state must be obtained before calcite can begin to precipitate (Mitchell, 2006a). In this case, strontium is essentially inhibiting crystal growth by blocking nucleation sites and prohibiting the collision of Ca^{2+} and CO_3^{2-}.

The VZRP is a challenging site. Initial exploration of the site demonstrated extreme changes in the regional gradient and overall transience of the flowfield. Unexpected changes such as these during an experiment may cause unforeseen results, or even the inability to use the data to create, validate, or compare with a running model. If more knowledge of the flowfield were obtained, surprising and confusing results may be avoided. The hydrology of the VZRP is ephemeral, and the challenges associated with this reflects the fact that reactive transport analyses must be generally dependent on a robust understanding of the flow field.

The temperature in the field was measured at 18C. The input into PHREEQC and relevant values in the thermodynamic database are programmed at 25C. This temperature discrepancy has a significant potential to affect the ureolysis rate and the mechanisms of calcite precipitation. Ureolysis increases with temperature. Fujita (2008) noted that an increase from 12C to 22C increased ureolysis by more than a factor of 10. Similar findings also occur in Mitchell (2005). Calcite exhibits retrograde solubility: an increase in temperature will decrease the solubility. This is potentially catastrophic for the VZRP remediation application; running the model at a false higher temperature will provide less soluble calcite, decreasing the margin of safety. Theoretically, an increased temperature will increase ureolysis, thus increasing calcite precipitation and decreasing calcite solubility. To mitigate this effect, the database could be re-assessed with K values pertinent to 18C and the sensitivity to temperature could be evaluated.

Another critical addition to the modeling code will be microbial life. Modeling bacterial activity itself (not only as a fictive species) will induce many changes within the system. The presence of microbes can alter the saturation indices for carbonate minerals and can serve as nucleation sites for precipitation reactions (Fujita, 2004). Microbial attachment and detachment may also play a role in the level of uniformity of ureolysis and subsequent calcite precipitation throughout the well field. Inclusion of microbial life would help mitigate the need for the general assumptions and approximations inherent in our application of the Fidaleo and Lavecchia kinetics. This kinetic approximation, however could be improved without the addition of a bacterial within PHREEQC. The reaction network could be further explored with inversion software such as UCODE. This technique could provide us with parameter approximations that are more appropriate for the VZRP application. Another option would be to create a set of experiments to establish our own kinetic parameters, instead of those developed for jack-bean urease.

A correlation between calcite precipitation (and potentially solid solution precipitation with strontium) and changes is permeability and porosity would be a useful topic to research. Precipitation may decrease permeability and porosity, lending to a number of unknown ramifications such as increased pore velocity or even clogging or the formation of preferential pathways.

An interesting and useful exercise may be to compare these model results to those of a different modeling code. Geochemist's Workbench, PumpIt, and TOUGHREACT are all modeling platforms that include the ability to model this application. For example, TOUGHREACT may be used. The reaction network for this application within

PHREEQC2 is largely the same as that applied to the column simulations currently modeled with TOUGHREACT. Thus, TOUGHREACT's Eulerian formulation can be utilized for verification of the PHREEQC2 and streamtube ensemble simulation, which is considered Lagrangian. Conversely, PHREEQC2 could be used to validate results produced by TOUGHREACT's columnar modeling. Ideally, comparison between the models, regardless of application, should yield similar results.

6. Conclusions

An innovative bioremediation strategy that involves the co-precipitation of strontium with calcite via urea hydrolysis has been suggested to immobilize the contaminant at the Idaho National Technology and Engineering Center (INTEC). To evaluate the potential of this remediation technique, a variable velocity streamtube ensemble with a kinetic rate formulation is applied to field results.

This model can be easily adjusted for different sites with different chemistry and transport parameters. The benefit of a streamtube ensemble is the ability to predict breakthroughs without knowledge of subsurface heterogeneity. Site exploration is costly, potentially inaccurate, and often impossible. Normalization of a tracer test incorporates many of the underground unknowns, eliminating the need for extensive knowledge of the aquifer properties.

This exercise introduced dissolution potential to the VZRP system. Previously, all analysis performed on the site suggested that calcite remained supersaturated, thus ensuring permanent strontium immobilization. However, a simple batch run on the initial conditions found in well 2024 demonstrated that calcite is actually undersaturated and will precipitate when the ambient water inevitably returns to the system.

A variable velocity streamtube ensemble is an appropriate choice for systems with kinetic reactions with multiple components, with kinetic reaction rates that vary in space, when the reactions involve multiple phases (e.g. heterogeneous reactions), and/or when they impact physical characteristics (porosity/permeability). Ureolytically driven calcite precipitation exhibits all of these characteristics: it is a multi-component system involving kinetic degradation of urea to produce ammonium, bicarbonate, and pH. This ultimately results in calcite precipitation (formation of a solid) that will also affect the system's porosity and permeability. Modeling for the VZRP demonstrated that variable velocity within streamtubes does effect the quantity and location of calcite precipitation along the streamline. This knowledge is important because a constant velocity ensemble has the potential to inappropriately over or under predict calcite precipitation, and thus strontianite immobilization. An over prediction would be an inefficient use of computational and experimental resources; an under prediction may result in radioactive contaminant leaching into the Snake River Plain Aquifer.

Upon evaluation of the sensitivity of the number of streamtubes, an interesting conclusion was developed: the number of streamtubes is proportional to the degree of

mixing. The single streamtube exhibits complete lateral mixing. Adjustment of the longitudinal mixing can be obtained by changing the dispersivity (a customizable parameter within PHREEQC). With increasing numbers of streamtubes, less lateral mixing is apparent. The ensemble with 17 streamtubes exhibited less lateral mixing than both the 7 and 1 streamtube ensembles. Again, the longitudinal mixing can be adjusted by changing the dispersivity.

This study demonstrates that it is possible to model the immobilization of strontium within a calcite precipitation matrix as a result of bacterial ureolysis using a Lagrangian technique. Utilization of a non-reactive tracer test provides the model with the appropriate travel times for each streamtube. Additionally, sufficient knowledge of the chemical properties of the aquifer and the reaction network provide an adequate foundation to build a chemical model. Although this model may be improved in a variety of ways, it is still capable of predicting self-consistent and theoretically stable results in the form of breakthrough curves and calcite precipitation profiles.

8. References

Baker, K., Hull, L., Bennett, J., Ansley, S., Heath, G. (2004). "Conceptual models of flow through a heterogeneous, layered Vadose zone under a percolation pond." *Idaho National Engineering and Environmental Laboratory*. Accessed 3 June 2008 from <http://www.osti.gov/em52/interim_reports/86679interim.pdf>.

Bethke, Craig M. *Geochemical and Biogeochemical Reaction Modeling*. New York: Cambridge University Press, 2008. Print.

Booster, J.L., van Meurs, G.A., Pruiksma, J.P., van Paassen, L.A., Harkes, M.P., and Whiffin, V.S. (2008). "1D modelling of microbially induced calcite precipitation for geotechnical applications." Proceedings. International conference on BioGeoCivil Engineering, Delft, 2008.

Charbeneau, R. *Groundwater Hydraulics and Pollutant Transport*. New Jersey: Prentice-Hall, Inc., 2000. Print.

Cirpka, O., and Kitanidis, P. (2001). "Travel-time based model of bioremediation using circulation wells." *Ground Water*, 39(3), 422-432.

Crane, M., and Blunt, M. (1999). "Streamline-based simulation of solute transport." *Water Resources Research*, 35(10), 3061-3078.

Curti, E. (1999). "Coprecipitation of radionuclides with calcite: Estimation of partition coefficients based on a review of laboratory investigations and geochemical data." *Applied Geochemistry*, 14, 433-445.

Fidaleo, M. and Lavecchia, R. (2003). "Kinetic study of enzymatic urea hydrolysis in the pH range 4-9." *Chem. Biochem. Eng. Q.,* 17(4), 311-318.

Fujita, Y., Redden, G., Ingram, J., Cortez, M., Ferris, F., and Smith, R. (2004). "Strontium incorporation into calcite generated by bacterial ureolysis." *Geochimica et Cosmochimica Acta*, 68(15), 3261-3270.

Fujita, Y., Taylor, J., Gresham, T., Delwiche, M., Colwell, F., McLing, T., Petzke, L., and Smith, R. (2008). "Stimulation of microbial urea hydrolysis in groundwater to enhance calcite precipitation." *Environmental Science and Technology*, 42, 3025-3032.

Ginn, T. R., C.S. Simmons, and B.D. Wood (1995) "Stochastic-Convective Transport with Nonlinear Reaction: Biodegradation with Microbial Growth" *Water Resources Research*, Vol. 31, 2689-2700.

Ginn, T. R. Stochastic-convective transport with nonlinear reactions and mixing: Finite streamtube ensemble formulation for multicomponent reaction systems with intra-streamtube dispersion, J. Contaminant Hydrology, 47:1-28, 2001.

Ginn, T. R., E. M. Murphy, A. Chilakapati, U. Seeboonruang, Stochastic-convective transport with nonlinear reactions and mixing: Application to intermediate-scale experiments in aerobic biodegradation in saturated porous media, J. Contaminant Hydrology, 48:121-149, 2001.

Ginn, T. (2009a) Lecture on Potential Theory. Engineering: Civil 272B.

Ginn, T. (2009b) Lecture on Method of Characteristics in Residence-Time Distributions. Engineering: Civil 272B.

Harkes, M.P., Booster, J.L., van Paassen, L.A., van Loosdrecht, M.C.M., and Whiffin, V.S. (2008). "Microbial induced carbonate precipitation as ground improvement method – bacterial fixation and empirical correlation CaCO3 vs strength." Proceedings. International conference on BioGeoCivil Engineering, Delft, 2008.

Jensen, N.G. (2007) Lecture on Root Finding Methods. Engineering and Applied Science, Davis: 115.

Langmuir, D. *Aqueous Environmental Geochemistry*. New Jersey: Prentice-Hall Inc., 1997. Print.

Luo, J., and Kitanidis, P. (2004). "Fluid residence times within a recirculation zone created by an extraction-injection well pair." *Journal of Hydrology*, 295, 149-162.

Luo, J., Wu, W., Fienen, M., Jardine, P., Mehlhorn, T., Watson, D., Cirpka, O., Criddle, C., and Kitanidis, P. (2006). "A nested-cell approach for in situ remediation." *Ground Water*, 44(2), 266-274.

Luo, J., Cirpka, O. (2008). "Travel-time based descriptions of transport and mixing in heterogeneous domains." *Water Resources Research*, 44, W09407.

Mathsoft Engineering and Education, Inc. (2005). Mathcad Version 13.

Martinez, B. (2009). "Bio-mediated soil improvement: Load transfer mechanisms at the micro- and macro- scales." Proceedings. Advances in Ground Improvement: Research to Practice in the United States and China, American Society of Civil Engineers, Florida, 2009.

Mitchell, A., and Ferris, F.G. (2006a). "Effect of strontium contaminants upon the size and solubility of calcite crystals precipitated by the bacterial hydrolysis of urea." *Environmental Science and Technology*, 40, 1008-10a4.

Mitchell, A., and Ferris, F.G. (2006b). "The influence of *Bacillus pasteurii* on the nucleation and growth of calcium carbonate." *Geomicrobiology Journal*, 23, 213-226.

Morel, F., and Hering, J. *Principles and Applications of Aquatic Chemistry*. New York: John Wiley and Sons, Inc., 1993. Print.

Muller, D. (1956). "A method for solving algebraic equations using an automatic computer." *Mathematical Tables and Other Aids to Computation*, American Mathematical Society, 10(56), 208-215.

Parkhurst, D., and C. Appelo. (1999). "User's guide to PHREEQC (Version 2) – A computer program for speciation, batch-reaction, one-dimensional transport, and inverse geochemical calculations." Water-Resources Investigations Report 99-4259.

Pingitore, N.E., Lytle, F.W., Davies, B.M., Eastman, M.P., Eller, P.G. and Larson, E.M. (1992). "Mode of incorporation of Sr2+ in calcite: Determination by X-ray absorption spectroscopy." *Geochimica et Cosmochimica Acta*, 56, 1531-1538.

Pollock, D. (1988). "Semianalytical computation of path lines for finite-difference models." *Ground water*, 26(6), 743-750.

Seshadri, V. *The Inverse Gaussian Distribution: A Case Study in Exponential Families*. New York: Oxford University Press Inc., 1993. Print.

Seeboonruang U. and Ginn, T. R. (2006) "Upscaling Heterogeneity in Aquifer Reactivity via Exposure-time Concept: Forward Modeling," Journal of Contaminant Hydrology, 84 (3-4): 127-154 March 2006.

Simmons, C., Ginn, T., and Wood, B. (1995). "Stochastic-convective transport with nonlinear reaction: Mathematical framework." *Water Resources Research*, 31(11), 2675-2688.

Spycher, N. (2009). Personal correspondance.

Tanis, R. and Naylor, A. (1968). "Physical and chemical studies of a low-molecular-weight form of Urease." *Biochemical Journal*, 108(5), 771-777.

Taylor, J. (2008). "VZRP Summer 2008." Presentation. Calcite Workshop, Center for Advanced Energy Studies, Idaho, 2008.

Tesoriero, A.J. and Pankow, J.F. (1996). "Solid solution partitioning of Sr2+, Ba2+, and Cd2+ to calcite." *Geochemica et Cosmochimica Acta*, 60(6), 1053-1063.

Tipton, K. and Dixon, H. (1979). "Effects of pH on enzymes." *Methods in Enzymology*, 63, 183-234.

US Department of Energy, (2003). "Bioremediation of metals and radionuclides, what it is and how it works." Natural and Accelerated Bioremediation Research Program.

Warren, L.A. , Maurice, P.A. , Parmar, N. and Ferris, F.G. (2001). "Microbially mediated calcium carbonate precipitation: Implications for interpreting calcite precipitation and for solid-phase capture of inorganic contaminants." *Geomicrobiology Journal*, 18(1), 93-115.

Wood, W. and Low, W. (1986). "Aqueous geochemistry and diagenesis in the eastern Snake River Plain Aquifer system, Idaho." *Geological Society of America Bulletin*, v. 97, 1456-1466.

Young, T. (2008) Lecture on Activity Coefficients. Engineering: Civil 245A.

9. Appendix

Appendix A: PHREEQC Input File

```
TITLE Ureolysis for the Co-precipitation of Trace Strontium with Calcite
**********
PLEASE NOTE: This problem requires database file minteq.v4-ns6b!!
**********
Example 10 has solid solutions
SOLUTION_MASTER_SPECIES        #Urea is not in the database, including this here as well as the SOLUTION_SPECIES below establishes it as a component
   Urea Urea  0.0 1.0    1.   #Defines the element, species, alkalinity, formula (here 1 Urea = 1 Urea), element weight
        Z Z- 0.0 1.0 1.
SOLUTION_SPECIES
  Urea = Urea
   log_k      0.0
  Z- = Z-                    # from Nic's F&L summary notes 2008Oct19-INLcal-FidaleoCheck
   log_k                0.0                # must put soln master species on left
  Z- + 2H+ = H2Z+
        log_k          14.017
  Z- + H+ = HZ
   log_k                7.896
  Z- + H+ + AmmH+ = HZAmmH+
        log_k          9.81

EXCHANGE_MASTER_SPECIES                   #Defines "X" as the exchange species.  This is used instead of surface complexation, which could be addressed later
        X       X-

EXCHANGE_SPECIES                          #This is taken from wateq4f db, not found in the minteq.v4 db
        X- = X-
        log_k          0.0

        Na+ + X- = NaX
        log_k          0.0
        -gamma         4.0     0.075

        K+ + X- = KX
        log_k          0.7
        -gamma         3.5     0.015
```

```
        H+ + X- = HX
        log_k           1.0

        AmmH+ + X- = AmmHX
        log_k           0.6

#       NH4+ + X- = NH4X
#       log_k           0.6

        Ca+2 + 2X- = CaX2
        log_k           0.8
        -gamma          5.0     0.165

        Mg+2 + 2X- = MgX2
        log_k           0.6
        -gamma          5.5     0.2

        Sr+2 + 2X- = SrX2
        log_k           0.91
        -gamma          5.26    0.121

# change to 1-N
##############################################################################
#######################

SOLUTION 1-17 Initially in Aquifer   #these values from joannas spreadsheet
      pH      7.33
      pe      4.0    # O2(g)   -0.7
      temp    25
      units   mol/kgw
      Ca      1.015769e-3
      C       0.003361057      #Calcite 0 #TIC from 7-18 Summary file
                  Sr                2.961653e-6
      Cl      1.183539e-3         #          charge                    #Charge is commented out.
There are no obvious differences if it is commented out or left in
                  Nitri     0
      Mg                    0.455462e-3
      Na          1.742079e-3     #charge
      K           0.061384e-3
      Z           2.083e-7
      F           0.013159e-3
                  Br                0.007759e-3
                  Sulfate 0.228801e-3
```

```
# change to 1-N
##############################################################################
#######################

EXCHANGE 1-17
	-equil with solution 1-17	# I did not find a notable difference when I set
equilibrium from just Solution 1 to Solution 1-20, I'm not quite sure what the program is
actually doing, and would probably require a detailed look into the output file
	X	.0005		# This value was chosen because it works...

#SOLID_SOLUTIONS 1-50
#	Ca(x)Sr(1-x)CO3
#		-comp	Calcite	0
#		-comp	Strontianite	0
#		-Gugg_nondim	3.43	-1.82		# Taken from Example 14 for
strontianite and aragonite solid solutions

# change to 1-N
##############################################################################
#######################

EQUILIBRIUM_PHASES 1-17
	Calcite	0.0	0
USE solution 1					# Moved from before
solid_solutions, and added save and end below
SAVE solution 1-17
END

SOLUTION 0 Br Urea injectate	# Solution 0 is required for transport.  This is what
is injected through the simulation.  Taken from the "tank" values.
	pH	7.75
	pe	4.0	# O2(g)	-0.7
	temp	25
	units	mol/kgw
	Ca	0.970607e-3
	C	3.731548e-3
		Sr		2.639808e-6
	Cl	0.499817e-3	#	charge		#Charge is commented out.
There are no obvious differences if it is commented out or left in
		Nitri	0.000435e-3
		Amm		0.014680e-3
	Mg		0.458341e-3
	Na		1.331895e-3
	K		1.961211e-3
	Z		2.083e-7	#this is the value from F&L good for a starting pt, possible
inversion later?
```

```
        F           0.007369e-3
                    Br              1.810297e-3
                    Sulfate 0.195091e-3
                    Urea    16.45504e-3

RATES # Urea hydrolysis rate (Fidaleo and Lavecchia, 2003)
        ureolysis     #crazy comments are for plugging in k(25) instead of exp[Ea...] term.
Must compare still.
        -start
                30 Km=parm(1)
                60 Kp=parm(2)
                90 k=parm(3)
                94 f2 = MOL("Urea")/(Km+MOL("Urea"))
                96 f3 = Kp/(Kp+MOL("AmmH+"))
                100 rate = k*480000/60*MOL("HZ")*f2*f3
                110 moles = rate*TIME           #time units are in SECONDS
                200 SAVE moles
        -end

# change to 1-N
##########################################################################
########################

KINETICS 1-17         #aka Bob Smith's Kinetics
ureolysis
      -Formula  Urea  -1.0   H2O -2  AmmH+  2  CO3-2  1   # Hydrolysis of urea
      -parms  3.21e-3 1.22e-2 1.83e-2


# change cells, lengths, shifts, and timestep
##########################################################################
########################

USER_GRAPH  # Plots speciation including moles of mineral phases, this works with
TRANSPORT, must change print cells to 50, comment out punch freq
-headings Time Urea(mmol/kgw) AmmH+(mmol/kgw) Ca(mmol/kgw) Calcite(mmol) Br
pH
-chart_title "Ureolysis for the Co-precipitation of Sr-90"
-axis_titles "Time" "Molality" "pH"
-axis_scale x_axis 0 550 20 5
-axis_scale y_axis 0 16 1 0.5
-axis_scale secondary_y_axis 6 10 0.5 0.1
-initial_solutions false
-plot_concentration_vs time
-start
10 GRAPH_X TOTAL_TIME
```

```
20 GRAPH_Y MOL("Urea")*1e3 MOL("AmmH+")*1e3 MOL("Ca+2")*1e3
EQUI("Calcite")*1e3 MOL("Br-")*1e3
30 GRAPH_SY -LA("H+")
#30 GRAPH_SY S_S("Calcite")*1e3 #S_S("Strontianite")*1e4
-end

TRANSPORT                    # Length units in METERS
      -cells        17
                -length                 0.0902155
0.0605641
0.0506666
0.0454522
0.0422896
0.0402776
0.0390207
0.0383265
0.0381042
0.0383265
0.0390207
0.0402776
0.0422896
0.0454522
0.0506666
0.0605641
0.0902155


      -shifts       217                 # run for as long as needed to match SS for longest
tube: 230mins/dt = shifts (approx)
                -time_step              1.06            # actual is 1.059
#               -diffc          0.0e-9              # from example 11
      -dispersivity   0.002             # from example 11, does mixruns?
      -correct_disp   true
                -punch          17                      # this defines which cells will be
recorded, comment for calcite over length
                -punch_frequency 1                      # the frequencies refer to which
shifts will be recorded, uncomment for calcite over length
                -print_cells    17      # for plotting molalities over time ONLY
#               -print_cells    1-17            # for plotting calcite over length ONLY
#               -print_frequency 1-17

#SAVE solution 1-17
END
```

```
SOLUTION 0 #injection off, no Br or urea... same as 1-17 (assume ambient gw is same as initial conds)
	pH	 7.33
	pe	 4.0	# O2(g)	-0.7
	temp	 25
	units	 mol/kgw
	Ca	 1.015769e-3
	C	 0.003361057	#Calcite 0 #TIC from 7-18 Summary file
		Sr		2.961653e-6
	Cl	 1.183539e-3	#	charge		#Charge is commented out. There are no obvious differences if it is commented out or left in
		Nitri	0
	Mg		0.455462e-3
	Na		1.742079e-3	#charge
	K		0.061384e-3
	Z		2.083e-7
	F		0.013159e-3
		Br		0.007759e-3
		Sulfate	0.228801e-3

# change cells, lengths, shifts, and timestep
##########################################################################################

TRANSPORT			# Length units in METERS
	-shifts	300			# run for as long as needed to match SS for longest tube: 240mins/dt = shifts (approx)



PRINT
	-reset true



# To run any of the following user graph statements, remove comment denotation for that block.  Note: some of these work with transport, others do not.

# change time axes to appropriate values
##########################################################################################



#USER_GRAPH  # Plots calcite pptn profile over the column, must change print freq to 1-50 in transport
```

```
#-headings Distance Calcite(mmol)
#-chart_title "Ureolysis for the Co-precipitation of Sr-90"
#-axis_titles "Distance" "Moles"
#-axis_scale x_axis 0 1 0.5 0.1
#-axis_scale y_axis 0 0.5 0.1 0.05
#-initial_solutions false
#-plot_concentration_vs x
#-start
#10 GRAPH_X DIST
#20 GRAPH_Y EQUI("Calcite")*1e3
#-end

#USER_GRAPH  # Plots BTC of Cl, this works with TRANSPORT
#-headings Time Cl(mmol/kgw)
#-chart_title "Ureolysis for the Co-precipitation of Sr-90"
#-axis_titles "Time" "Molality" "Moles"
#-axis_scale x_axis 0 10000 5000 1000
#-axis_scale y_axis 0 3 1 0.5
#-axis_scale secondary_y_axis 0 1 0.5 0.1
#-initial_solutions false
#-plot_concentration_vs time
#-start
#10 GRAPH_X TOTAL_TIME
#20 GRAPH_Y MOL("Cl-")*1e3
#-end

END
```

Appendix B: Section of a PHREEQC Output File

```
   Input file: C:\Users\Tess\AppData\Local\Temp\phrq0000.tmp
  Output file: C:\Users\Tess\Desktop\from flash\calcite\Streamtubes\Constant
Velocity\7tubes aug20\2024\may 13\st1 allchem aug26 tail.out
Database file: C:\Program Files\Phreeqc\Databases\minteq.v4-ns6b.dat.txt

------------------
Reading data base.
------------------

        SOLUTION_MASTER_SPECIES
        SOLUTION_SPECIES
        SOLUTION_SPECIES
        PHASES
        PHASES
        SURFACE_MASTER_SPECIES
        SURFACE_SPECIES
        END
-----------------------------------
Reading input data for simulation 1.
-----------------------------------

        TITLE Ureolysis for the Co-precipitation of Trace Strontium with Calcite
        **********
        PLEASE NOTE: This problem requires database file minteq.v4-ns6b!!
        **********
        Example 10 has solid solutions
        SOLUTION_MASTER_SPECIES        #Urea is not in the database, including
this here as well as the SOLUTION_SPECIES below establishes it as a component
            Urea Urea  0.0 1.0    1.    #Defines the element, species, alkalinity, formula
(here 1 Urea = 1 Urea), element weight
                Z Z- 0.0 1.0 1.
        SOLUTION_SPECIES
          Urea = Urea
           log_k       0.0
          Z- = Z-                    # from Nic's F&L summary notes 2008Oct19-INLcal-
FidaleoCheck
           log_k                 0.0                  # must put soln master species on left
          Z- + 2H+ = H2Z+
                log_k            14.017
```

```
Z- + H+ = HZ
 log_k                  7.896
Z- + H+ + AmmH+ = HZAmmH+
        log_k           9.81
EXCHANGE_MASTER_SPECIES                 #Defines "X" as the exchange species.  This is used instead of surface complexation, which could be addressed later
        X       X-
EXCHANGE_SPECIES                        #This is taken from wateq4f db, not found in the minteq.v4 db
        X- = X-
        log_k           0.0
        Na+ + X- = NaX
        log_k           0.0
        gamma4.0        0.075
        K+ + X- = KX
        log_k           0.7
        gamma3.5        0.015
        H+ + X- = HX
        log_k           1.0
        AmmH+ + X- = AmmHX
        log_k           0.6
        Ca+2 + 2X- = CaX2
        log_k           0.8
        gamma5.0        0.165
        Mg+2 + 2X- = MgX2
        log_k           0.6
        gamma5.5        0.2
        Sr+2 + 2X- = SrX2
        log_k           0.91
        gamma5.26       0.121
SOLUTION 1-17 Initially in Aquifer   #these values from joannas spreadsheet
    pH      7.33
    pe      4.0    # O2(g)   -0.7
    temp    25
    units   mol/kgw
    Ca      1.015769e-3
    C       0.003361057      #Calcite 0 #TIC from 7-18 Summary file
            Sr              2.961653e-6
    Cl      1.183539e-3      #       charge                  #Charge is commented out.  There are no obvious differences if it is commented out or left in
            Nitri   0
    Mg              0.455462e-3
    Na          1.742079e-3     #charge
    K           0.061384e-3
    Z           2.083e-7
    F           0.013159e-3
```

```
                    Br              0.007759e-3
                    Sulfate 0.228801e-3
        EXCHANGE 1-17
            equilibrate with solution 1-17      # I did not find a notable difference when I
set equilibrium from just Solution 1 to Solution 1-20, I'm not quite sure what the program
is actually doing, and would probably require a detailed look into the output file
            X       .0005               # This value was chosen because it works...
        EQUILIBRIUM_PHASES 1-17
            Calcite         0.0     0
        USE solution 1                                          # Moved from before
solid_solutions, and added save and end below
        SAVE solution 1-17
        END
-----
TITLE
-----

 Ureolysis for the Co-precipitation of Trace Strontium with Calcite
**********
PLEASE NOTE: This problem requires database file minteq.v4-ns6b!!
**********
Example 10 has solid solutions

-------------------------------------------
Beginning of initial solution calculations.
-------------------------------------------

Initial solution 1.       Initially in Aquifer

----------------------------Solution composition------------------------------

        Elements          Molality       Moles

        Br              7.759e-06   7.759e-06
        C               3.361e-03   3.361e-03
        Ca               1.016e-03   1.016e-03
        Cl              1.184e-03   1.184e-03
        F               1.316e-05   1.316e-05
        K               6.138e-05   6.138e-05
        Mg               4.555e-04   4.555e-04
        Na               1.742e-03   1.742e-03
        Sr              2.962e-06   2.962e-06
        Sulfate           2.288e-04   2.288e-04
        Z               2.083e-07   2.083e-07

---------------------------Description of solution----------------------------
```

pH = 7.330
pe = 4.000
Activity of water = 1.000
Ionic strength = 6.218e-03
Mass of water (kg) = 1.000e+00
Total alkalinity (eq/kg) = 3.077e-03
Total CO2 (mol/kg) = 3.361e-03
Temperature (deg C) = 25.000
Electrical balance (eq) = 1.282e-05
Percent error, 100*(Cat-|An|)/(Cat+|An|) = 0.14
Iterations = 6
Total H = 1.110173e+02
Total O = 5.551692e+01

----------Distribution of species----------

Species	Molality	Log Activity	Log Molality	Log Activity	Gamma
OH-	2.343e-07	2.152e-07	-6.630	-6.667	-0.037
H+	5.085e-08	4.677e-08	-7.294	-7.330	-0.036
H2O	5.551e+01	9.999e-01	1.744	-0.000	0.000
Br	7.759e-06				
Br-	7.759e-06	7.137e-06	-5.110	-5.146	-0.036
C(4)	3.361e-03				
HCO3-	3.011e-03	2.776e-03	-2.521	-2.557	-0.035
H2CO3	2.920e-04	2.920e-04	-3.535	-3.535	0.000
CaHCO3+	3.819e-05	3.525e-05	-4.418	-4.453	-0.035
MgHCO3+	9.656e-06	8.880e-06	-5.015	-5.052	-0.036
CO3-2	3.886e-06	2.783e-06	-5.410	-5.556	-0.145
CaCO3	3.007e-06	3.007e-06	-5.522	-5.522	0.000
NaHCO3	2.496e-06	2.496e-06	-5.603	-5.603	0.000
MgCO3	7.235e-07	7.235e-07	-6.141	-6.141	0.000
SrHCO3+	9.791e-08	9.038e-08	-7.009	-7.044	-0.035
NaCO3-	8.985e-08	8.285e-08	-7.046	-7.082	-0.035
SrCO3	3.606e-09	3.606e-09	-8.443	-8.443	0.000
Ca	1.016e-03				
Ca+2	9.524e-04	6.819e-04	-3.021	-3.166	-0.145
CaHCO3+	3.819e-05	3.525e-05	-4.418	-4.453	-0.035
CaSulfate	2.206e-05	2.206e-05	-4.656	-4.656	0.000
CaCO3	3.007e-06	3.007e-06	-5.522	-5.522	0.000
CaF+	9.370e-08	8.633e-08	-7.028	-7.064	-0.036
CaOH+	3.173e-09	2.929e-09	-8.499	-8.533	-0.035
Cl	1.184e-03				
Cl-	1.184e-03	1.089e-03	-2.927	-2.963	-0.036

F	1.316e-05				
F-	1.261e-05	1.160e-05	-4.899	-4.936	-0.036
MgF+	4.420e-07	4.068e-07	-6.355	-6.391	-0.036
CaF+	9.370e-08	8.633e-08	-7.028	-7.064	-0.036
NaF	1.170e-08	1.170e-08	-7.932	-7.932	0.000
HF	8.025e-10	8.025e-10	-9.096	-9.096	0.000
SrF+	9.020e-11	8.224e-11	-10.045	-10.085	-0.040
HF2-	3.853e-14	3.539e-14	-13.414	-13.451	-0.037
H2F2	1.726e-18	1.726e-18	-17.763	-17.763	0.000
H(0)	3.093e-26				
H2	1.547e-26	1.549e-26	-25.811	-25.810	0.001
K	6.138e-05				
K+	6.132e-05	5.641e-05	-4.212	-4.249	-0.036
KSulfate-	6.117e-08	5.640e-08	-7.213	-7.249	-0.035
Mg	4.555e-04				
Mg+2	4.366e-04	3.126e-04	-3.360	-3.505	-0.145
MgHCO3+	9.656e-06	8.880e-06	-5.015	-5.052	-0.036
MgSulfate	8.034e-06	8.034e-06	-5.095	-5.095	0.000
MgCO3	7.235e-07	7.235e-07	-6.141	-6.141	0.000
MgF+	4.420e-07	4.068e-07	-6.355	-6.391	-0.036
MgOH+	2.899e-08	2.679e-08	-7.538	-7.572	-0.034
Na	1.742e-03				
Na+	1.738e-03	1.599e-03	-2.760	-2.796	-0.036
NaHCO3	2.496e-06	2.496e-06	-5.603	-5.603	0.000
NaSulfate-	1.315e-06	1.213e-06	-5.881	-5.916	-0.035
NaCO3-	8.985e-08	8.285e-08	-7.046	-7.082	-0.035
NaF	1.170e-08	1.170e-08	-7.932	-7.932	0.000
O(0)	0.000e+00				
O2	0.000e+00	0.000e+00	-40.676	-40.675	0.001
Sr	2.962e-06				
Sr+2	2.803e-06	2.007e-06	-5.552	-5.697	-0.145
SrHCO3+	9.791e-08	9.038e-08	-7.009	-7.044	-0.035
SrSulfate	5.657e-08	5.657e-08	-7.247	-7.247	0.000
SrCO3	3.606e-09	3.606e-09	-8.443	-8.443	0.000
SrF+	9.020e-11	8.224e-11	-10.045	-10.085	-0.040
SrOH+	3.098e-12	2.855e-12	-11.509	-11.544	-0.036
Sulfate	2.288e-04				
Sulfate-2	1.973e-04	1.412e-04	-3.705	-3.850	-0.145
CaSulfate	2.206e-05	2.206e-05	-4.656	-4.656	0.000
MgSulfate	8.034e-06	8.034e-06	-5.095	-5.095	0.000
NaSulfate-	1.315e-06	1.213e-06	-5.881	-5.916	-0.035
KSulfate-	6.117e-08	5.640e-08	-7.213	-7.249	-0.035
SrSulfate	5.657e-08	5.657e-08	-7.247	-7.247	0.000
HSulfate-	7.013e-10	6.456e-10	-9.154	-9.190	-0.036
Z	2.083e-07				
HZ	1.528e-07	1.530e-07	-6.816	-6.815	0.001

Z-	4.519e-08	4.157e-08	-7.345	-7.381	-0.036
H2Z+	1.028e-08	9.458e-09	-7.988	-8.024	-0.036

----------Saturation indices----------

Phase	SI	log IAP	log KT	
Anhydrite	-2.66	-7.02	-4.36	CaSulfate
Aragonite	-0.42	-8.72	-8.30	CaCO3
Artinite	-7.51	2.09	9.60	MgCO3:Mg(OH)2:3H2O
Brucite	-5.69	11.15	16.84	Mg(OH)2
Calcite	-0.24	-8.72	-8.48	CaCO3
Celestite	-2.93	-9.55	-6.62	SrSulfate
CH4(g)	-69.81	-110.86	-41.05	CH4
CO2(g)	-2.07	-20.22	-18.15	CO2
Dolomite(disordered)	-1.24	-17.78	-16.54	CaMg(CO3)2
Dolomite(ordered)	-0.69	-17.78	-17.09	CaMg(CO3)2
Epsomite	-5.23	-7.36	-2.13	MgSulfate:7H2O
Fluorite	-2.54	-13.04	-10.50	CaF2
Gypsum	-2.41	-7.02	-4.61	CaSulfate:2H2O
Halite	-7.36	-5.76	1.60	NaCl
Huntite	-5.94	-35.90	-29.97	CaMg3(CO3)4
Hydromagnesite	-16.32	-25.09	-8.77	Mg5(CO3)4(OH)2:4H2O
Lime	-21.21	11.49	32.70	CaO
Magnesite	-1.60	-9.06	-7.46	MgCO3
Mg(OH)2(active)	-7.64	11.15	18.79	Mg(OH)2
MgF2	-5.25	-13.38	-8.13	MgF2
Mirabilite	-8.33	-9.44	-1.11	Na2Sulfate:10H2O
Natron	-9.84	-11.15	-1.31	Na2CO3:10H2O
Nesquehonite	-4.39	-9.06	-4.67	MgCO3:3H2O
O2(g)	-37.77	45.32	83.09	O2
Periclase	-10.43	11.15	21.58	MgO
Portlandite	-11.31	11.49	22.80	Ca(OH)2
SrF2	-6.99	-15.57	-8.58	SrF2
Strontianite	-1.98	-11.25	-9.27	SrCO3
Thenardite	-9.76	-9.44	0.32	Na2Sulfate
Thermonatrite	-11.78	-11.15	0.64	Na2CO3:H2O

Beginning of initial exchange-composition calculations.

Exchange 1.

X 5.000e-04 mol

Species	Moles	Equiv-alents	Equivalent Fraction	Log Gamma
CaX2	1.891e-04	3.781e-04	7.563e-01	-0.141
MgX2	5.445e-05	1.089e-04	2.178e-01	-0.139
NaX	9.786e-06	9.786e-06	1.957e-02	-0.036
KX	1.733e-06	1.733e-06	3.467e-03	-0.037
SrX2	7.160e-07	1.432e-06	2.864e-03	-0.141
HX	2.635e-09	2.635e-09	5.271e-06	0.000

Beginning of batch-reaction calculations.

Reaction step 1.

Using solution 1. Initially in Aquifer
Using exchange 1. Exchange assemblage after simulation 1.
Using pure phase assemblage 1.

----------Phase assemblage----------

Phase	SI	log IAP	log KT	Moles in assemblage: Initial	Final	Delta
Calcite	-0.24	-8.72	-8.48	0.000e+00	0	0.000e+00

----------Exchange composition----------

X 5.000e-04 mol

Species	Moles	Equiv-alents	Equivalent Fraction	Log Gamma
CaX2	1.891e-04	3.781e-04	7.563e-01	-0.141
MgX2	5.445e-05	1.089e-04	2.178e-01	-0.139
NaX	9.786e-06	9.786e-06	1.957e-02	-0.036
KX	1.733e-06	1.733e-06	3.467e-03	-0.037
SrX2	7.160e-07	1.432e-06	2.864e-03	-0.141
HX	2.635e-09	2.635e-09	5.271e-06	0.000

----------Solution composition----------

Elements	Molality	Moles
Br	7.759e-06	7.759e-06

C	3.361e-03	3.361e-03
Ca	1.016e-03	1.016e-03
Cl	1.184e-03	1.184e-03
F	1.316e-05	1.316e-05
K	6.138e-05	6.138e-05
Mg	4.555e-04	4.555e-04
Na	1.742e-03	1.742e-03
Sr	2.962e-06	2.962e-06
Sulfate	2.288e-04	2.288e-04
Z	2.083e-07	2.083e-07

----------Description of solution----------

pH = 7.330 Charge balance
pe = 5.300 Adjusted to redox equilibrium
Activity of water = 1.000
Ionic strength = 6.218e-03
Mass of water (kg) = 1.000e+00
Total alkalinity (eq/kg) = 3.077e-03
Total CO2 (mol/kg) = 3.361e-03
Temperature (deg C) = 25.000
Electrical balance (eq) = 1.282e-05
Percent error, 100*(Cat-|An|)/(Cat+|An|) = 0.14
Iterations = 1
Total H = 1.110173e+02
Total O = 5.551692e+01

----------Distribution of species----------

Species	Molality	Log Activity	Log Molality	Log Activity	Gamma
OH-	2.343e-07	2.152e-07	-6.630	-6.667	-0.037
H+	5.085e-08	4.677e-08	-7.294	-7.330	-0.036
H2O	5.551e+01	9.999e-01	1.744	-0.000	0.000
Br	7.759e-06				
Br-	7.759e-06	7.137e-06	-5.110	-5.146	-0.036
C(4)	3.361e-03				
HCO3-	3.011e-03	2.776e-03	-2.521	-2.557	-0.035
H2CO3	2.920e-04	2.920e-04	-3.535	-3.535	0.000
CaHCO3+	3.819e-05	3.525e-05	-4.418	-4.453	-0.035
MgHCO3+	9.656e-06	8.880e-06	-5.015	-5.052	-0.036
CO3-2	3.886e-06	2.783e-06	-5.410	-5.556	-0.145
CaCO3	3.007e-06	3.007e-06	-5.522	-5.522	0.000
NaHCO3	2.496e-06	2.496e-06	-5.603	-5.603	0.000
MgCO3	7.235e-07	7.235e-07	-6.141	-6.141	0.000

SrHCO3+	9.791e-08	9.038e-08	-7.009	-7.044	-0.035
NaCO3-	8.985e-08	8.285e-08	-7.046	-7.082	-0.035
SrCO3	3.606e-09	3.606e-09	-8.443	-8.443	0.000
Ca	1.016e-03				
Ca+2	9.524e-04	6.819e-04	-3.021	-3.166	-0.145
CaHCO3+	3.819e-05	3.525e-05	-4.418	-4.453	-0.035
CaSulfate	2.206e-05	2.206e-05	-4.656	-4.656	0.000
CaCO3	3.007e-06	3.007e-06	-5.522	-5.522	0.000
CaF+	9.370e-08	8.633e-08	-7.028	-7.064	-0.036
CaOH+	3.173e-09	2.929e-09	-8.499	-8.533	-0.035
Cl	1.184e-03				
Cl-	1.184e-03	1.089e-03	-2.927	-2.963	-0.036
F	1.316e-05				
F-	1.261e-05	1.160e-05	-4.899	-4.936	-0.036
MgF+	4.420e-07	4.068e-07	-6.355	-6.391	-0.036
CaF+	9.370e-08	8.633e-08	-7.028	-7.064	-0.036
NaF	1.170e-08	1.170e-08	-7.932	-7.932	0.000
HF	8.025e-10	8.025e-10	-9.096	-9.096	0.000
SrF+	9.020e-11	8.224e-11	-10.045	-10.085	-0.040
HF2-	3.853e-14	3.539e-14	-13.414	-13.451	-0.037
H2F2	1.726e-18	1.726e-18	-17.763	-17.763	0.000
H(0)	7.770e-29				
H2	3.885e-29	3.890e-29	-28.411	-28.410	0.001
K	6.138e-05				
K+	6.132e-05	5.641e-05	-4.212	-4.249	-0.036
KSulfate-	6.117e-08	5.640e-08	-7.213	-7.249	-0.035
Mg	4.555e-04				
Mg+2	4.366e-04	3.126e-04	-3.360	-3.505	-0.145
MgHCO3+	9.656e-06	8.880e-06	-5.015	-5.052	-0.036
MgSulfate	8.034e-06	8.034e-06	-5.095	-5.095	0.000
MgCO3	7.235e-07	7.235e-07	-6.141	-6.141	0.000
MgF+	4.420e-07	4.068e-07	-6.355	-6.391	-0.036
MgOH+	2.899e-08	2.679e-08	-7.538	-7.572	-0.034
Na	1.742e-03				
Na+	1.738e-03	1.599e-03	-2.760	-2.796	-0.036
NaHCO3	2.496e-06	2.496e-06	-5.603	-5.603	0.000
NaSulfate-	1.315e-06	1.213e-06	-5.881	-5.916	-0.035
NaCO3-	8.985e-08	8.285e-08	-7.046	-7.082	-0.035
NaF	1.170e-08	1.170e-08	-7.932	-7.932	0.000
O(0)	6.687e-36				
O2	3.343e-36	3.348e-36	-35.476	-35.475	0.001
Sr	2.962e-06				
Sr+2	2.803e-06	2.007e-06	-5.552	-5.697	-0.145
SrHCO3+	9.791e-08	9.038e-08	-7.009	-7.044	-0.035
SrSulfate	5.657e-08	5.657e-08	-7.247	-7.247	0.000
SrCO3	3.606e-09	3.606e-09	-8.443	-8.443	0.000

SrF+	9.020e-11	8.224e-11	-10.045	-10.085	-0.040
SrOH+	3.098e-12	2.855e-12	-11.509	-11.544	-0.036
Sulfate	2.288e-04				
Sulfate-2	1.973e-04	1.412e-04	-3.705	-3.850	-0.145
CaSulfate	2.206e-05	2.206e-05	-4.656	-4.656	0.000
MgSulfate	8.034e-06	8.034e-06	-5.095	-5.095	0.000
NaSulfate-	1.315e-06	1.213e-06	-5.881	-5.916	-0.035
KSulfate-	6.117e-08	5.640e-08	-7.213	-7.249	-0.035
SrSulfate	5.657e-08	5.657e-08	-7.247	-7.247	0.000
HSulfate-	7.013e-10	6.456e-10	-9.154	-9.190	-0.036
Z	2.083e-07				
HZ	1.528e-07	1.530e-07	-6.816	-6.815	0.001
Z-	4.519e-08	4.157e-08	-7.345	-7.381	-0.036
H2Z+	1.028e-08	9.458e-09	-7.988	-8.024	-0.036

----------Saturation indices----------

Phase	SI	log IAP	log KT	
Anhydrite	-2.66	-7.02	-4.36	CaSulfate
Aragonite	-0.42	-8.72	-8.30	CaCO3
Artinite	-7.51	2.09	9.60	MgCO3:Mg(OH)2:3H2O
Brucite	-5.69	11.15	16.84	Mg(OH)2
Calcite	-0.24	-8.72	-8.48	CaCO3
Celestite	-2.93	-9.55	-6.62	SrSulfate
CH4(g)	-80.21	-121.26	-41.05	CH4
CO2(g)	-2.07	-20.22	-18.15	CO2
Dolomite(disordered)	-1.24	-17.78	-16.54	CaMg(CO3)2
Dolomite(ordered)	-0.69	-17.78	-17.09	CaMg(CO3)2
Epsomite	-5.23	-7.36	-2.13	MgSulfate:7H2O
Fluorite	-2.54	-13.04	-10.50	CaF2
Gypsum	-2.41	-7.02	-4.61	CaSulfate:2H2O
Halite	-7.36	-5.76	1.60	NaCl
Huntite	-5.94	-35.90	-29.97	CaMg3(CO3)4
Hydromagnesite	-16.32	-25.09	-8.77	Mg5(CO3)4(OH)2:4H2O
Lime	-21.21	11.49	32.70	CaO
Magnesite	-1.60	-9.06	-7.46	MgCO3
Mg(OH)2(active)	-7.64	11.15	18.79	Mg(OH)2
MgF2	-5.25	-13.38	-8.13	MgF2
Mirabilite	-8.33	-9.44	-1.11	Na2Sulfate:10H2O
Natron	-9.84	-11.15	-1.31	Na2CO3:10H2O
Nesquehonite	-4.39	-9.06	-4.67	MgCO3:3H2O
O2(g)	-32.57	50.52	83.09	O2
Periclase	-10.43	11.15	21.58	MgO
Portlandite	-11.31	11.49	22.80	Ca(OH)2
SrF2	-6.99	-15.57	-8.58	SrF2

```
Strontianite     -1.98  -11.25   -9.27  SrCO3
Thenardite       -9.76   -9.44    0.32  Na2Sulfate
Thermonatrite   -11.78  -11.15    0.64  Na2CO3:H2O
```

Appendix C: Section of the PHREEQC minteq.v4 De-coupled Database

```
#  $Id: minteq.v4.dat 85 2005-02-02 16:13:00Z dlpark $
#NS 11/06 use sverjensky data for Pb-S complexes
# NS6  start from  NS4, add Oxy for decoupled oxygen
#NS 7/06  decouple CuI and CuII
#NS 6/2006 add nitrogen gas
#NS 6/2006 couple Cu(I) and Cu(II) with HS/SO4
#N.S. 6/2006 Also modify Zn and Cu sulfide complexes
#N.S. 6/2006 Replace data for FeS (solid and aqueous) with Rickard 2006
#N.S. 10/05 decoupled redox for FeII/FeIII, SO4/HS-, NO3/NO3/NH4
SOLUTION_MASTER_SPECIES
Alkalinity      CO3-2           2.0     HCO3    61.0173
E               e-              0       0       0
O               H2O             0       O       16.00
O(-2)           H2O             0       O
O(0)            O2              0       O
Oxy             Oxy             0       32.00   32.00
Ag              Ag+             0.0     Ag      107.868
Al              Al+3            0.0     Al      26.9815
As              H3AsO4                  -1.0    As      74.9216
As(3)           H3AsO3                  0.0     As
As(5)           H3AsO4                  -1.0    As
B               H3BO3                   0.0     B       10.81
Ba              Ba+2            0.0     Ba      137.33
Be              Be+2            0.0     Be      9.0122
Br              Br-             0.0     Br      79.904
C               CO3-2           2.0     CO3     12.0111
C(4)            CO3-2           2.0     CO3     12.0111
Cyanide         Cyanide-        1.0     Cyanide 26.0177
Dom_a           Dom_a           0.0     C       12.0111
Dom_b           Dom_b           0.0     C       12.0111
Dom_c           Dom_c           0.0     C       12.0111
Ca              Ca+2            0.0     Ca      40.078
Cd              Cd+2            0.0     Cd      112.41
Cl              Cl-             0.0     Cl      35.453
Co              Co+3            -1.0    Co      58.9332
Co(2)           Co+2            0.0     Co
Co(3)           Co+3            -1.0    Co
Cr              CrO4-2                  1.0     Cr      51.996
Cr(2)           Cr+2            0.0     Cr
Cr(3)           Cr(OH)2+        0.0     Cr
Cr(6)           CrO4-2                  1.0     Cr
```

Cup	Cup+	0.0	63.546	63.546	
Cu	Cu+2	0.0	Cu	63.546	
#Cu(1)	Cu+	0.0	Cu		
#Cu(2)	Cu+2	0.0	Cu		
F	F-	0.0	F	18.9984	
Fe	Fe+3	-2.0	Fe	55.847	
Fe(3)	Fe+3	-2.0	Fe		
Feii	Feii+2	0.0	55.847	55.847	
H	H+	-1.0	H	1.0079	
H(0)	H2	0	H		
H(1)	H+	-1.0	H		
Hg	Hg(OH)2		0.0	Hg	200.59
Hg(0)	Hg	0.0	Hg		
Hg(1)	Hg2+2	0.0	Hg		
Hg(2)	Hg(OH)2		0.0	Hg	
I	I-	0.0	I	126.904	
K	K+	0.0	K	39.0983	
Li	Li+	0.0	Li	6.941	
Mg	Mg+2	0.0	Mg	24.305	
Mn	Mn+3	0.0	Mn	54.938	
Mn(2)	Mn+2	0.0	Mn		
Mn(3)	Mn+3	0.0	Mn		
Mn(6)	MnO4-2		0.0	Mn	
Mn(7)	MnO4-	0.0	Mn		
Mo	MoO4-2		0.0	Mo	95.94
N	NO3-	0.0	N	14.0067	
N(5)	NO3-	0.0	N		
#N(-3)	NH4+	0.0	N		
#N(3)	Nitri-	0.0	N		
Nitri	Nitri-	0.0	46.0067	46.0067	
Amm	AmmH+	0.0	17.0304	17.0304	
Naq	Naq	0.0	28.0134	28.0134	
Ngas	Ngas	0.0	28.0134	28.0134	
Na	Na+	0.0	Na	22.9898	
Ni	Ni+2	0.0	Ni	58.69	
P	PO4-3	2.0	P	30.9738	
Pb	Pb+2	0.0	Pb	207.2	
Sulfate	Sulfate-2	0.0	96.066	96.066	
S	HS-	1.0	S	32.066	
#S(0)	S	0.0	S		
#S(6)	Sulfate-2	0.0	SO4		
Sb	Sb(OH)6-	0.0	Sb	121.75	
Sb(3)	Sb(OH)3		0.0	Sb	
Sb(5)	Sb(OH)6-	0.0	Sb		
Se	SeO4-2		0.0	Se	78.96
Se(-2)	HSe-	0.0	Se		

Se(4)	HSeO3-		0.0	Se	
Se(6)	SeO4-2		0.0	Se	
Si	H4SiO4		0.0	SiO2	28.0843
Sn	Sn(OH)6-2	0.0	Sn	118.71	
Sn(2)	Sn(OH)2		0.0	Sn	
Sn(4)	Sn(OH)6-2	0.0	Sn		
Sr	Sr+2	0.0	Sr	87.62	
Tl	Tl(OH)3		0.0	Tl	204.383
Tl(1)	Tl+	0.0	Tl		
Tl(3)	Tl(OH)3		0.0	Tl	
U	UO2+2		0.0	U	238.029
U(3)	U+3	0.0	U		
U(4)	U+4	-4.0	U		
U(5)	UO2+	0.0	U		
U(6)	UO2+2		0.0	U	
V	VO2+	-2.0	V	50.94	
V(2)	V+2	0.0	V		
V(3)	V+3	-3.0	V		
V(4)	VO+2	0.0	V		
V(5)	VO2+	-2.0	V		
Zn	Zn+2	0.0	Zn	65.39	
Benzoate	Benzoate-	0.0	121.116		121.116
Phenylacetate	Phenylacetate-	0.0	135.142		135.142
Isophthalate	Isophthalate-2	0.0	164.117		164.117
Diethylamine	Diethylamine	1.0	73.138	73.138	
Butylamine	Butylamine	1.0	73.138	73.138	
Methylamine	Methylamine	1.0	31.057	31.057	
Dimethylamine	Dimethylamine		1.0	45.084	45.084
Hexylamine	Hexylamine	1.0	101.192		101.192
Ethylenediamine	Ethylenediamine		2.0	60.099	60.099
Propylamine	Propylamine	1.0	59.111	59.111	
Isopropylamine	Isopropylamine		1.0	59.111	59.111
Trimethylamine	Trimethylamine		1.0	59.111	59.111
Citrate	Citrate-3	2.0	189.102		189.102
Nta	Nta-3	1.0	188.117		188.117
Edta	Edta-4	2.0	288.214		288.214
Propionate	Propionate-	1.0	73.072	73.072	
Butyrate	Butyrate-	1.0	87.098	87.098	
Isobutyrate	Isobutyrate-	1.0	87.098	87.098	
Two_picoline	Two_picoline	1.0	93.128	93.128	
Three_picoline	Three_picoline		1.0	93.128	93.128
Four_picoline	Four_picoline	1.0	93.128	93.128	
Formate	Formate-		0.0	45.018	45.018
Isovalerate	Isovalerate-	1.0	101.125		101.125
Valerate	Valerate-	1.0	101.125		101.125
Acetate	Acetate-		1.0	59.045	59.045

```
Tartarate       Tartarate-2     0.0     148.072         148.072
Glycine                 Glycine-        1.0     74.059 74.059
Salicylate      Salicylate-2    1.0     136.107         136.107
Glutamate       Glutamate-2     1.0     145.115         145.115
Phthalate       Phthalate-2     1.0     164.117         164.117
SOLUTION_SPECIES
e- = e-
        log_k 0
H2O = H2O
        log_k 0
Oxy = Oxy
        log_k 0
Ag+ = Ag+
        log_k 0
Al+3 = Al+3
        log_k 0
H3AsO4 = H3AsO4
        log_k 0
H3BO3 = H3BO3
        log_k 0
Ba+2 = Ba+2
        log_k 0
Be+2 = Be+2
        log_k 0
Br- = Br-
        log_k 0
CO3-2 = CO3-2
        log_k 0
Cyanide- = Cyanide-
        log_k 0
Dom_a = Dom_a
        log_k 0
Dom_b = Dom_b
        log_k 0
Dom_c = Dom_c
        log_k 0
Ca+2 = Ca+2
        log_k 0
Cd+2 = Cd+2
        log_k 0
Cl- = Cl-
        log_k 0
Co+3 = Co+3
        log_k 0
CrO4-2 = CrO4-2
        log_k 0
```

```
Cup+ = Cup+
        log_k 0
Cu+2 = Cu+2
        log_k 0
F- = F-
        log_k 0
Fe+3 = Fe+3
        log_k 0
Feii+2 = Feii+2
        log_k 0
H+ = H+
        log_k 0
Hg(OH)2 = Hg(OH)2
        log_k 0
I- = I-
        log_k 0
K+ = K+
        log_k 0
Li+ = Li+
        log_k 0
Mg+2 = Mg+2
        log_k 0
Mn+3 = Mn+3
        log_k 0
MoO4-2 = MoO4-2
        log_k 0
NO3- = NO3-
        log_k 0
Nitri- = Nitri-
        log_k 0
Naq   = Naq
        log_k 0
Ngas = Ngas
        log_k 0
AmmH+ = AmmH+
        log_k 0
Na+ = Na+
        log_k 0
Ni+2 = Ni+2
        log_k 0
PO4-3 = PO4-3
        log_k 0
Pb+2 = Pb+2
        log_k 0
#SO4-2 = SO4-2
        log_k 0
```

```
Sulfate-2 = Sulfate-2
        log_k 0
HS- = HS-
        log_k 0
Sb(OH)6- = Sb(OH)6-
        log_k 0
SeO4-2 = SeO4-2
        log_k 0
H4SiO4 = H4SiO4
        log_k 0
Sn(OH)6-2 = Sn(OH)6-2
        log_k 0
Sr+2 = Sr+2
        log_k 0
Tl(OH)3 = Tl(OH)3
        log_k 0
UO2+2 = UO2+2
        log_k 0
VO2+ = VO2+
        log_k 0
Benzoate- = Benzoate-
        log_k 0
Phenylacetate- = Phenylacetate-
        log_k 0
Isophthalate-2 = Isophthalate-2
        log_k 0
Zn+2 = Zn+2
        log_k 0
Diethylamine = Diethylamine
        log_k 0
Butylamine = Butylamine
        log_k 0
Methylamine = Methylamine
        log_k 0
Dimethylamine = Dimethylamine
        log_k 0
Hexylamine = Hexylamine
        log_k 0
Ethylenediamine = Ethylenediamine
        log_k 0
Propylamine = Propylamine
        log_k 0
Isopropylamine = Isopropylamine
        log_k 0
Trimethylamine = Trimethylamine
        log_k 0
```

```
Citrate-3 = Citrate-3
        log_k 0
Nta-3 = Nta-3
        log_k 0
Edta-4 = Edta-4
        log_k 0
Propionate- = Propionate-
        log_k 0
Butyrate- = Butyrate-
        log_k 0
Isobutyrate- = Isobutyrate-
        log_k 0
Two_picoline = Two_picoline
        log_k 0
Three_picoline = Three_picoline
        log_k 0
Four_picoline = Four_picoline
        log_k 0
Formate- = Formate-
        log_k 0
Isovalerate- = Isovalerate-
        log_k 0
Valerate- = Valerate-
        log_k 0
Acetate- = Acetate-
        log_k 0
Tartarate-2 = Tartarate-2
        log_k 0
Glycine- = Glycine-
        log_k 0
Salicylate-2 = Salicylate-2
        log_k 0
Glutamate-2 = Glutamate-2
        log_k 0
Phthalate-2 = Phthalate-2
        log_k 0
SOLUTION_SPECIES
#Fe+3 + e- = Fe+2
#       log_k   13.032
#       delta_h -42.7   kcal
#       -gamma          0       0
                #               Id:             2802810
                #       log K source:   Bard85
                #     Delta H source:   Bard85
                #T and ionic strength:
H3AsO4 + 2e- + 2H+ = H3AsO3 + H2O
```

```
        log_k   18.898
        delta_h-125.6  kcal
        -gamma          0       0
                #               Id:             600610
                #       log K source:   Bard85
                #     Delta H source:   MTQ3.11
                #T and ionic strength:
Sb(OH)6- + 2e- + 3H+ = Sb(OH)3 + 3H2O
        log_k   24.31
        delta_h0        kcal
        -gamma          0       0
                #               Id:             7407410
                #       log K source:   Bard85
                #     Delta H source:   MTQ3.11
                #T and ionic strength:
UO2+2 + 3e- + 4H+ = U+3 + 2H2O
        log_k   0.42
        delta_h-42      kcal
        -gamma          0       0
                #               Id:             8908930
                #       log K source:   MTQ3.11
                #     Delta H source:   MTQ3.11
                #T and ionic strength:
UO2+2 + 2e- + 4H+ = U+4 + 2H2O
        log_k   9.216
        delta_h-144.1  kcal
        -gamma          0       0
                #               Id:             8918930
                #       log K source:   MTQ3.11
                #     Delta H source:   MTQ3.11
                #T and ionic strength:
UO2+2 + e- = UO2+
        log_k   2.785
        delta_h-13.8   kcal
        -gamma          0       0
                #               Id:             8928930
                #       log K source:   MTQ3.11
                #     Delta H source:   MTQ3.11
                #T and ionic strength:
e- + Mn+3 = Mn+2
        log_k   25.35
        delta_h-107.8  kcal
        -gamma          0       0
                #               Id:             4704710
                #       log K source:   Bard85
                #     Delta H source:   MTQ3.11
```

```
                #T and ionic strength:
Co+3 + e- = Co+2
        log_k   32.4
        delta_h0        kcal
        -gamma          0       0
                #               Id:             2002010
                #       log K source:   Bard85
                #     Delta H source:   MTQ3.11
                #T and ionic strength:

#need this entry, otherwise code will not run
#Cu+2 + 0.125HS- + 0.5H2O = Cup +0.125Sulfate-2 + 1.125H+
#       log_k   -1.5175         #N.S. balance with HS/SO4
#       delta_h0        kcal
#      -no_check
#       -gamma          0       0


#Cu+2 + e- = Cu+
#       log_k   2.69
#       delta_h6.9      kcal
#       -gamma          0       0
                #               Id:             2302310
                #       log K source:   Bard85
                #     Delta H source:   MTQ3.11
                #T and ionic strength:
V+3 + e- = V+2
        log_k   -4.31
        delta_h0        kcal
        -gamma          0       0
                #               Id:             9009010
                #       log K source:   Bard85
                #     Delta H source:   MTQ3.11
                #T and ionic strength:
VO+2 + e- + 2H+ = V+3 + H2O
        log_k   5.696
        delta_h0        kcal
        -gamma          0       0
                #               Id:             9019020
                #       log K source:   Bard85
                #     Delta H source:   MTQ3.11
                #T and ionic strength:
VO2+ + e- + 2H+ = VO+2 + H2O
        log_k   16.903
        delta_h-122.7   kcal
        -gamma          0       0
```

```
                #               Id:          9029030
                #       log K source:    Bard85
                #     Delta H source:    MTQ3.11
                #T and ionic strength:
#SO4-2 + 9H+ + 8e- = HS- + 4H2O
#       log_k   33.66
#       delta_h-60.14  kcal
#       -gamma          0       0
                #               Id:          7307320
                #       log K source:    MTQ3.11
                #     Delta H source:    MTQ3.11
                #T and ionic strength:
Sn(OH)6-2 + 2e- + 4H+ = Sn(OH)2 + 4H2O
        log_k   19.2
        delta_h0        kcal
        -gamma          0       0
                #               Id:          7907910
                #       log K source:    Bard85
                #     Delta H source:    MTQ3.11
                #T and ionic strength:
Tl(OH)3 + 2e- + 3H+ = Tl+ + 3H2O
        log_k   45.55
        delta_h0        kcal
        -gamma          0       0
                #               Id:          8708710
                #       log K source:    Bard85
                #     Delta H source:    MTQ3.11
                #T and ionic strength:
HSeO3- + 6e- + 6H+ = HSe- + 3H2O
        log_k   44.86
        delta_h0        kcal
        -gamma          0       0
                #               Id:          7607610
                #       log K source:    Bard85
                #     Delta H source:    MTQ3.11
                #T and ionic strength:
SeO4-2 + 2e- + 3H+ = HSeO3- + H2O
        log_k   36.308
        delta_h-201.2  kcal
        -gamma          0       0
                #               Id:          7617620
                #       log K source:    Bard85
                #     Delta H source:    MTQ3.11
                #T and ionic strength:
0.5Hg2+2 + e- = Hg
        log_k   6.5667
```

delta_h-45.735 kcal
-gamma 0 0
Id: 3600000

Appendix D: MathCad File for Determining Streamtube Lengths

Finding hop lengths, x, between 2024 and 2025 for a alpha = pi/7.
The graphic to the right depicts the variables used for this formulation.

Units in feet and minutes.

Luo, J., Kitanidis, P.K. 2004. Fluid residence times within a recirculation zone created by an extraction-injection well pair. Journal of Hydrology 295 (2004) 149-162

$N := 3$ $k := 1..N-1$

$j := 1..N$ $kp := 0..N-1$

$rw := 0.2$ $n := 0.4$

$tau := 39.36$ $factor := 1$

$b := \frac{5.5}{factor}$

$Qu := 1gpm$ $Qu = 0.134\frac{ft^3}{min}$

$Q := 0.13$

$C := \frac{-Q}{4\cdot\pi}$ $L := 3.29438$ for 2024 to 2025, includes well radii

$dt := \frac{tau}{N}$ $dt = 1.064$

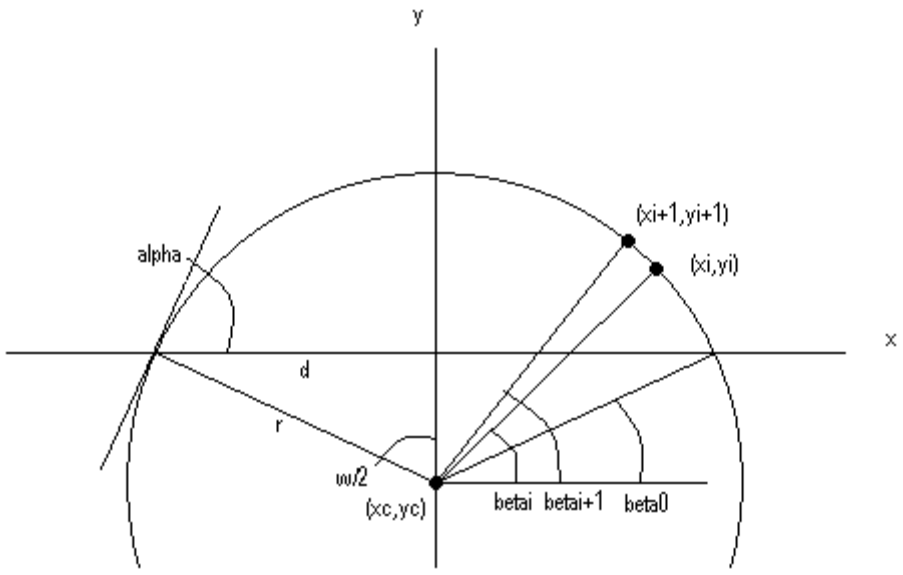

$\alpha := \frac{\pi}{7}$ $\omega := 2\cdot\alpha$ $\beta_0 := \frac{\pi}{2} - \alpha$ $\beta_0 = 1.122$

$d := \frac{L}{2}$ $r := \frac{d}{\sin(\alpha)}$ $y_c := -r\cdot\cos(\alpha)$ $y_c = -3.42$

To include well radius:

$rwangx0 := \operatorname{atan}\left(\frac{|y_c|}{d - rw}\right)$ $rwangx0 = 1.183$

$rwang := \operatorname{atan}\left(\frac{-y_c + rw\cdot\sin(\alpha)}{d - rw\cdot\cos(\alpha)}\right)$ $rwang = 1.188$

$rwy := rw\cdot\sin(\alpha)$ $rwy = 0.108$

$rwx := d - rw\cdot\cos(\alpha)$ $rwx = 1.422$

$\beta_1 := rwang$ $\beta_1 = 1.188$

α defines which streamtube we are evaluating

According to the graphic here and as shown in Figure 3 of Luo & Kit 2004, yc is below the origin, and thus should be negative. The formula for y coordinates in the paper is: $y=yc+r\sin(\beta)$. For streamlines with $0<\alpha<\pi/2$ yc will be negative.

rwangx0 is the angle β corresponding to (d-rw,0). This is the starting angle if we are starting at the well radius.

rwang is the angle β corresponding to where the streamline arc intersects with the well radius. (rwx,rwy). this is the value that should be used for β1 because it is actually on the streamline.

To calculate factor: $factorold := 1$ $b := \frac{5.5}{factorold}$

$$v(\beta) := \frac{Q \cdot d}{2 \cdot \pi \cdot n \cdot b \cdot r \cdot \left(r \cdot \sin(\beta) + y_c\right)}$$

$$factor := \frac{1}{tau}\left(\int_{rwang}^{\pi - rwang} \frac{r}{v(\beta)}\, d\beta\right)$$

$factor = 5.484$ $b := \frac{5.5}{factor}$

To calculate first length:

$$v(\beta) := \frac{Q \cdot d}{2 \cdot \pi \cdot n \cdot b \cdot r \cdot \left(r \cdot \sin(\beta) + y_c\right)}$$

$$t31(\beta 2) := \int_{\beta_1}^{\beta 2} \frac{r}{v(\beta)}\, d\beta - dt$$

$guess := 1.2$ $\beta 2 := guess$

$angle1 := root\left(t31(\beta 2), \beta 2\right)$

$angle1 = 1.232$

$delta\beta := angle1 - \beta_1$

$delta\beta = 0.045$

$dist1 := \left(root\left(t31(\beta 2), \beta 2\right) - \beta_1\right) \cdot r$

$dist1 = 0.17$

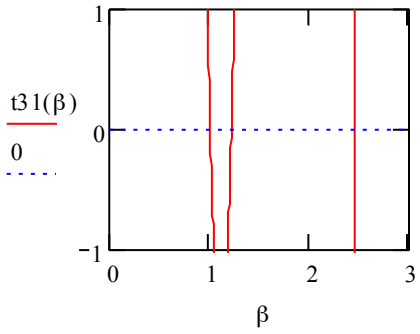

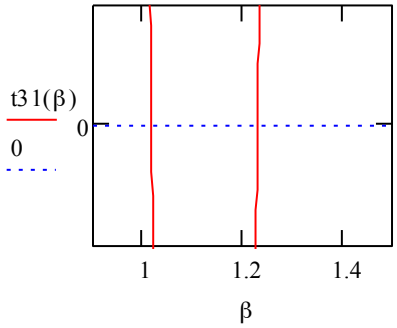

To calculate all lengths:

$cxxx(N) :=$ | angold ← angle1

$ttime(new, old) :=$ | d ← angold | $\int_{old}^{new} \frac{r}{v(\beta)}\, d\beta - dt$ | for k ∈ 0.. N

| | $delta_k \leftarrow (root(ttime(d, angold), d) - angold)\cdot r$

| | $angnew_k \leftarrow root(ttime(d, angold), d)$

| | angold ← $angnew_k$

| | d ← angold

| return delta

angle1 = 1.232

angle1 := β_1

cintervals := cxxx(36) Input N-1

$total := \sum_{i=0}^{36} cintervals_i$ total = 2.908

$totdist := (\pi - 2\cdot rwang)\cdot r$ totdist = 2.908

$constvellength := \frac{totdist}{N}$ constvellength = 0.079

feet := 0.079ft

meter := feet

meter = 0.024m

Unit conversions and uniform velocity divisions

$phrqstandard := \frac{total}{N}\,ft$ $\quad phrqstandard = 0.079ft$

$phrqstandard = 0.0239586m$

$tophrq := cintervals \cdot ft$

Appendix E: MathCad File for Deconvolution

TRACER TEST UREA ONE: 7-18-8

ref: Seshadri, V., *The Inverse Gaussian Distribution: A Case Study in Exponential Families,* Oxford University Press, New York, New York, 1993.

$Co1 := 1$

$\tau 0 := 0$ $\quad \Delta 1 := 230$

del1 is the time of pumping, but 190 fits data better.

$\lambda := 450$ $\quad \mu := 55$ $\quad \sigma := \left(\frac{\mu^3}{\lambda}\right)^{\frac{1}{2}}$

$$pdfc(\tau) := \left(\frac{\lambda}{2\cdot\pi\cdot\tau^3}\right)^{\frac{1}{2}} \cdot \exp\left[\frac{-\lambda\cdot(\tau-\mu)^2}{2\cdot\mu^2\cdot\tau}\right]$$

$$pdfc(\tau) := \left(\frac{\mu^3}{2\cdot\pi\cdot\tau^3\cdot\sigma^2}\right)^{\frac{1}{2}} \cdot \exp\left[-\mu\cdot\frac{(\tau-\mu)^2}{2\cdot\sigma^2\cdot\tau}\right]$$

$$cdfc(\tau) := \int_0^{\tau} pdfc(t)\,dt$$

$$cdf(\tau) := if(\tau < \tau 0, 0, cdfc(\tau))$$

D := READPRN("TestOneUreaBr.txt")

time24 := $D^{\langle 0 \rangle}$ Br24 := $D^{\langle 1 \rangle}$

time26 := $D^{\langle 2 \rangle}$ Br26 := $D^{\langle 3 \rangle}$

i := 0.. last(time24)

cumulative fitter

$$c24m(t) := .24 \cdot (if(t < \Delta 1, cdf(t), cdf(t) - cdf(t - \Delta 1)))$$

$$c26m(t) := .77 \cdot (if(t < \Delta 1, cdf(t), cdf(t) - cdf(t - \Delta 1)))$$

$c24_i := c24m(time24_i)$ $c26_i := c26m(time26_i)$

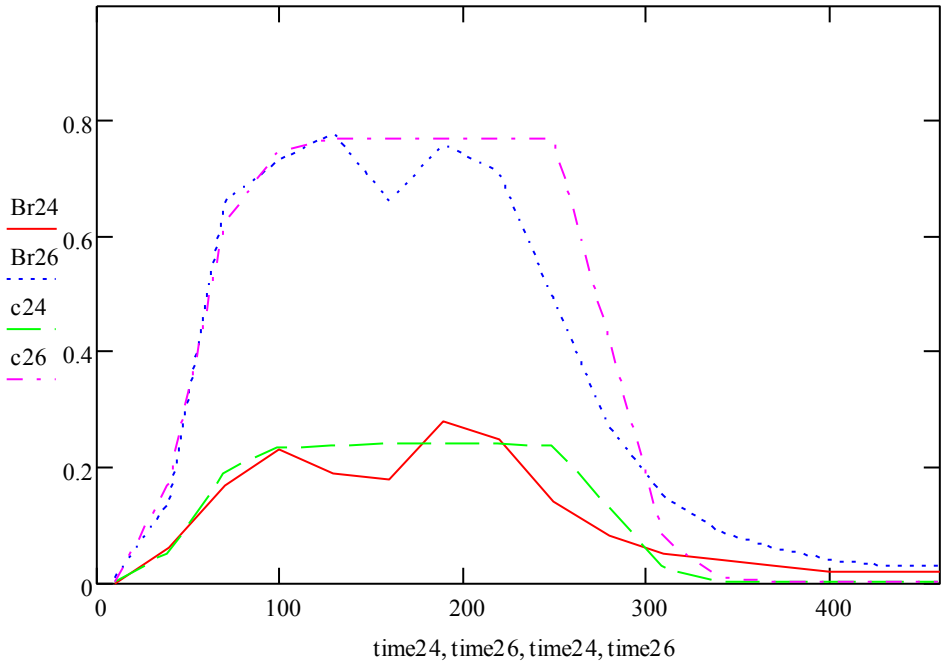

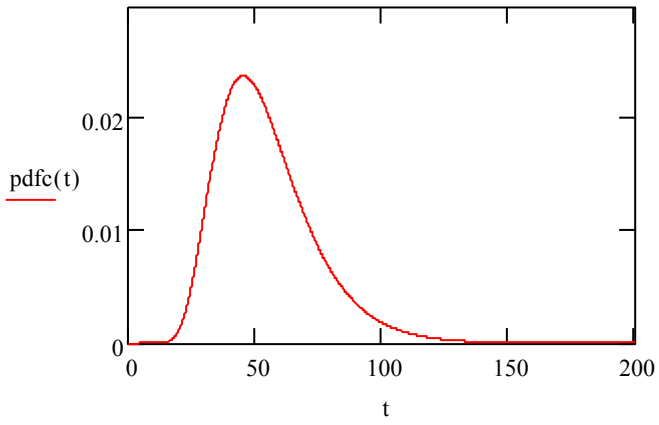

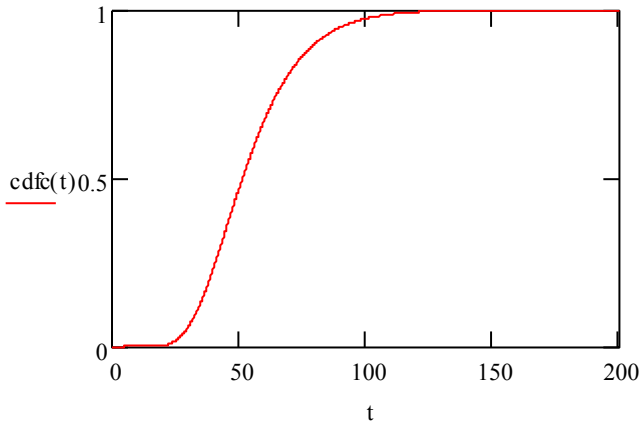

For 2026:

$j := 0..6$

$g1 := 50$

$y_j := \frac{j+1}{7}$ $\quad y = \begin{pmatrix} 0.143 \\ 0.286 \\ 0.429 \\ 0.571 \\ 0.714 \\ 0.857 \\ 1 \end{pmatrix}$ $\quad r_j := \text{root}\left(\text{cdfc}(g1) - y_j, g1\right)$

$r_6 := 154.46$

$$\overrightarrow{cdfc(r)} = \begin{pmatrix} 0.143 \\ 0.286 \\ 0.429 \\ 0.571 \\ 0.714 \\ 0.857 \\ 1 \end{pmatrix}$$

$tout_0 := 0$

$tout_{j+1} := r_j$

$$tout = \begin{pmatrix} 0 \\ 36.022 \\ 42.705 \\ 48.745 \\ 55.177 \\ 63.02 \\ 74.843 \\ 154.461 \end{pmatrix}$$

$$tt_j := \frac{tout_{j+1} + tout_j}{2}$$

$$\overrightarrow{tt = \begin{pmatrix} 18.011 \\ 39.363 \\ 45.725 \\ 51.961 \\ 59.098 \\ 68.931 \\ 114.652 \end{pmatrix}}$$

$rtt := round(tt, 3)$

$N_0 := 17$

$$dt := \frac{rtt_0}{N_0}$$

$dt = 1.059$

$k := 1..6$

$rdt := round(dt, 3)$

$$N_k := \frac{tt_k}{dt}$$

$$N = \begin{pmatrix} 17 \\ 37.154 \\ 43.158 \\ 49.044 \\ 55.781 \\ 65.062 \\ 108.216 \end{pmatrix}$$

$$\overrightarrow{N = \begin{pmatrix} 17 \\ 37 \\ 43 \\ 49 \\ 56 \\ 65 \\ 108 \end{pmatrix}}$$

$rN := round(N, 0)$

$$\text{roundcheck} := \text{rdt} \cdot \text{rN}$$

$$\text{roundcheck} = \begin{pmatrix} 18.003 \\ 39.183 \\ 45.537 \\ 51.891 \\ 59.304 \\ 68.835 \\ 114.372 \end{pmatrix} \qquad \text{rtt} = \begin{pmatrix} 18.011 \\ 39.363 \\ 45.725 \\ 51.961 \\ 59.098 \\ 68.931 \\ 114.652 \end{pmatrix}$$

$$\text{newdt} := \frac{\text{rtt}}{\text{rN}} \qquad \left| \text{newdt} = \begin{pmatrix} 1.059 \\ 1.064 \\ 1.063 \\ 1.06 \\ 1.055 \\ 1.06 \\ 1.062 \end{pmatrix} \right| \qquad \left| \text{rN} = \begin{pmatrix} 17 \\ 37 \\ 43 \\ 49 \\ 56 \\ 65 \\ 108 \end{pmatrix} \right| \qquad \left| \text{rtt} = \begin{pmatrix} 18.011 \\ 39.363 \\ 45.725 \\ 51.961 \\ 59.098 \\ 68.931 \\ 114.652 \end{pmatrix} \right|$$